

Article

A SHORT SURVEY OF MATTER-ANTIMATTER EVOLUTION IN THE PRIMORDIAL UNIVERSE

Johann Rafelski , Jeremiah Birrell , Andrew Steinmetz , and Cheng Tao Yang 

Department of Physics, The University of Arizona, Tucson, Arizona 85721, USA

* Correspondence: JohannR@arizona.edu

Version April 20, 2023 submitted to Universe

Abstract: In celebration of Remo Ruffini’s birthday, his contributions to astrophysics and cosmology and the large number of students he mentored, (see Fig. 1) we offer here a survey of the matter-antimatter evolution of the primordial Universe. While the origin of matter-antimatter asymmetry has remained one of the big questions in modern cosmology today, for much of the Universe’s early history, antimatter still played a large role in its evolution. We take the position of the standard model Λ -CDM Universe without invoking additional novel and unexplored physics. We study and explore the evolution of the Universe implementing the known baryonic asymmetry. We present the composition of the Universe across its temperature history while emphasizing the epochs where antimatter content is essential to our understanding. Special topics will include the creation of matter from quark-gluon plasma (QGP), the free-streaming of the neutrinos, the vanishing of the muons, magnetism in the electron-positron cosmos, and a better understanding of the environment where Big Bang Nucleosynthesis (BBN) occurred producing the light elements. We suggest that the methods used in exploring the early Universe may also provide new insights in the study of exotic stellar cores, magnetars, as well as gamma-ray burst (GRB) events. Further investigation is required in pushing known physics to its extremes in the unique laboratory of the matter-antimatter early Universe.

Keywords: Particles, Plasmas and Electromagnetic Fields in Cosmology; Quarks to Cosmos;



Figure 1. Remo Ruffini (right) at work. Photo by Johann Rafelski.

Contents

19	1	Timeline of particles and plasmas in the Universe	2
20	1.1	Guide to $130 \text{ GeV} > T > 20 \text{ keV}$	2
21	1.2	The Five Plasma Epochs	3
22	1.3	The Λ -CDM Universe	7

23	2 QGP Epoch	9
24	2.1 Conservation Laws in QGP	9
25	2.2 Heavy flavor: bottom and charm in QGP	12
26	3 Hadronic Epoch	15
27	3.1 The Formation of Matter	15
28	3.2 Cosmological Strangeness Abundance	17
29	3.3 Pion Abundance in the Early Universe	21
30	4 Leptonic Epoch	24
31	4.1 Thermal Degrees of Freedom	24
32	4.2 Muon Abundance in the Early Universe	24
33	4.3 Neutrino Masses and Oscillation	26
34	4.4 Neutrino freezeout in early Universe	28
35	4.5 Effective Number of Neutrinos	30
36	5 Electron-Positron Epoch	32
37	5.1 Electron-Positron Density Compared to Baryons	33
38	5.2 Energy Eigenvalues	34
39	5.3 Landau eigen-energies in cosmology	35
40	5.4 Electron-positron statistical physics	37
41	5.5 Charge neutrality and chemical potential	39
42	5.6 Magnetization	40
43	6 Summary	42
44	6.1 Primordial Plasma Outlook	42
45	6.2 Application to Novel Stellar Objects	42
46	References	42

47 1. Timeline of particles and plasmas in the Universe

48 1.1. Guide to $130 \text{ GeV} > T > 20 \text{ keV}$

49 This survey of the early Universe begins with quark-gluon plasma (QGP) at a temperature of 130 GeV
 50 and ends with the electron-positron e^\pm epoch which was the final phase of the Universe to contain
 51 significant quantities of antimatter. Under the assumption of a homogeneous Universe, this final
 52 cosmic soup of antimatter survived until the Universe cooled to a temperature of 20 keV. This work
 53 presumes that in our casual domain, the Universe is matter dominated.

54 A more detailed description of particles and plasmas follows in Sect. 1.2. We have adopted
 55 the standard Λ -CDM model of a cosmological constant (Λ) and cold dark matter (CDM) where the
 56 Universe undergoes dynamical expansion as described in the Friedmann–Lemaître–Robertson–Walker
 57 (FLRW) metric. The contemporary and recent history of the Universe in terms of energy density as a
 58 function of time and temperature is shown in Fig. 2. The Universe’s past is obtained from integrating
 59 backwards the proposed modern composition of the Universe which contains 69% dark energy, 26%
 60 dark matter, 5% baryons, and $< 1\%$ photons and neutrinos in terms of energy density. The method
 61 used to obtain these results are found in Sect. 1.3.

62 After the general overview, we take the opportunity to enlarge in some detail our more recent
 63 work in special topics. In Sect. 2, we describe the chemical potentials of the QGP plasma species
 64 leading up to hadronization, Hubble expansion of the QGP plasma, and the abundances of heavy
 65 quarks. In Sect. 3 we discuss the formation of matter during hadronization, the role of strangeness, and
 66 the unique circumstances which led to pions remaining abundant well after all other hadrons were

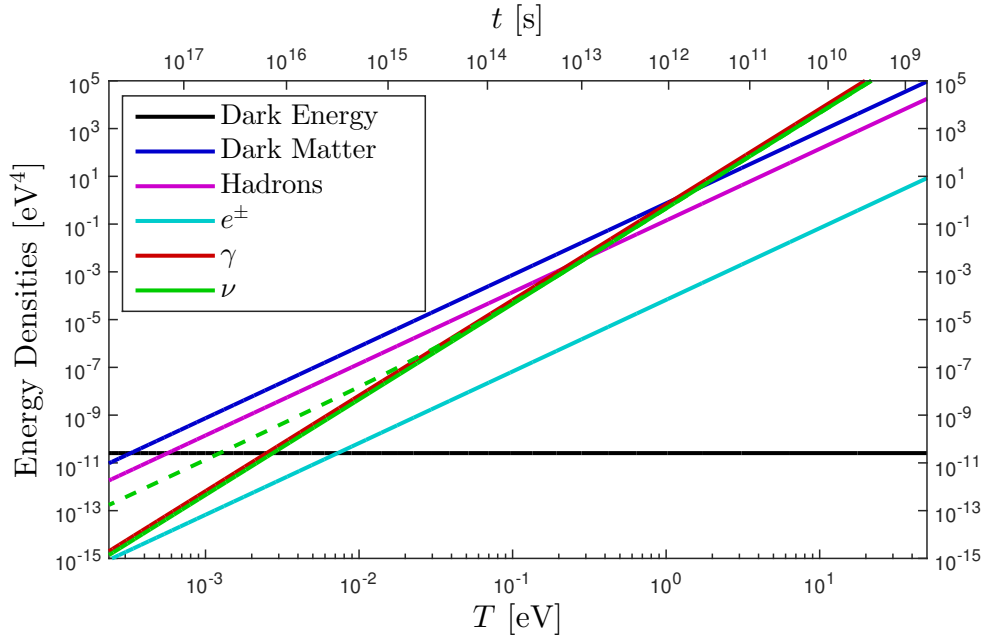


Figure 2. Contemporary era: 69% dark energy, 26% dark matter, 5% baryons, < 1% photons and neutrinos. Solid neutrino line shows massless neutrinos while the dashed line shows 1 massless and 2×0.1 eV neutrinos (Neutrino mass choice is just for illustration. Other values are possible).

67 diluted or decayed. We review the roles of muons and neutrinos in the leptonic epoch in Sect. 4. The
 68 e^\pm plasma epoch is described in Sect. 5 which is the final stage of the universe where antimatter played
 69 an important role. Here we introduce the statistical physics description of electrons and positron
 70 gasses, their relation to the baryon density, and the magnetization of the e^\pm plasma prior to the
 71 disappearance of the positrons shortly after Big Bang Nucleosynthesis (BBN). A more careful look
 72 at the effect of the dense e^\pm plasma on BBN is underway [99]. One interesting feature of having an
 73 abundant e^\pm plasma is the possibility of magnetization in the early Universe. We begin to address this
 74 using spin-magnetization and mean-field theory where all the spins respond to the collective bulk
 75 magnetism self generated by the plasma. We stop our survey at a temperature of 20 keV with the
 76 disappearance of the positrons signifying the end of antimatter dynamics at cosmological scales.

77 This primordial Universe is a plasma physics laboratory with unique properties not found in
 78 laboratory or stellar environments due to the high amount of antimatter present nearly non-relativistic
 79 temperatures. We suggest that astrophysics systems where positrons content is considered should
 80 be explored. Possibilities for novel stellar objects with significant positron content is discussed.
 81 While the disappearance of baryonic matter is well described in the literature, it has not always been
 82 appreciated how late leptonic ($\bar{\mu} = \mu^+$ and $\bar{e} = e^+$) antimatter remains a significant presence in the
 83 Universe's evolutionary history. We show that the e^\pm epoch is a prime candidate to tackle up to
 84 here several unrelated cosmic mysteries such as early Universe matter in-homogeneity, the origin
 85 of cosmic magnetic fields. While the plasma epochs of the early Universe are in our past, plasmas
 86 which share features with the primordial Universe might possibly exist with dynamics relevant to
 87 gamma-ray burst (GRB), black holes, [1–3,8] and magnetars in the contemporary Universe today. While
 88 the literature contains many comprehensive reviews of observational cosmology, the recombination
 89 period, BBN, and inflationary epochs, we aim to fill the niche of a general overview of the antimatter
 90 content of the universe with details absent from more general texts like Kolb and Turner [105].

91 1.2. The Five Plasma Epochs

92 At an early time in the standard cosmology model, the Universe began as a fireball with extremely high
 93 temperature and high energy density. The ultra-relativistic plasma produced in the early Universe

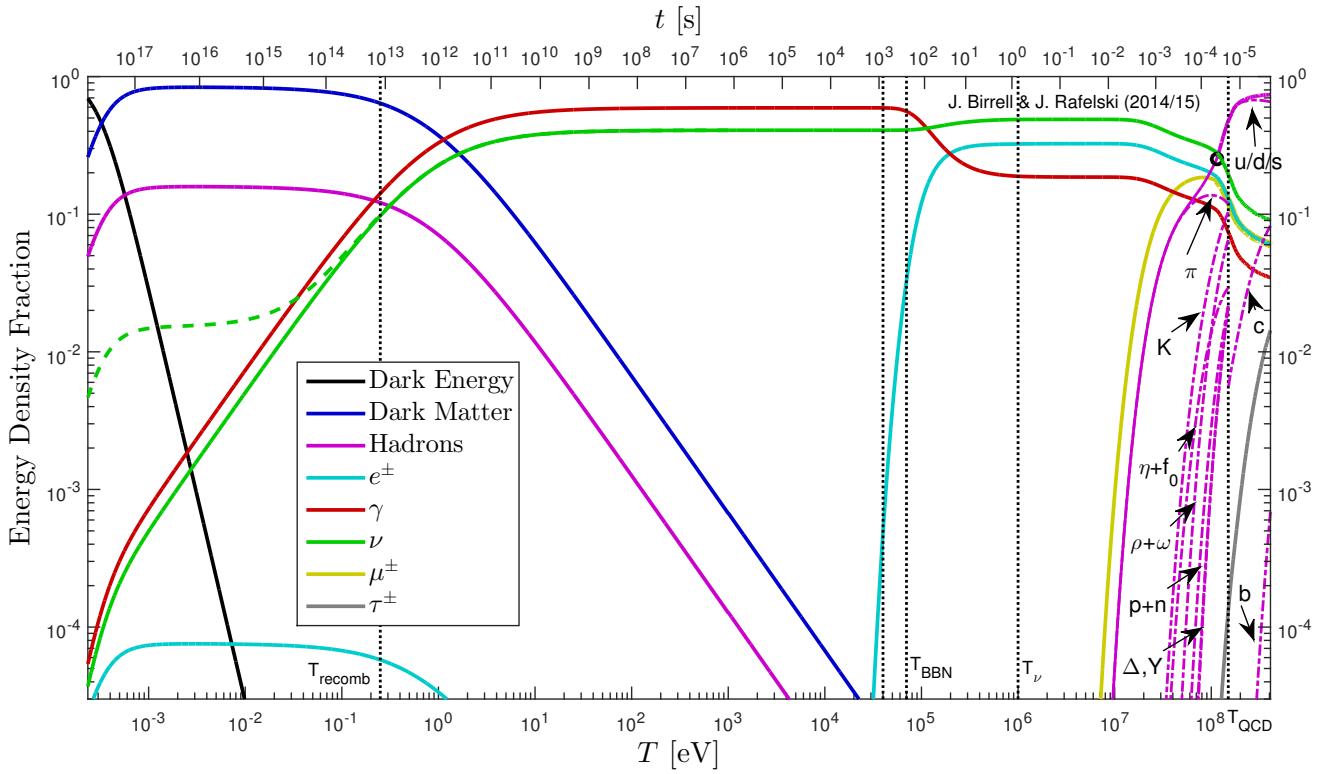


Figure 3. Evolution of the differing matter and radiation components of the Universe over cosmological timescales from contemporary observational cosmology to the QGP epoch of the Universe. Key temperatures are listed for specific transitions between epochs. Solid neutrino line shows massless neutrinos while the dashed line shows 1 massless and 2×0.1 eV neutrinos (Neutrino mass choice is just for illustration. Other values are possible).

94 contained almost a perfect symmetry between matter and antimatter except for a small discrepancy of
 95 one part in 10^9 which remains a mystery today. This fireball then underwent several phases changes
 96 which dramatically evolved the gross properties as the Universe expanded and cooled. Evolutionary
 97 processes in the primordial Universe are taken to be adiabatic. We present an overview of particle
 98 families across all epochs Fig. 3 in the Universe, as a function of temperature and thus time. The comic
 99 plasma, after the electroweak symmetry breaking epoch and presumably inflation, occurred in the
 100 early Universe in the following sequence:

- 101 1. **Primordial quark-gluon plasma:** At early times when the temperature was between $130 \text{ GeV} >$
 102 $T > 150 \text{ MeV}$, we have the building blocks of Universe as we know them today including the
 103 leptons, vector bosons, and all three families of de-confined quarks and gluons which propagated
 104 freely. As all hadrons are dissolved into their constituents during this time, strongly interacting
 105 particles u, d, s, t, b, c, g controlled the fate of the Universe. Here we will only look at the late-stage
 106 evolution at around 150 MeV .
- 107 2. **Hadronic epoch:** Around the hadronization temperature $T_h \approx 150 \text{ MeV}$, a phase transformation
 108 occurred forcing the strongly interacting particles such as quarks and gluons to condense into
 109 confined states. It is here where matter as we know it today forms and the Universe becomes
 110 hadronic-matter dominated. In the temperature range $150 \text{ MeV} > T > 20 \text{ MeV}$ the Universe is
 111 rich in physics phenomena involving strange mesons and (anti)baryons including (anti)hyperon
 112 abundances [97,109].
- 113 3. **Lepton-photon epoch:** For temperature $10 \text{ MeV} > T > 2 \text{ MeV}$, the Universe contained
 114 relativistic electrons, positrons, photons, and three species of neutrinos/antineutrinos. Muons

vanish partway through this temperature scale. In this range, neutrinos were still coupled to the charged leptons via the weak interaction. [110]. During this time the expansion of the Universe is controlled by leptons and photons almost on equal footing.

4. **Final antimatter epoch:** After neutrinos decoupled and become free-streaming, referred to as neutrino freezeout, from the cosmic plasma at $T = 2$ MeV, the cosmic plasma was dominated by electrons, positrons, and photons. We have shown in [99] that this plasma existed until $T \approx 0.02$ MeV such that BBN occurred within a rich electron-positron plasma. This is the last time the Universe will contain a significant fraction of its content in antimatter.
5. **Moving towards matter dominated Universe:** The final major plasma stage in the Universe began after the annihilation of the majority of e^\pm pairs leaving behind a residual amount of electrons determined by the baryon asymmetry in the Universe and charge conservation. The Universe was still opaque to photons at this point and remained so until the recombination period at $T \approx 0.26$ eV starting the era of observational cosmology with the CMB. This final epoch of the primordial Universe will not be described in detail here, but is well covered in [42].

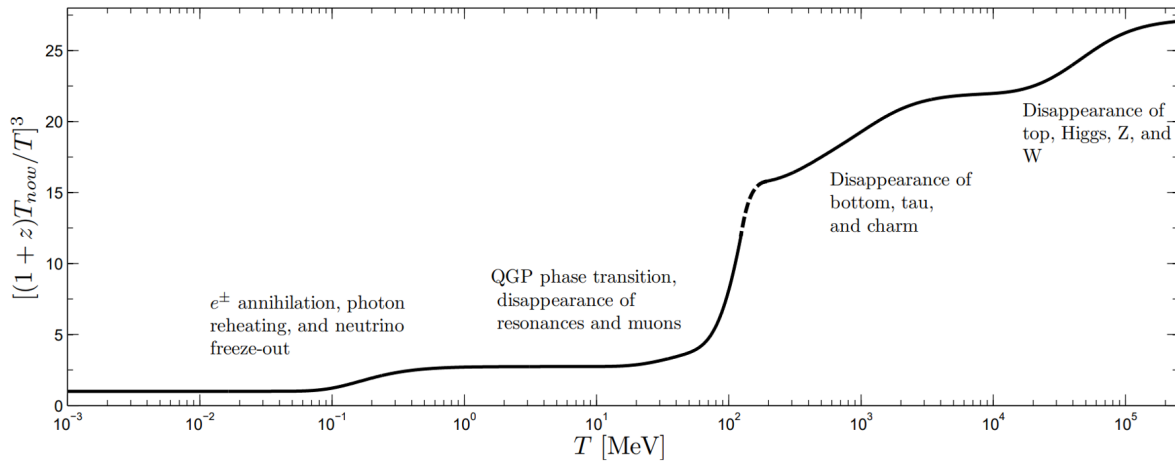


Figure 4. The evolution of the photon reheating (black line) process in terms of fractional temperature change in the Universe. Figure adapted from [124]. The dashed portion is a qualitative description subject to the exact model of QGP hadronization.

Each plasma outlined above contributes to the thermal behavior of the Universe over time. This is illustrated in Fig. 4 where the fractional drop in temperature during each plasma transformation is plotted. Each subsequent plasma lowers the available degrees of freedom (as the particle inventory is whittled away) as the Universe cools [124]. Each drop in degrees of freedom represents entropy being pumped into the photons as entropy is conserved (up until gravitational processes become relevant) in an expanding Universe. As there are no longer degrees of freedom to consume reheating the photon field further, the fractional temperature remains constant today.

In Figure 3 we begin on the right at the end of the QGP era. The first dotted vertical line shows the QGP phase transition and hadronization, near $T = 150$ MeV. The hadron era proceeds with the disappearance of muons, pions, and heavier hadrons. This constitutes a reheating period, with energy and entropy from these particles being transferred to the remaining e^\pm , photon, neutrino plasma. The black circle near $T = 115$ MeV denotes our change from 2 + 1-flavor lattice QCD data for the hadron energy density, taken from Borsanyi et al. [38], to an ideal gas model at lower temperature. We note that the hadron ideal gas energy density matches the lattice results to less than a percent at 115 MeV.

To the right of the QGP transition region, the solid hadron line shows the total energy density of quarks and gluons. From top to bottom, the dot-dashed hadron lines to the right of the transition show the energy density fractions of 2 + 1-flavor (u,d,s) lattice QCD matter (almost indistinguishable from the total energy density), charm, and bottom (both in the ideal gas approximation). To the left of the

147 transition the dot-dashed lines show the pion, kaon, $\eta + f_0$, $\rho + \omega$, nucleon, Δ , and Y contributions to
 148 the energy fraction.

149 Continuing to the second vertical line at $T = \mathcal{O}(1 \text{ MeV})$, we come to the annihilation of e^\pm and
 150 the photon reheating period. Notice that only the photon energy density increases here, as we
 151 assume here that neutrinos are already decoupled at this time and hence do not share in the reheating
 152 process, leading to a difference in photon and neutrino temperatures. This is not strictly correct but it is
 153 a reasonable simplifying assumption for the current purpose; see [110,119–121]. We next pass through
 154 a long period, from $T = \mathcal{O}(1 \text{ MeV})$ until $T = \mathcal{O}(1 \text{ eV})$, where the energy density is dominated by
 155 photons and free-streaming neutrinos. BBN occurs in the approximate range $T = 40 - 70 \text{ keV}$ and
 156 is indicated by the next two vertical lines. It is interesting to note that, while the hadron fraction is
 157 insignificant at this time, there is still a substantial background of e^\pm pairs during BBN as seen in
 158 Fig. 5 and until $T_{\text{split}} = 20.36 \text{ keV}$. For $T < T_{\text{split}}$ the positron density quickly vanishes because of
 159 annihilation leaving only a residual electron density as required by charge conservation.

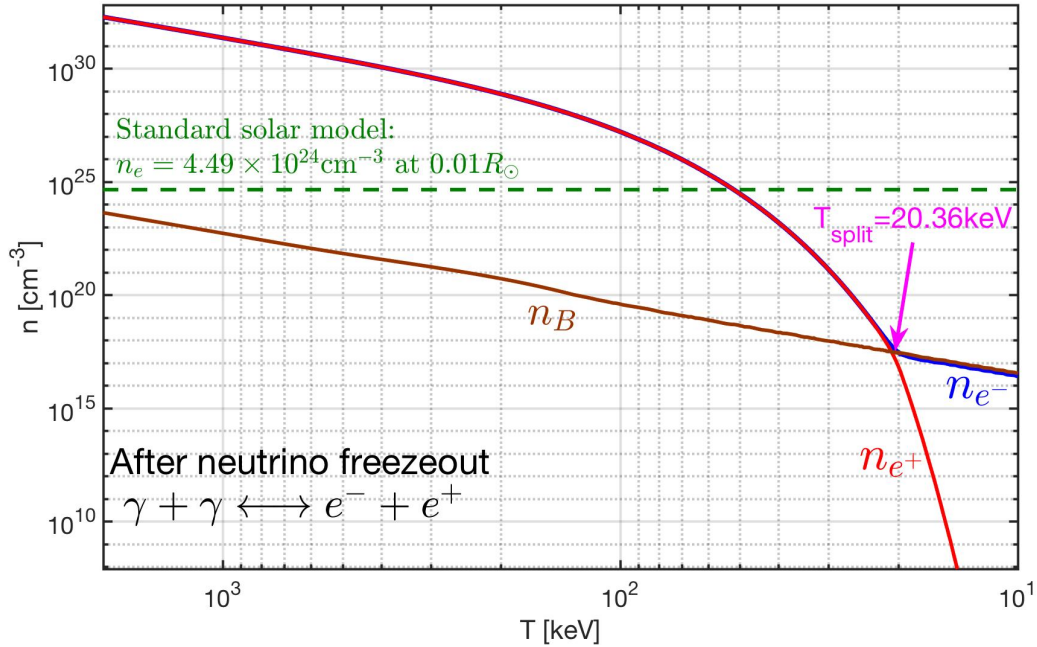


Figure 5. The e^\pm number densities as a function of temperature in the range $2 \text{ MeV} > T > 10 \text{ keV}$. The blue solid line is the electron density, the red solid line is the positron density, and the brown solid line is the baryon density. For comparison, we also show the green dotted line as the solar electron density within the stellar core. **Need reference!**

160 We then come to the beginning of the matter dominated regime, where the energy density is
 161 dominated by the combination of dark matter and baryonic matter. This transition is the result of the
 162 redshifting of the photon and neutrino energy, $\rho \propto T^4$, whereas for non-relativistic matter $\rho \propto a^{-3} \propto T^3$.
 163 Recombination and photon decoupling occurs near the transition to the matter dominated regime,
 164 denoted by the vertical line at $T = 0.25 \text{ eV}$.

165 Finally, as we move towards the present day CMB temperature of $T_{\gamma,0} = 0.235 \text{ MeV}$ on the left
 166 hand side, we have entered the dark energy dominated regime. For the present day values, we have
 167 used the energy densities proscribed by the Planck parameters Eq. (14) [40] and zero Universe spatial
 168 curvature. The photon energy density is fixed by the CMB temperature $T_{\gamma,0}$ and the neutrino energy
 169 density is fixed by $T_{\gamma,0}$ along with the photon to neutrino temperature ratio and neutrino masses. Both
 170 constitute $< 1\%$ of the current energy budget.

171 The Universe evolution and total energy densities were computed using massless neutrinos, but
 172 for comparison we show the energy density of massive neutrinos in the dashed green line. For the

173 dashed line we used two neutrino flavors with masses $m_\nu = 0.1$ eV and one massless flavor. Note that
 174 the inclusion of neutrino mass causes the leveling out of the neutrino energy density fraction during
 175 the matter dominated period, as compared to the continued redshifting of the photon energy.

176 1.3. The Λ -CDM Universe

Here we provide background on the standard Λ -CDM cosmological (FLRW-Universe) model that is used in the computation of the composition of the Universe over time. We use the spacetime metric with metric signature $(+1, -1, -1, -1)$ in spherical coordinates

$$ds^2 = c^2 dt^2 - a^2(t) \left[\frac{dr^2}{1 - kr^2} + r^2(d\theta^2 + \sin^2(\theta)d\phi^2) \right] \quad (1)$$

characterized by the scale parameter $a(t)$ of a spatially homogeneous Universe. The geometric parameter k identifies the Gaussian geometry of the spacial hyper-surfaces defined by co-moving observers. Space is a Euclidean flat-sheet for the observationally preferred value $k = 0$ [40–42]. In this case it can be more convenient to write the metric in rectangular coordinates

$$ds^2 = c^2 dt^2 - a^2(t) [dx^2 + dy^2 + dz^2]. \quad (2)$$

177 We will work in units where $\hbar = 1$, $c = 1$.

The global Universe dynamics can be characterized by two quantities: the Hubble parameter H , a strongly time dependent quantity on cosmological time scales, and the deceleration parameter q :

$$H(t)^2 \equiv \left(\frac{\dot{a}}{a} \right)^2 = \frac{8\pi G_N}{3} \rho_{tot}, \quad (3)$$

$$\frac{\ddot{a}}{a} = -qH^2, \quad q \equiv -\frac{a\ddot{a}}{\dot{a}^2}, \quad \dot{H} = -H^2(1 + q), \quad (4)$$

178 where G_N is the Newtonian gravitational constant and ρ_{tot} is the energy density of the Universe and
 179 composed of the various energy densities in the Universe. The deceleration parameter q is defined
 180 in terms of the second derivative of the scale parameter. In Fig. 6 (left) we illustrate the late stage
 181 evolution of the parameters H and q given in Eq. (3) and Eq. (4) compared to temperature. This
 182 illustrates how the Universe evolves according to the Friedmann equations Eq. (3) and Eq. (4) above.
 183 The deceleration begins radiation dominated with $q = 1$ and then transitions to matter dominated
 184 $q = 1/2$. The contemporary Universe is undergoing the transition from matter dominated to dark
 185 energy dominated where, barring the possibility of phantom energy, the deceleration will settle on the
 186 asymptotic value of $q = -1$ [124]. Part of the program of this survey is to connect this picture of late
 187 stage evolution to the very early universe during and prior to BBN. The current tension in Hubble
 188 parameter measurements [71–73] might benefit from closer inspection of the earlier denser periods.
 189 Fig. 6 (right) shows the close relationship between the redshift z and the Hubble parameter. Deviations
 190 separating the two occur from the transitions which changed the deceleration value.

The Einstein equations with a cosmological constant Λ corresponding to dark energy are:

$$G^{\mu\nu} = R^{\mu\nu} - \left(\frac{R}{2} + \Lambda \right) g^{\mu\nu} = 8\pi G_N T^{\mu\nu}, \quad R = g_{\mu\nu} R^{\mu\nu}. \quad (5)$$

The homogeneous and isotropic symmetry considerations imply that the stress energy tensor is determined by an energy density and an isotropic pressure

$$T_\nu^\mu = \text{diag}(\rho, -P, -P, -P). \quad (6)$$

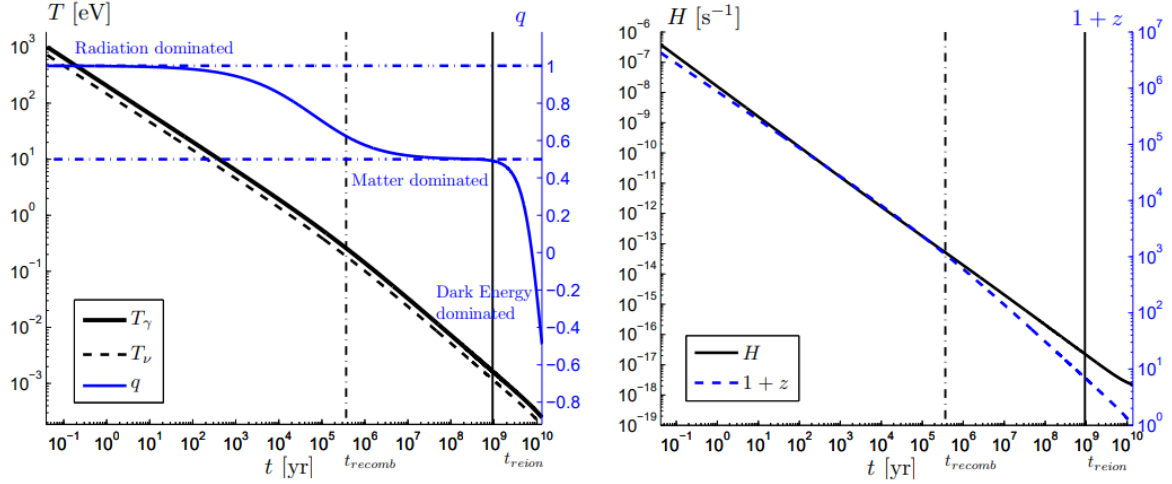


Figure 6. (left) The numerically solved later $t > 10^{-1}$ yr evolution of photon and neutrino background temperatures T_γ , T_ν (black and black dashed lines) and the deceleration parameter q (thin blue line) over the lifespan of the Universe. (right) The evolution of the Hubble parameter $1/H$ (black line) and redshift z (blue dashed line) which is related to the scale parameter $a(t)$. Figure adapted from [124].

It is common to absorb the Einstein cosmological constant Λ into the energy and pressure

$$\rho_\Lambda = \frac{\Lambda}{8\pi G_N}, \quad P_\Lambda = -\frac{\Lambda}{8\pi G_N} \quad (7)$$

191 and we implicitly consider this done from now on.

Two dynamically independent equations arise using the metric Eq. (1) in Eq. (5):

$$\frac{8\pi G_N}{3}\rho = \frac{\dot{a}^2 + k}{a^2} = H^2 \left(1 + \frac{k}{\dot{a}^2}\right), \quad \frac{4\pi G_N}{3}(\rho + 3P) = -\frac{\ddot{a}}{a} = qH^2. \quad (8)$$

We can eliminate the strength of the interaction, G_N , solving both these equations for $8\pi G_N/3$, and equating the result to find a relatively simple constraint for the deceleration parameter:

$$q = \frac{1}{2} \left(1 + 3\frac{P}{\rho}\right) \left(1 + \frac{k}{\dot{a}^2}\right). \quad (9)$$

For a spatially flat Universe, $k = 0$, note that in a matter-dominated era where $P/\rho \ll 1$ we have $q \simeq 1/2$; for a radiative Universe where $3P = \rho$ we find $q = 1$; and in a dark energy Universe in which $P = -\rho$ we find $q = -1$. Spatial flatness is equivalent to the assertion that the energy density of the Universe equals the critical density

$$\rho = \rho_{\text{crit}} \equiv \frac{3H^2}{8\pi G_N}. \quad (10)$$

The CMB power spectrum is sensitive to the deceleration parameter and the presence of spatial curvature modifies q . The Planck results [40–42] constrain the effective curvature energy density fraction,

$$\Omega_K \equiv 1 - \rho/\rho_{\text{crit}}, \quad (11)$$

to

$$|\Omega_K| < 0.005. \quad (12)$$

192 This indicates a nearly flat Universe. We will work here within an exactly spatially flat cosmological
193 model, $k = 0$.

As must be the case for any solution of Einstein's equations, Eq. (8) implies that the energy momentum tensor of matter is divergence free:

$$T^{\mu\nu}{}_{;\nu} = 0 \Rightarrow -\frac{\dot{\rho}}{\rho + P} = 3\frac{\dot{a}}{a} = 3H. \quad (13)$$

A dynamical evolution equation for $\rho(t)$ arises once we combine Eq. (13) with Eq. (8), eliminating H . Given an equation of state $P(\rho)$, solutions of this equation describes the dynamical evolution of matter in the Universe. In practice, we evolve the system in both directions in time. On one side, we start in the present era with the energy density fractions fit by Planck data [40],

$$H_0 = 67.74\text{km/s/Mpc}, \quad \Omega_b = 0.05, \quad \Omega_c = 0.26, \quad \Omega_\Lambda = 0.69, \quad (14)$$

194 and integrate backward in time. On the other hand, we start in the QGP era with an equation of state
 195 determined by an ideal gas of SM particles, combined with a perturbative QCD equation of state for
 196 quarks and gluons [38], and integrate forward in time. As the Universe continues to dilute from dark
 197 energy in the future, the cosmic equation of state is becoming well approximated by the de Sitter
 198 inflationary metric which is a special case of FLRW.

199 2. QGP Epoch

200 2.1. Conservation Laws in QGP

201 During the first $\approx 30 \mu\text{sec}$ after the Big Bang, the early Universe is a hot soup that containing the
 202 elementary primordial building blocks of matter [9]. In particular it contained the light quarks which
 203 are now hidden in protons and neutrons. Beyond this there were also electrons, photons, neutrinos,
 204 and massive strange and charm quarks. These interacting particle species were kept in chemical and
 205 thermal equilibrium with one another. Gluons which mediated the color interaction are very abundant
 206 as well. This primordial phase lasted as long as the temperature of the Universe was more than 110,000
 207 times than the expected temperature $T_\odot = 1.36 \text{ keV}$ ($1.58 \times 10^7 \text{ K}$) at the center of the Sun [47].

208 The conditions in the early universe and those created in relativistic collisions of heavy atomic
 209 nuclei differ somewhat: whereas the primordial quark-gluon plasma survives for about $30 \mu\text{sec}$
 210 in the Big Bang, the comparable extreme conditions created in ultra-relativistic nuclear collisions
 211 are extremely short-lived [49] on order of 10^{-23} seconds. As a consequence of the short lifespan of
 212 laboratory QGP in heavy ion collisions, they are not subject to the same weak interaction dynamics
 213 as the characteristic times for weak processes are too lengthy. Therefore our ability to recreate the
 214 conditions of the primordial QGP are limited due to the relativistic explosive disintegration of the
 215 extremely hot dense relativistic 'fireballs' created in modern accelerators. This disparity is seen in
 216 Fig. 7 where the chemical potential of QGP $\mu_q = \mu_B/3$ for various values of entropy-per-baryon s/B
 217 relevant to relativistic particle accelerators are plotted alongside the evolution of the cosmic hadronic
 218 plasma chemical potential. The QGP precipitates hadrons in cosmic fluid at a far higher entropy ratio
 219 than those accessible by terrestrial means and the two manifestations of QGP live far away from each
 220 other on the QCD phase diagram.

221 The work of Fromerth et. al. [109] allows us to parameterize the chemical potentials μ_d , μ_e , and
 222 μ_ν during this epoch as they are the lightest particles in each main thermal category: quarks, charged
 223 leptons, and neutral leptons. The quark chemical potential is determined by the following three
 224 constraints [109]:

1. Electric charge neutrality $Q = 0$, given by

$$Q \equiv \sum_f Q_f n_f(\mu_f, T) = 0 \quad (15)$$

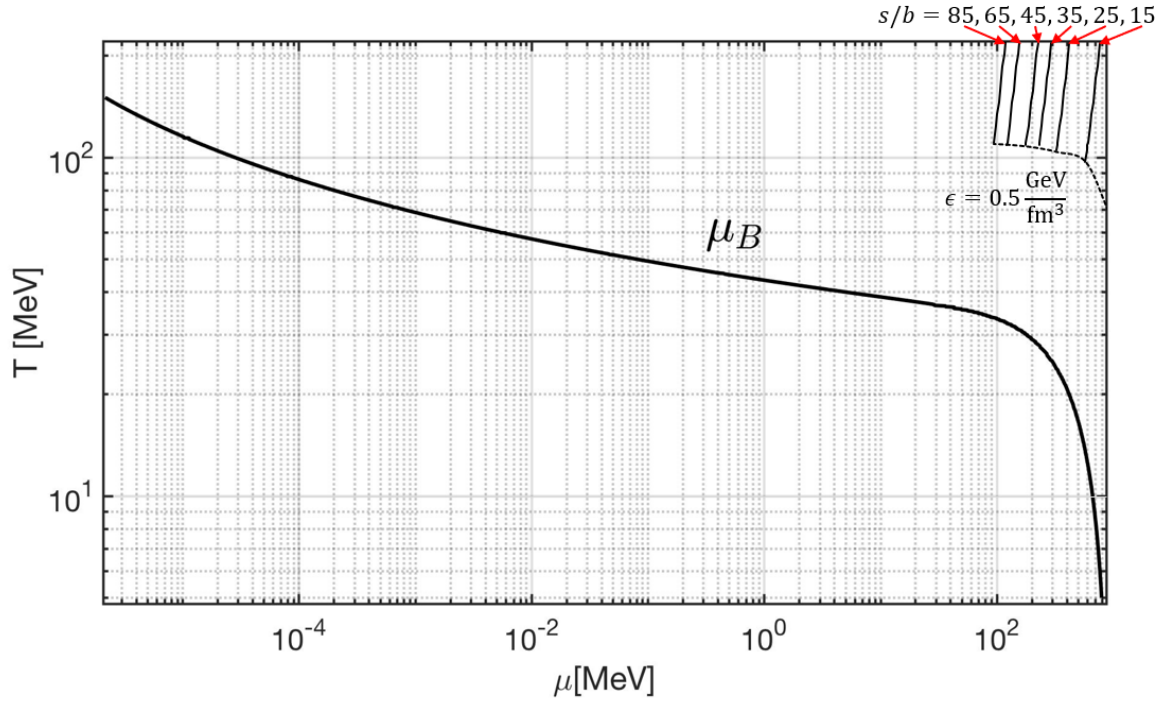


Figure 7. The evolution of the cosmic baryon chemical potential μ_B after hadronization (black line). Curves for QGP (thin black line) created in terrestrial accelerators for differing entropy-per-baryon s/B values are included [19]. The boundary (dashed line) where QGP condenses into hadrons is illustrated at an energy density of $0.5 \text{ GeV}/\text{fm}^3$.

225 where Q_f is the charge and n_f is the numerical density of each species f . Q is a conserved
 226 quantity in the Standard Model under global $U(1)_{EM}$ symmetry. This is summed is over all
 227 particles present in the QGP epoch.

2. Baryon number and lepton number neutrality $B - L = 0$, given by

$$B - L \equiv \sum_f (B_f - L_f) n_f(\mu_f, T) = 0 \quad (16)$$

228 where L_f and B_f are the lepton and baryon number for the given species f . This condition is
 229 phenomenologically motivated by baryogenesis and is exactly conserved in the Standard Model
 230 under global $U(1)_{B-L}$ symmetry. We note many Beyond-Standard-Model (BSM) models also
 231 retain this as an exact symmetry though Majorana neutrinos do not.

3. The entropy-per-baryon ratio s/n_B is a constant and can be written as

$$\frac{s}{n_B} = \frac{\sum_f s_f(\mu_f, T)}{\sum_f B_f n_f(\mu_f, T)} = \text{const} \quad (17)$$

232 where s_f is the entropy density of given species f . As the expanding Universe remains in thermal
 233 equilibrium, the entropy is conserved within a co-moving volume. The baryon number within
 234 a co-moving volume is also conserved. As both quantities dilute with $1/a(t)^3$ within a normal
 235 volume, the ratio of the two is constant. This constraint does not become broken until spatial
 236 inhomogeneities from gravitational attraction becomes significant leading to increases in local
 237 entropy.

At each temperature T , the above three conditions form a system of three coupled, nonlinear equations of the three chosen unknowns (here we have μ_d , μ_e , and μ_ν). In Fig. 8 we present numerical solutions to the conditions Eq. (15)-Eq. (17) and plot the chemical potentials as a function of time. As seen

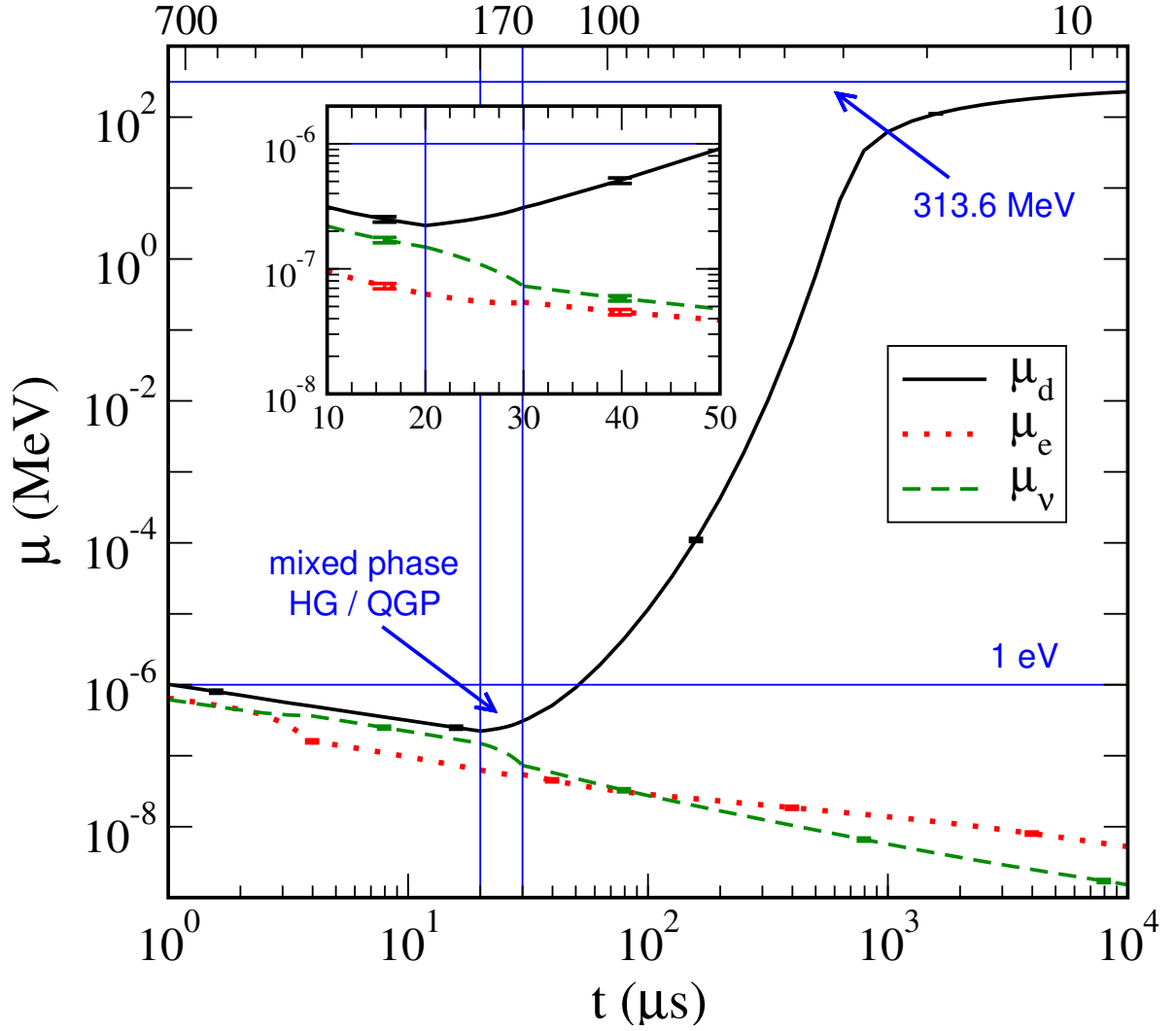


Figure 8. Plot of the down quark chemical potential (black), electron chemical potential (dotted red) and neutrino chemical potential (dashed green) as a function of time. (2003 unpublished, Fromerth & Rafelski) [125]

in the figure, the three potentials are in alignment during the QGP phase until the hadronization epoch where the down quark chemical potential diverges from the leptonic chemical potentials before reaching an asymptotic value at late times. This asymptotic value is given as approximately $1/3$ the mass of the nucleons and represents the confinement of the quarks into the protons and neutrons at the end of hadronization. This asymptotic limit is also shown in Fig. 9 where we present the down quark chemical potential for different values of the entropy-to-baryon ratio. While the s/n_B ratio has large consequences for the plasma at high temperatures, the chemical potential is insensitive to this parameter at low temperatures as it converged to an asymptotic value as the Universe cools. Therefore the entropy to baryon value today greatly controls the quark content when the Universe was very hot. We note that the distribution of quarks in the QGP plasma does not remain fixed to the Fermi-Dirac distribution for thermal and entropic equilibrium. The quark partition function is instead

$$\ln \mathcal{Z}_{\text{quarks}} = \sum_q \ln \left(1 + Y_q(t) e^{-\beta E_q} \right), \quad Y_q(t) = \gamma_q(t) \lambda_q \quad q = u, d, c, s, t, b, \quad (18)$$

238 which is summed over all quarks and their quantum numbers. In Eq. (18), λ_q is the quark fugacity
 239 while $\gamma_q(t)$ is the temporal inhomogeneity of the population distribution [125]. Because of nuclear

240 reactions, these distributions populate and depopulate over time which pulls the gas off entropic
 241 equilibrium while retaining temperature T with the rest of the universe [116]. When $\gamma \neq 1$, the entropy
 242 of the quarks is no longer minimized. As entropy in the cosmic expansion is conserved overall, this
 243 means the entropy gain or loss is then related to the entropy moving into the quarks or its products.

244 In practice, the generalized fugacity is always $\gamma = 1$ during the QGP epoch as the quarks in
 245 early universe remained in both thermal and entropic equilibrium. This is because the Universe's
 246 expansion was many orders of magnitude slower than the process reaction and decay timescales [116].
 247 However near the hadronization temperature, heavy quarks abundance and deviations from chemical
 248 equilibrium have not yet been studied in great detail. We show in [78,79] that the bottom quarks can
 249 deviate from chemical equilibrium $\gamma \neq 1$ by breaking the detailed balance between reactions of the
 quarks.

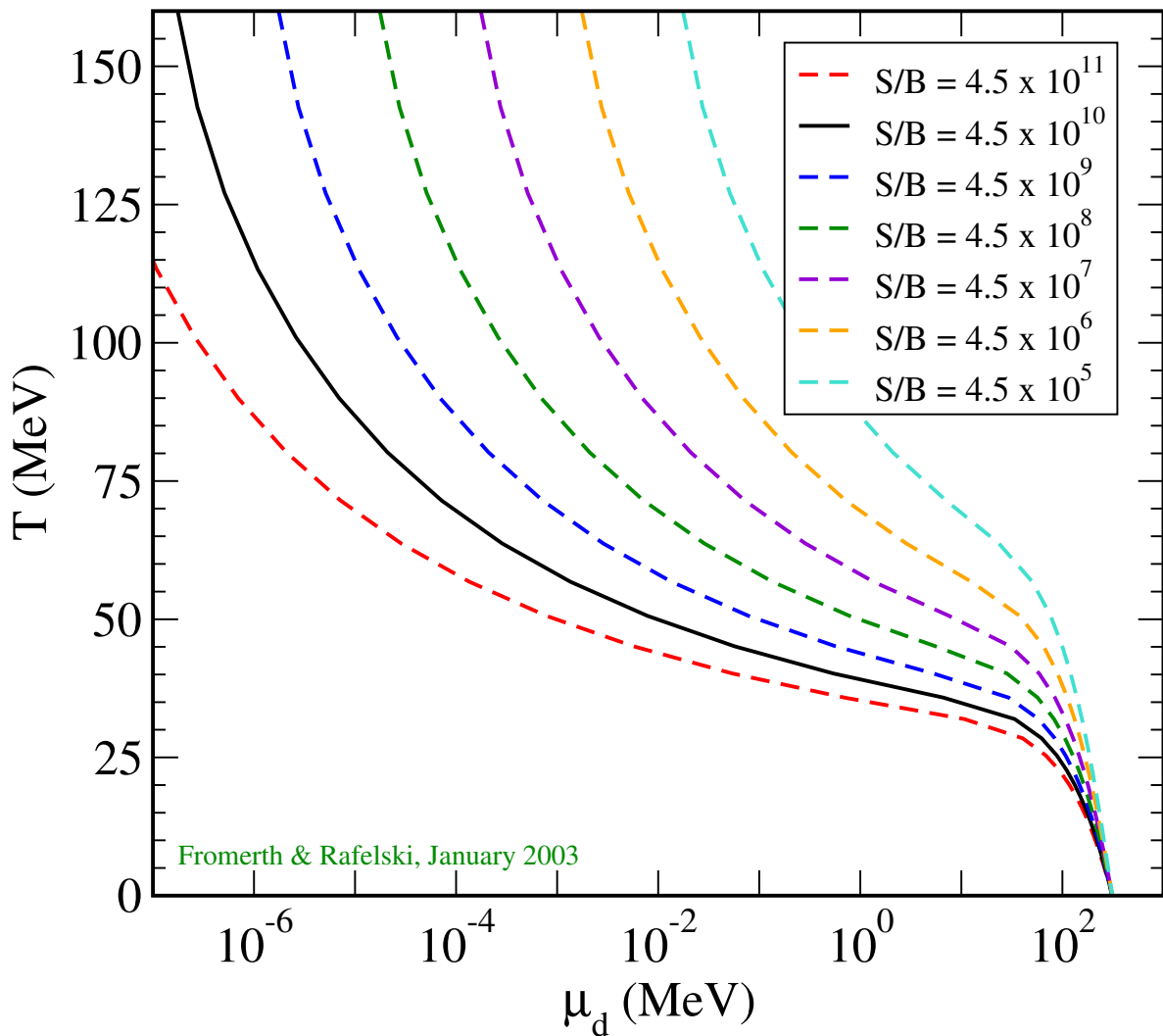


Figure 9. Plot of the down quark chemical potential μ_d as a function of temperature for differing values of entropy-to-baryon S/B ratios. (2003 unpublished, Fromerth & Rafelski) [125]

250

251 2.2. Heavy flavor: bottom and charm in QGP

In the QGP epoch, the up/down are massless quarks and retain the equilibrium via gluon/quark fusion. Strangeness retains the equilibrium via weak, electromagnetic, and strong interaction until $T \sim 12$ MeV [97]. In this section, we focus on the heavy bottom and charm quarks in QGP. In the

primordial QGP, the bottom/charm quarks can be produced via the strong interaction gluon/quark pair fusion processes and disappear via the weak interaction decay. We have

$$q + q \longrightarrow b + \bar{b}, c + \bar{c}, \quad g + g \longrightarrow b + \bar{b}, c + \bar{c} \quad (19)$$

for productions and

$$b \longrightarrow c + l + \nu_l, \quad b \longrightarrow c + q + \bar{q} \quad (20)$$

$$c \longrightarrow s + l + \nu_l, \quad c \longrightarrow s + q + \bar{q} \quad (21)$$

252 for decay. The detail calculation of production and decay rate can be found in [78,79].

In the early Universe within a temperature range $130 \text{ GeV} > T > 150 \text{ MeV}$ we have the following particles: photons, 8_c -gluons, W^\pm, Z^0 , three generations of 3_c -quarks and leptons in the primordial QGP. The Hubble parameter can be written as the sum of particle energy densities ρ_i for each species

$$H^2 = \frac{8\pi G_N}{3} (\rho_\gamma + \rho_{\text{lepton}} + \rho_{\text{quark}} + \rho_{g,W^\pm,Z^0}), \quad (22)$$

253 where G_N is Newton's constant of gravitation. Ultra-relativistic particles (which are effectively
254 massless) and radiation dominate the speed of expansion. The Universe's characteristic expansion
255 time constant $1/H$ is seen in Fig. 10. During QGP, the Hubble time is much larger than the lifespan
256 and production times of the bottom and charm quarks. Therefore, these heavier quark species remain
257 in equilibrium as their processes occur much faster than the expansion of the Universe.

258 In Fig. 10 (on top) we plot the relaxation time for production and decay of charm as a function
259 of temperature. It shows the relaxation time for c-quark production is faster than the c-quark decay
260 in QGP epoch, and both production and decay are faster than the Hubble time $1/H$. The faster
261 gluon/quark pair fusion keeps the charm quark in chemical equilibrium until hadronization. After
262 hadronization, charm quarks form heavy mesons that decay into multi-particles very fast. The Charm
263 disappears from particle inventory once the hadronization is formed.

In Fig. 10 (on bottom) we plot the relaxation time for production and decay of the bottom with different masses as a function of temperature. It shows that both production and decay are faster than the Hubble time $1/H$ and the relaxation time for b-quark production intersects with b-quark decay at different temperatures which depend on the mass of the bottom. This means that the bottom quark decoupling from the primordial plasma is driven by the production process slowing down at low temperature and not being able to keep up with the WI-decay rate of bottom quarks, and Hubble expansion rate is not relevance compare to the decay and production rates. The competition between decay and production reactions requires the study of dynamic bottom abundance in QGP. The dynamic equation of bottom abundance in the early universe can be written as

$$\frac{1}{V} \frac{dN_b}{dt} = (1 - Y_b^2) R_b^{\text{Source}} - Y_b R_b^{\text{Decay}}, \quad (23)$$

where Y_b is the general fugacity of bottom quarks, and R_b^{Source} and R_b^{Decay} are the thermal reaction rates per volume of production and decay of bottom quark, respectively. The bottom source rates are the gluon fusion rate and quark fusion, while the decay rate depends on whether we have free bottom quarks in plasma or they are bounded in the mesons. We study the dynamic equation for bottom abundance and solve the fugacity parameter of the bottom under adiabatic approximation [78,79], we have

$$Y_b = \frac{R_b^{\text{Decay}}}{2R_b^{\text{Source}}} \left[\sqrt{1 + \left(2R_b^{\text{Source}}/R_b^{\text{Decay}}\right)^2} - 1 \right] \quad (24)$$

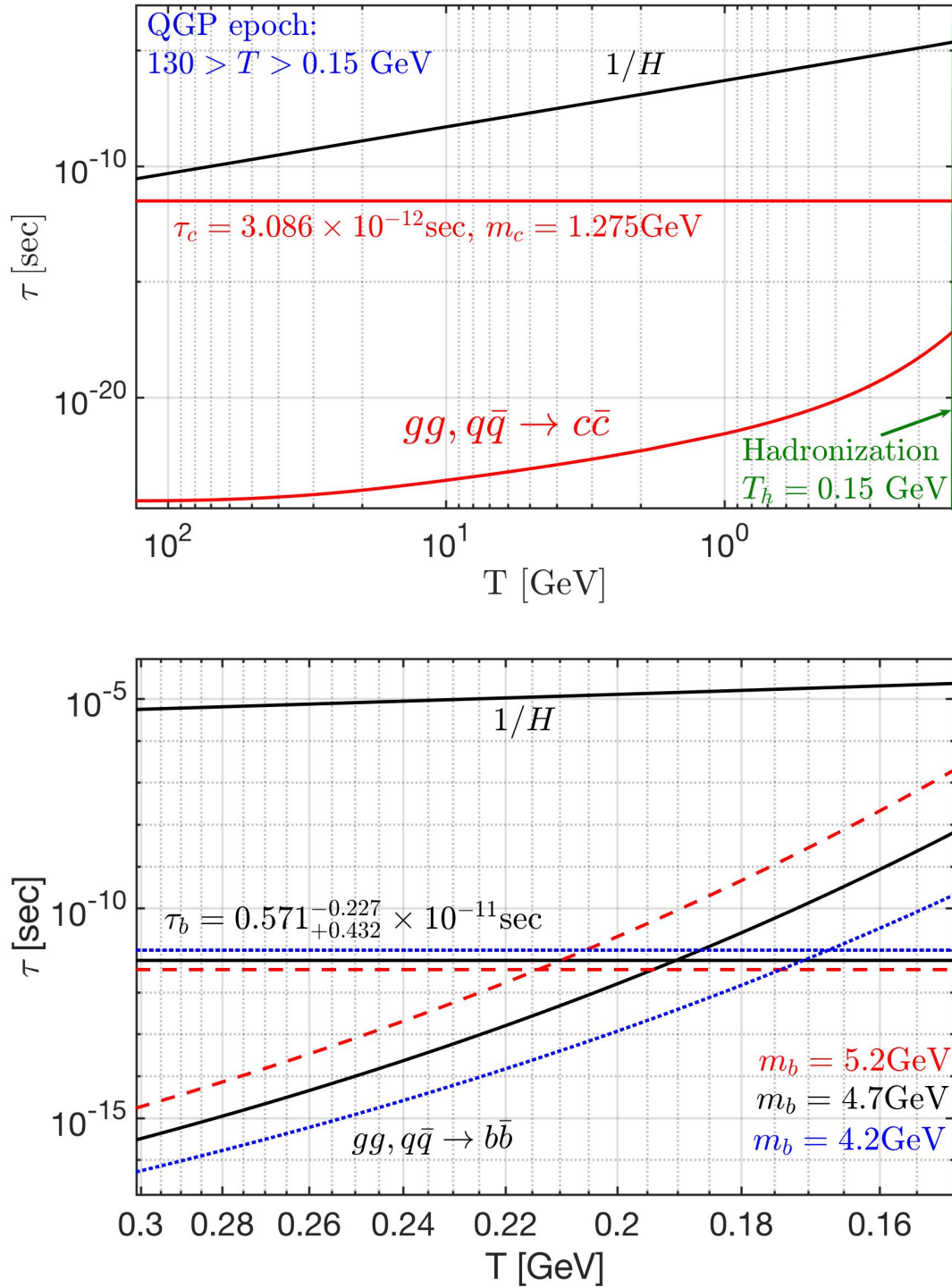


Figure 10. The relaxation time for charm (on top) and bottom (on bottom) production and decay as a function of temperature. On top: it shows that the relaxation time for c-quark production is faster than the c-quark decay in QGP. On bottom: it shows the competition between production and decay, and establishes the temperature era for the abundance non-equilibrium of bottom quarks. For comparison, we also show the Hubble time $1/H$ as a function of temperature.

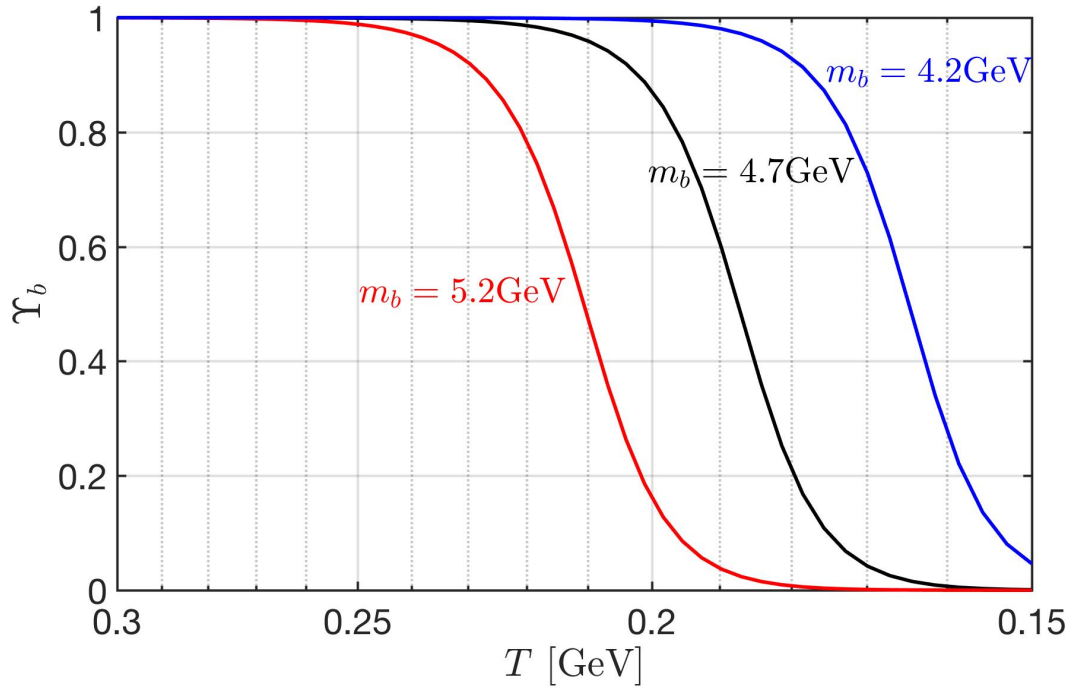


Figure 11. The fugacity of free bottom quark as a function of temperature in the early Universe for $m_b = 4.2\text{GeV}$ (blue), $m_b = 4.7\text{GeV}$ (black), and $m_b = 5.2\text{ GeV}$ (red). The prolonged non-equilibrium happens because the decay and reformation rates of bottom quarks are comparable to each other as the temperature of the universe cools down.

264 In Fig.(11) we show the fugacity of the bottom quarks as a function of temperature $T = 0.3 \sim$
 265 0.15 GeV for different masses of bottom quarks. In all cases, we have prolonged non-equilibrium and
 266 this happens since the decay and reformation rates of bottom quarks are comparable to each other. It
 267 also shows that the smaller mass of the bottom quark slows the strong interaction formation rate to the
 268 value of weak decay near the phase transformation of QGP to HG phase.

269 In this case, the bottom flavor breaks the detail balance and disappearance from particle inventory
 270 during the epoch $T = 0.3 \sim 0.15\text{ GeV}$ which is the essential condition for departure from the
 271 thermal equilibrium. Our results provide a strong motivation to explore the physics of baryon
 272 non-conservation involving the bottom quarks or bottonium mesons in a thermal environment. Given
 273 that the non-equilibrium of bottom flavor arises at a relatively low QGP temperature allows the
 274 possibility for baryogenesis to be occurred in primordial QGP hadronization [78,79]. This result
 275 is of pivotal importance in the QGP study as it establishes the temperature era for the abundance
 276 non-equilibrium of bottom quarks.

277 3. Hadronic Epoch

278 3.1. The Formation of Matter

279 It is in this epoch that the matter of the universe, including all the baryons which make up visible
 280 matter today, was created [125]. Unlike the fundamental particles, such as the quarks or W and Z, the
 281 mass of these hadrons is not due to the Higgs mechanism, but rather from the condensation of the
 282 QCD vacuum [9,17,18]. The quarks from which protons and neutrons are made have a mass more
 283 than 100 times smaller than these nucleons. The dominant matter mass-giving mechanism is popularly
 284 called quark confinement. Light quarks are compressed by the quantum vacuum structure into a small
 285 space domain a hundred times smaller than their natural 'size'. That costs a lot of energy which is

286 the nucleon mass. The remaining few percent of mass are than due to the fact that quarks also have
 287 inertial mass provided by the Higgs mechanism as well as the electromagnetic mass for particles with
 288 charge. At a temperature of $T_h \approx 150$ MeV the quarks and gluons became confined condensing into the
 289 hadrons (both baryons and mesons). During this period, the number of baryon-antibaryon pairs was
 290 sufficiently high that the asymmetry (of 1 in 10^9) would be essentially invisible until a temperature of
 291 between 40 – 50 MeV. We note that CPT symmetry is protected by the lack of asymmetry in normal
 292 SM reactions to some large factor by the accumulation of scattering events. CPT is similarly restricted
 293 by the mass difference in the Kaons via the difference in strange-antistrange masses.

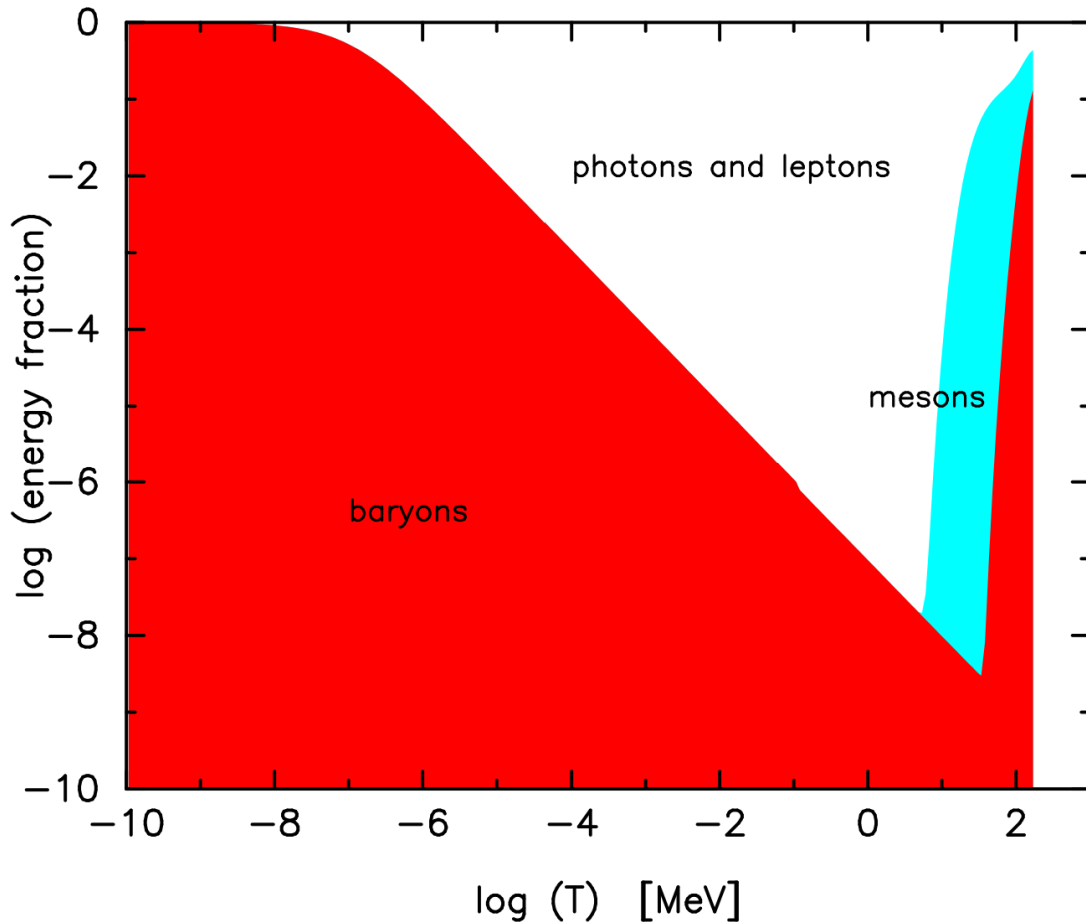


Figure 12. The hadronic content of the luminous Universe as a function of temperature. This figure is a zoom into the right side of Fig. 3. (2003 unpublished, Fromerth & Rafelski) [125]

294 In Fig. 12, we present the fraction of visible radiation and matter split between the baryons,
 295 mesons, and light and leptons. For a brief period in the early Universe, the hadrons contribution to the
 296 energy density of the universe dwarfed that of radiation and leptons [125]. This circumstance would
 297 not be true again until the late universe after recombination though by that point dark matter would
 298 become the dominant form of matter in the cosmos.

The chemical potential of baryons can be determined by the conserved baryon-per-entropy ratio in adiabatic universe expansion. Considering the net baryon density in early Universe with temperature range $150 \text{ MeV} > T > 5 \text{ MeV}$ [97]:

$$\begin{aligned} \frac{(n_B - n_{\bar{B}})}{s} &= \frac{1}{s} [(n_p - n_{\bar{p}}) + (n_n - n_{\bar{n}}) + (n_Y - n_{\bar{Y}})] \\ &= \frac{45}{2\pi^4 g_*^s} \sinh \left[\frac{\mu_B}{T} \right] F_N \left[1 + \frac{F_Y}{F_N} \sqrt{\frac{1 + e^{-\mu_B/T} F_Y/F_K}{1 + e^{\mu_B/T} F_Y/F_K}} \right]. \end{aligned} \quad (25)$$

where we employ the phase-space function F_i for sets of nucleon N , kaon K , and hyperon Y particles defined in Ref. [116], Section 11.4.

$$F_N = \sum_{N_i} g_{N_i} W(m_{N_i}/T), \quad N_i = n, p, \Delta(1232), \quad (26)$$

$$F_K = \sum_{K_i} g_{K_i} W(m_{K_i}/T), \quad K_i = K^0, \bar{K}^0, K^\pm, K^* (892), \quad (27)$$

$$F_Y = \sum_{Y_i} g_{Y_i} W(m_{Y_i}/T), \quad Y_i = \Lambda, \Sigma^0, \Sigma^\pm, \Sigma(1385), \quad (28)$$

where g_{N_i, K_i, Y_i} are the degenerate factors, $W(x) = x^2 K_2^B(x)$ with K_2^B is the modified Bessel functions of integer order "2". The baryon-per-entropy ratio can be obtained from present-day measurement of $(n_B - n_{\bar{B}})/n_\gamma$, and we obtain: [97]:

$$\frac{n_B - n_{\bar{B}}}{s} = \left. \frac{n_B - n_{\bar{B}}}{s} \right|_{t_0} = (0.865 \pm 0.008) \times 10^{-10}, \quad (29)$$

299 The value can be obtained by given $(n_B - n_{\bar{B}})/n_\gamma = (0.609 \pm 0.06) \times 10^{-9}$, as well as the entropy per
300 particle for a massless boson $\sigma/n|_{\text{boson}} \approx 3.60$ and massless fermion $\sigma/n|_{\text{fermion}} \approx 4.20$.

301 Considering the inventory of the Universe strange mesons and baryons, we have reevaluated
302 the temperature of the baryon disappearance. In Fig. 13 we solve Eq.(25) numerically and plot the
303 baryon(antibaryon) number density as a function of temperature in the range $150 \text{ MeV} > T > 5 \text{ MeV}$.
304 The temperature where antibaryons disappear from the Universe inventory can be defined when the
305 ratio $n_{\bar{B}}/(n_B - n_{\bar{B}}) = 1$. This condition is reached in an expanding Universe at $T = 38.2 \text{ MeV}$ (vertical
306 black dotted line) which is agree with qualitatively results in Ref. [105].

307 The antibaryon disappearance temperature does not depend on the baryon and lepton number
308 neutrality $L = B$, it only depends on the baryon-per-entropy ratio assumed to be constant during
309 Universe evolution. The assumption of comoving baryon number conservation is justified by the
310 wealth of particle physics experiments, and the comoving entropy conservation in an adiabatic evolving
311 Universe is a common assumption.

312 3.2. Cosmological Strangeness Abundance

313 As energy contained in the quark-gluon plasma is used up to create matter and antimatter particles, the
314 high abundance of strange quark pairs present in the plasma is preserved as exotic forms containing
315 strange particles. After hadronization, both charm quarks and strange quarks can form heavy mesons.
316 With time strangeness and charmness decays as they are heavier than the usual quarks and antiquarks.
317 However, unlike charm which disappears from the particle inventory quickly, strangeness can still
318 persist [97] in the Universe until $T \approx \mathcal{O}(10 \text{ MeV})$.

We illustrate this by considering an unstable strange particle S decaying into two particles 1 and 2 which themselves have no strangeness content. In a dense and high-temperature plasma with particles

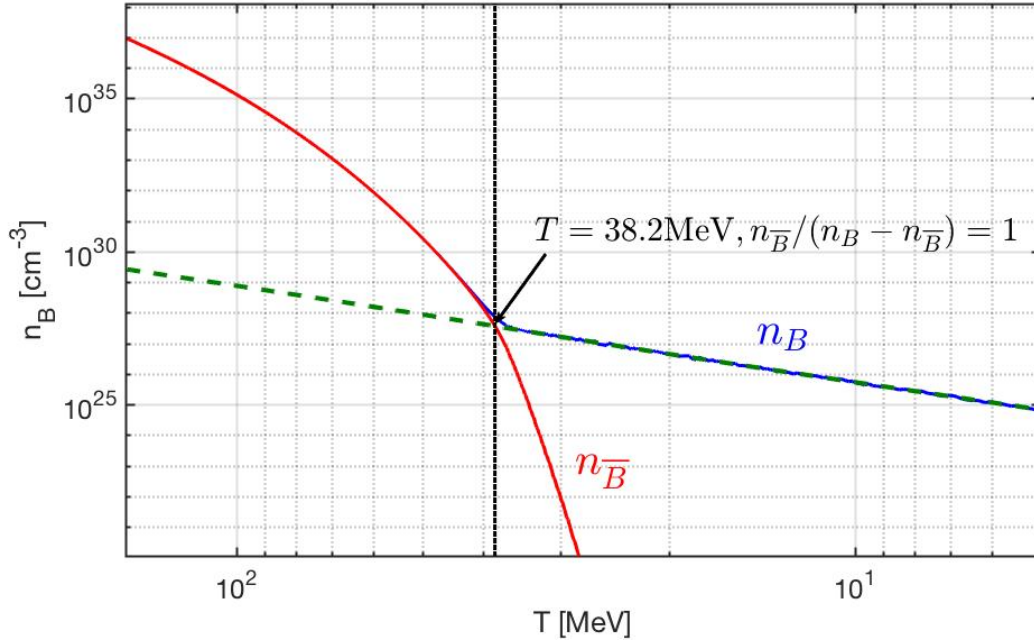
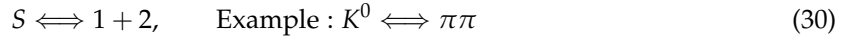


Figure 13. The baryon(antibaryon) number density as a function of temperature in the range $150 \text{ MeV} > T > 5 \text{ MeV}$. The blue solid line is the baryon density, the red solid line is the antibaryon density. The black dotted line represents $T = 38.2 \text{ MeV}$ when the ratio $n_{\bar{B}}/(n_B - n_{\bar{B}}) = 1$ which define the condition where $n_{\bar{B}}$ disappear from the Universe. The temperature we reevaluated is agree with the results in Ref. [105]

1 and 2 in thermal equilibrium, the inverse reaction populates the system with particle S . This is written schematically as



The natural decay of the particles concerned provides also the intrinsic strength of the inverse, strangeness production reaction. As long as both decay and production reactions are possible, particle S abundance remains in thermal equilibrium. This balance between production and decay rates is called detailed balance. The thermal reaction rate per time and volume for two body-to-one particle reactions $1 + 2 \rightarrow 3$ has been presented before [114,115]. In full kinetic and chemical equilibrium, the reaction rate per time per volume is given by [115] :

$$R_{12 \rightarrow 3} = \frac{g_3}{(2\pi)^2} \frac{m_3}{\tau_3^0} \int_0^\infty \frac{p_3^2 dp_3}{E_3} \frac{e^{E_3/T}}{e^{E_3/T} \pm 1} \Phi(p_3), \quad (31)$$

where τ_3^0 is the vacuum lifetime of particle 3. The positive sign “+” is for the case when particle 3 is a boson, and negative sign “-” for fermion. The function $\Phi(p_3)$ for the non-relativistic limit $m_3 \gg p_3, T$ can be written as

$$\Phi(p_3 \rightarrow 0) = 2 \frac{1}{(e^{E_1/T} \pm 1)(e^{E_2/T} \pm 1)}. \quad (32)$$

319 When the back reactions are faster than the Universe expansion, which condition(s) we
 320 characterize in the following, we can explore the Universe composition assuming both kinetic and
 321 particle abundance equilibrium (chemical equilibrium). In Fig. 14 we solve the chemical potential

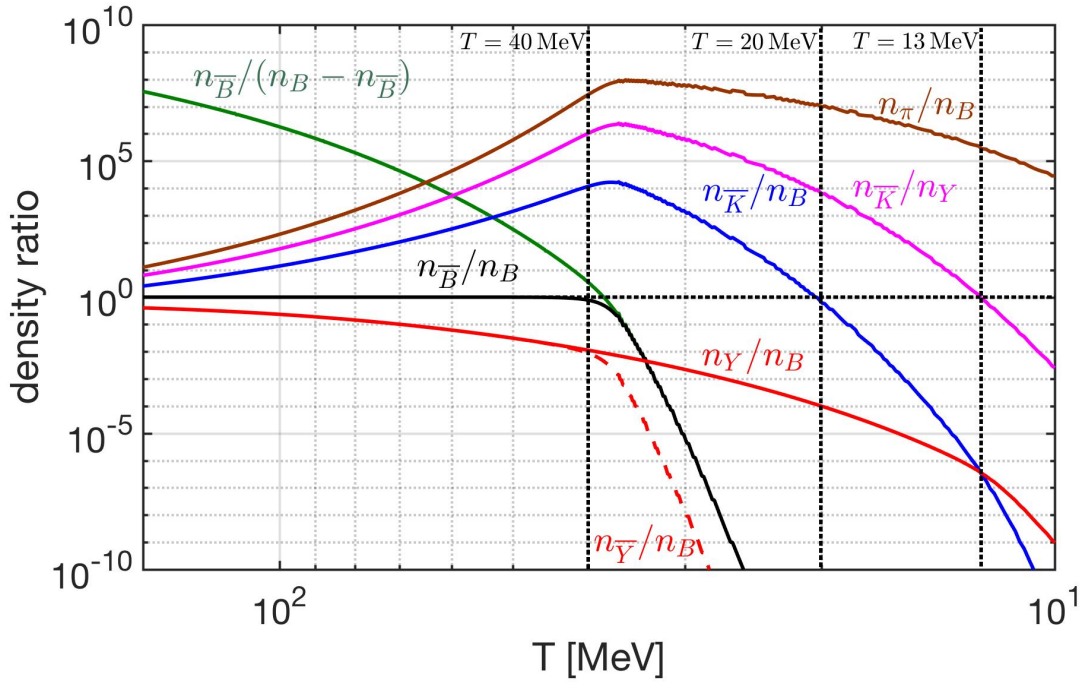


Figure 14. Ratios of hadronic particle number densities as a function of temperature $150 \text{ MeV} > T > 10 \text{ MeV}$ in the early Universe with baryon B yields: pions π (brown line), kaons $K(q\bar{s})$ (blue), antibaryon \bar{B} (black), hyperon Y (red) and anti-hyperons \bar{Y} (dashed red). Also shown \bar{K}/Y (purple).

322 of strangeness numerically and show the chemical equilibrium particle abundance ratios of the
 323 composition of hadronic Universe [97]. We have

- 324 • In the temperature range $150 \text{ MeV} > T > 40 \text{ MeV}$ the Universe is rich in physics phenomena
 325 involving strange mesons, (anti)baryons including (anti)hyperon abundances. Pions $\pi(q\bar{q})$ are
 326 the most abundant hadrons because of their low mass and the inverse decay reaction $\gamma\gamma \rightarrow \pi^0$,
 327 which assures chemical equilibrium [114]. It is important to realize that hadrons always are a
 328 part of the evolving Universe, a point not much discussed in literature.
- 329 • For temperature $150 \text{ MeV} > T > 20 \text{ MeV}$ the Universe is meson-dominant and the strangeness
 330 is dominantly present in the meson sector with $s = \bar{s}$. For temperature $T < 20 \text{ MeV}$, the Universe
 331 becomes baryon-dominant. Below temperature $T < 13 \text{ MeV}$, strangeness is present dominantly
 332 in hyperons, we have $(s - \bar{s}) \neq 0$.

333 In Fig. 15 we shows important source reactions for strange quark abundance in baryons and mesons,
 334 considering both open and hidden strangeness ($s\bar{s}$ -content). The important reactions are $l^- + l^+ \rightarrow \phi$,
 335 $\rho + \pi \rightarrow \phi$, $\pi + \pi \rightarrow K_S$, $\Lambda \leftrightarrow \pi + N$, and $\mu^\pm + \nu \rightarrow K^\pm$. Muons and pions are coupled through
 336 electromagnetic reactions $\mu^+ + \mu^- \leftrightarrow \gamma + \gamma$ and $\pi^0 \leftrightarrow \gamma + \gamma$ to the photon background and retain
 337 their chemical equilibrium respectively [113,114]. The large $\phi \leftrightarrow K + K$ rate assures ϕ and K are in
 338 relative chemical equilibrium. Once the primordial Universe expansion rate, given as the inverse of
 339 the Hubble parameter $1/H$, overwhelms the strongly temperature-dependent back-reaction, the decay
 340 $S \rightarrow 1 + 2$ occurs out of balance and particle S disappears from the Universe. In order to determine
 341 where exactly strangeness disappears from the Universe inventory we explore the magnitudes of a
 342 relatively large number of different rates of production and decay processes, and compare these with
 343 the Hubble time constant [97]. We have

- 344 • **Strangeness in meson era:** The relevant interaction rates competing with Hubble time involving
 345 strongly interacting mesons are the reactions $\pi + \pi \leftrightarrow K$, $\mu^\pm + \nu \rightarrow K^\pm$, $l^+ + l^- \rightarrow \phi$, $\rho + \pi \leftrightarrow \phi$,
 346 and $\pi + \pi \leftrightarrow \rho$. These relaxation time τ are compared with Hubble time in Fig. 16. In Table 1

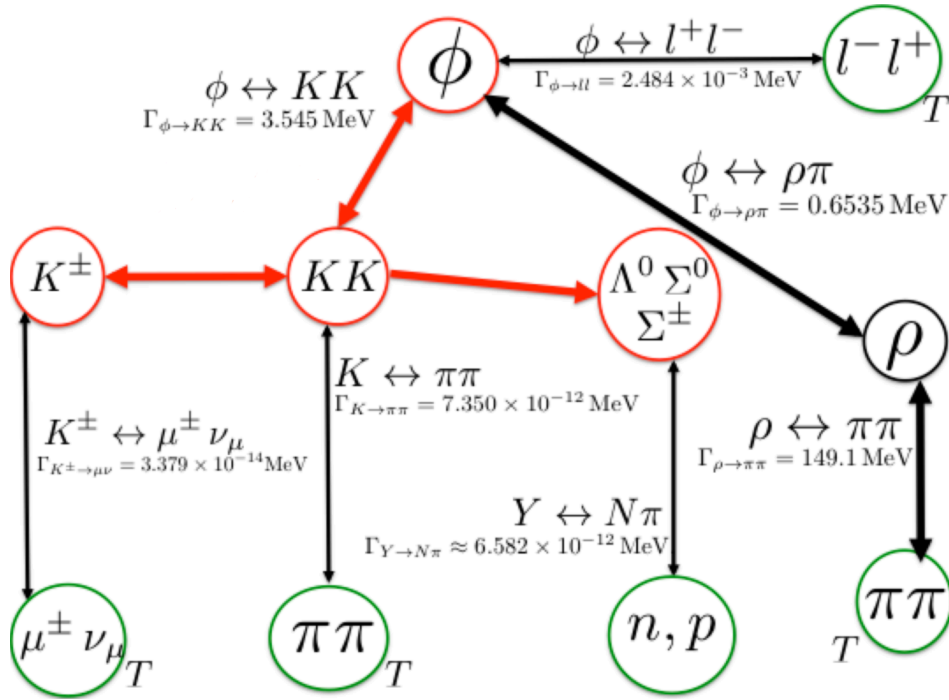


Figure 15. The strangeness abundance of changing reactions in the primordial Universe. The red circles show strangeness carrying hadronic particles; red thick lines denote effectively instantaneous reactions. Black thick lines show relatively strong hadronic reactions.

Table 1. The characteristic strangeness reaction and their freezeout temperature and temperature width in early Universe.

Reactions	Freezeout Temperature (MeV)	ΔT_f (MeV)
$\mu^\pm \nu \rightarrow K^\pm$	$T_f = 33.8 \text{ MeV}$	3.5 MeV
$e^+ e^- \rightarrow \phi$	$T_f = 24.9 \text{ MeV}$	0.6 MeV
$\mu^+ \mu^- \rightarrow \phi$	$T_f = 23.5 \text{ MeV}$	0.6 MeV
$\pi\pi \rightarrow K$	$T_f = 19.8 \text{ MeV}$	1.2 MeV
$\pi\pi \rightarrow \rho$	$T_f = 12.3 \text{ MeV}$	0.2 MeV

347 we show the characteristic strangeness reactions and their freezeout temperatures in the early
348 Universe.

349 It shows that once the reactions freezeout from the cosmic plasma, the corresponding detailed
350 balance is broken and the inverse decay reactions are acting like a "hole" in the strangeness
351 abundance "pot". The first freezeout reaction is the weak interaction $\mu^\pm + \nu_\mu \rightarrow K^\pm$ at $T_f^{K^\pm} =$
352 33.8 MeV , and followed by the electromagnetic process $l^- + l^+ \rightarrow \phi$ at $T_f^\phi = 23 \sim 25 \text{ MeV}$. At
353 $T_f^K = 19.8 \text{ MeV}$ the hadronic reaction $\pi + \pi \rightarrow K$ becomes slower than the Hubble expansion.
354 The reactions $\gamma + \gamma \rightarrow \pi$ and $\rho + \pi \leftrightarrow \phi$ are faster compared to $1/H$. However, the $\rho \rightarrow \pi + \pi$
355 lifetime (black dashed line in Fig. 16) is faster than the reaction $\rho + \pi \leftrightarrow \phi$; Hence most of
356 ρ -meson decays faster and cannot contribute to the strangeness creation in the meson sector.
357 Below the temperature $T < 20 \text{ MeV}$, all the detail balances in the strange meson reactions are
358 broken and the strangeness in the meson sector should disappear rapidly, were it not for the
359 small number of baryons present in the Universe.

360 • **Strangeness in hyperons era:** In order to understand strangeness in hyperons, we evaluated the
361 reaction $\pi + N \rightarrow K + \Lambda$, the strangeness exchange reaction $\bar{K} + N \rightarrow \Lambda + \pi$, and the strangeness
362 decay $\Lambda \rightarrow N + \pi$, in detail. The general form for thermal reaction rate per volume is discussed
363 in [116] (Eq.(17.16), Chapter 17). In Fig. 17 we saw that for $T < 20 \text{ MeV}$, the reactions for the

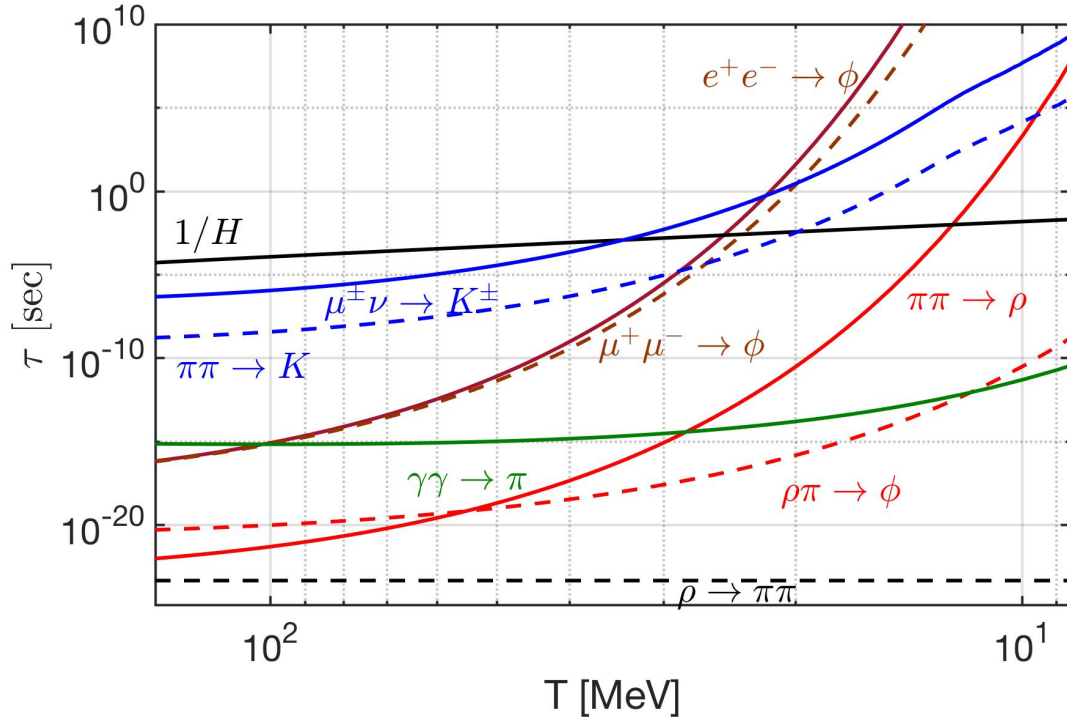


Figure 16. The hadronic relaxation reaction times in meson sector as a function of temperature T , are compared to Hubble time $1/H$ (black solid line). At the bottom, the horizontal black-dashed line is the natural (vacuum) lifespan of ρ .

364 hyperon Λ production is dominated by $\bar{K} + N \leftrightarrow \Lambda + \pi$. Both strangeness and anti-strangeness
 365 disappear from the Universe via the reactions $\Lambda \rightarrow N + \pi$ and $K \rightarrow \pi + \pi$, keeping the $s = \bar{s}$.
 366 Beginning with $T = 12.9$ MeV, the dominant reaction is $\Lambda \leftrightarrow N + \pi$, which shows that at a lower
 367 temperature we still have (very little) strangeness remnant in the Λ . In this case, the strangeness
 368 abundance becomes asymmetric and we have $s \gg \bar{s}$ in the early Universe. Hence, strange
 369 hyperons and anti hyperons could enter into dynamic nonequilibrium condition including
 370 $\langle s - \bar{s} \rangle \neq 0$.

371 The primary conclusion of the study of strangeness production and content in the early Universe,
 372 following on QGP hadronization, is that the relevant temperature domains indicate a complex interplay
 373 between baryon and meson (strange and non-strange) abundances and non-trivial decoupling from
 374 equilibrium for strange and non-strange mesons.

375 3.3. Pion Abundance in the Early Universe

376 In early universe, the π^0 vacuum life span $\tau_{\pi^0}^0 = (8.4 \pm 0.6) \times 10^{-17}$ sec is rather short compare to the
 377 Hubble expansion time $1/H = (10^{-3} \sim 10^{-4})$ sec. In this case, one is tempted to presume that the
 378 decay process dominates and π^0 disappears in early Universe. However, there must be a detailed
 379 balance in the thermal bath: the production process in a suitable environment must be able to form π^0
 380 with strength corresponding to the decay process lifespan.

In general, π^0 in the QED plasma is produced predominantly in the thermal two-photon fusion:

$$\gamma + \gamma \rightarrow \pi^0. \quad (33)$$

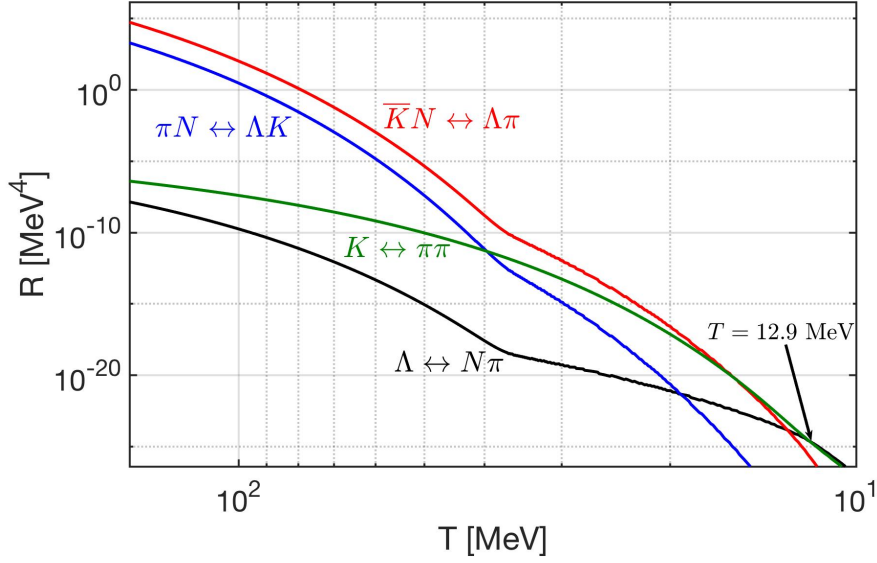


Figure 17. Thermal reaction rate R per volume and time for important hadronic strangeness production and exchange processes as a function of temperature $150 \text{ MeV} > T > 10 \text{ MeV}$ in the early Universe.

These formation processes are the inverse of the decay process of π^0 . The smallness of the electron-formation of π^0 is characterized by the small branching ratio in π^0 decay $B = \Gamma_{ee}/\Gamma_{\gamma\gamma} = 6.2 \pm 0.5 \times 10^{-8}$. For π^\pm can be produced in $\pi^0\pi^0$ charge exchange scattering:

$$\pi^0 + \pi^0 \rightarrow \pi^+ + \pi^-, \quad \gamma + \gamma \rightarrow \pi^+ + \pi^-, \quad e^+ + e^- \rightarrow \pi^+ + \pi^-. \quad (34)$$

We find that for π^\pm production, the last two processes are much slower compared to the first, in case that π^0 density is near chemical equilibrium. The general form for invariant production rates and relaxation time is discussed in paper [114], we have for $\gamma\gamma \rightarrow \pi^0$

$$R_{\gamma\gamma \rightarrow \pi^0} = \int \frac{d^3 p_\pi}{(2\pi)^3 2E_\pi} \int \frac{d^3 p_{2\gamma}}{(2\pi)^3 2E_{2\gamma}} \int \frac{d^3 p_{1\gamma}}{(2\pi)^3 2E_{1\gamma}} (2\pi)^4 \delta^4(p_{1\gamma} + p_{2\gamma} - p_\pi) \times \sum_{spin} |\langle p_{1\gamma} p_{2\gamma} | M | p_\pi \rangle|^2 f_\pi(p_\pi) f_\gamma(p_{1\gamma}) f_\gamma(p_{2\gamma}) Y_\gamma^{-2} Y_{\pi^0}^{-1} e^{u \cdot p_\pi / T}. \quad (35)$$

where Y_i is the fugacity of particle i . For π^\pm production, we have

$$R_{12 \leftrightarrow \pi^+ \pi^-} = \frac{g_1 g_2}{32\pi^4} \frac{T}{1 + I} \int_{s_{th}}^{\infty} ds \sigma(s) \frac{(s - (m_1 + m_2)^2)(s - (m_1 - m_2)^2)}{\sqrt{s}} K_1(\sqrt{s}/T), \quad (36)$$

381 (compared to reference [116] our definition is changed $R_{12 \rightarrow 34} \rightarrow R_{12 \rightarrow 34}/(Y_1 Y_2)$) where m_1 and m_2 ,
382 g_1 and g_2 , Y_1 and Y_2 are masses, degeneracy and fugacities of initial interacting particles.

Fig 18 Fig. 16 discussion only. shows the invariant production rates R of pion for the different processes considered as a function of temperature $T \in [3, 50] \text{ MeV}$. It shows that $\gamma + \gamma \rightarrow \pi^0$ (solid blue line) is the dominant mechanism of π^0 production. The other solid line with dots corresponds to $e^+ + e^- \rightarrow \pi^0$ reaction which in essence remains, in comparison, insignificant. Its importance follows from the fact that it provides the second most dominant path to π_0 formation at the lowest temperatures considered. Since the $\gamma + \gamma \rightarrow \pi^0$ is the dominant mechanism of pion production, then we can ask the question: at what temperature in the expanding early Universe does this reaction ‘freeze’ out, that is the π^0 decay overwhelms the production rate and the yield falls away from chemical equilibrium yield. To answer this question, we study the dynamic equation of π^0 which describes

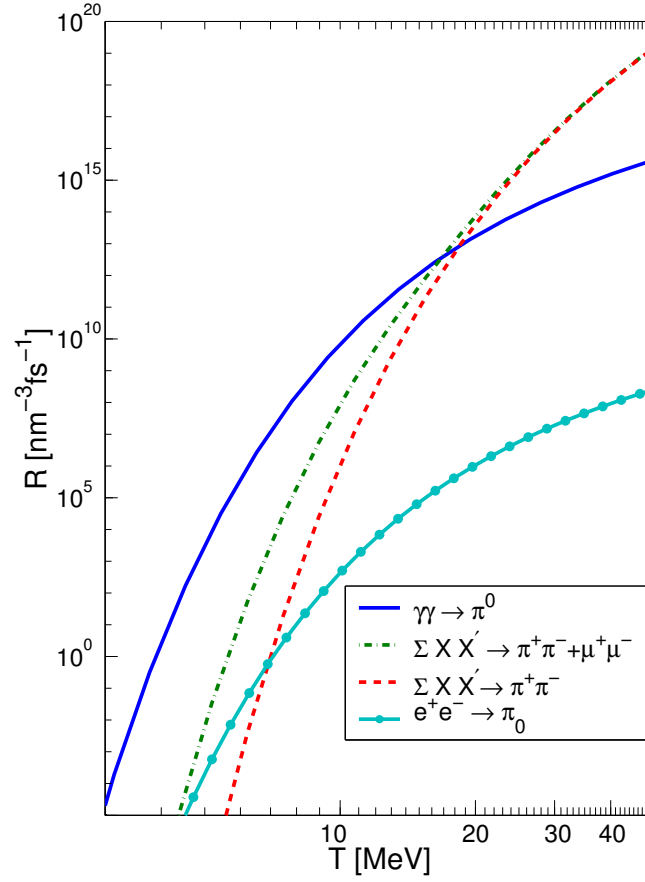


Figure 18. Remove figure. Salvage text? The invariant pion production rates as a function of temperature T . The sum of formation rates of charged pion pairs (dashed, red) by all reactions: $\pi^0 + \pi^0 \rightarrow \pi^+ + \pi^-$, $\gamma + \gamma \rightarrow \pi^+ + \pi^-$, $e^+ + e^- \rightarrow \pi^+ + \pi^-$. We also present the sum of all reactions leading to either a charged pion pair, or muon pair (dot-dashed, green) lines with reactions: $\gamma + \gamma \rightarrow \mu^+ + \mu^-$, $e^+ + e^- \rightarrow \mu^+ + \mu^-$. Figure adapted from [114]

the evolution of π^0 number density in early universe [109]. Omitting all sub-dominant processes, the dynamic equation of π^0 abundance can be written as:

$$\frac{d}{dt} Y_{\pi^0} = \frac{1}{\tau_T} Y_{\pi^0} + \frac{1}{\tau_S} Y_{\pi^0} + \frac{1}{\tau_{\pi^0}} (Y_\gamma^2 - Y_{\pi^0}) \quad (37)$$

where τ_T and τ_S are the kinematic relaxation time for the evolution of the temperature and entropy, and τ_{π^0} is the chemical relaxation time for π^0 . We have

$$\frac{1}{\tau_T} \equiv -T^3 g^* \frac{d(n_\pi / (Y_3 g^* T^3)) / dT}{dn_\pi / dY_3} \dot{T}, \quad \frac{1}{\tau_S} \equiv -\frac{n_\pi / Y_3}{dn_\pi / dY_3} \frac{d \ln(g^* V T^3)}{dT} \dot{T}, \quad \tau_{\pi^0} = \frac{dn_{\pi^0} / dY_{\pi^0}}{R_{\pi^0}} \quad (38)$$

Where n_{π^0} is the number density of pion and we introduced the minus sign above in order to have $\tau_T, \tau_S > 0$. Entropy is conserved in the expanding Universe, and in the radiation-dominated Universe we have $d(T^3 V) / dT = 0$, and hence $1 / \tau_S = 0$. The effect of universe expansion and dilution of number density is described by $1 / \tau_T$. Comparing τ_T to the chemical relaxation time τ_{π^0} can provide the

quantitative condition for freezeout from chemical equilibrium. In the case, of massive pion $m_\pi \gg T$, we have [117]

$$\tau_T \approx \frac{T}{m_\pi H}. \quad (39)$$

383 In Fig.(?) Fig. 16 discussion only. we compare the relaxation time of τ_{π^0} to the Hubble time $1/H$, it
 384 shows that $\tau_{\pi^0} \ll 1/H$. In such a case, the yield of π^0 is expected to be chemical equilibrium. Since
 385 the decay rate is compensated by the production rate, and within 100 the chemical equilibrium yield is
 386 attained even as its thermal number density gradually decreases. This phenomenon can be attributed
 387 to the high population of photons. In such an environment, it remains probable to find high-energy
 388 photons to fuse into π^0 in the early universe.

389 4. Leptonic Epoch

390 4.1. Thermal Degrees of Freedom

The leptonic epoch dominated by photons and both charged and neutral leptons is notable for being the last time where neutrinos played an active role in the Universe's thermal dynamics before decoupling and becoming free-streaming. In the early stage of this plasma after the hadronization era ended $T \approx \mathcal{O}(10 \text{ MeV})$, neutrinos represented the highest energy density followed by the light charged leptons and then finally the photons. The differing energy densities were related by

$$\rho_{e^\pm} \approx \left(2 \times \frac{7}{8}\right) \rho_\gamma, \quad \rho_\nu \approx \left(3 \times \frac{7}{8}\right) \rho_\gamma. \quad (40)$$

391 The reason for this hierarchy is because of the degrees of freedom [124] available in each species in
 392 thermal equilibrium. The factor of $7/8$ arises from the difference in pressure contribution from bosons
 393 versus fermions [124]. While photons only exhibit two helicity degrees of freedom, the charged light
 394 leptons could manifest as both matter (electrons), antimatter (positrons) and as well as two helicities
 395 yielding $2 \times 2 = 4$. The neutral leptons made up of the neutrinos however had three thermally active
 396 species $3 \times 2 = 6$ boosting their energy density in that period to more than any other contribution.
 397 The muon-antimuon energy density was also controlled by its degrees of freedom matching that of e^\pm
 398 until $T \approx 100 \text{ GeV}$ when the heavier lepton no longer satisfied the ultra-relativistic (and thus massless)
 399 limit. This separation of the two lighter charge lepton dynamics is seen in Fig. 3.

400 The measured degrees of freedom also adds a constraint on the question whether neutrinos are
 401 Dirac or Majorana particles. If neutrinos are Dirac-like and have right-handed components, then it is
 402 necessary these fields do not become sufficiently populated thermally during this epoch as it would
 403 drive the neutrino effective degrees of freedom N_{eff}^V away from three. The neutrino degrees of freedom
 404 will be more fully discussed in Sect. 4.5.

405 4.2. Muon Abundance in the Early Universe

406 Muon abundance is an important quantity required for the understanding of several fundamental
 407 questions regarding the properties of the primordial Universe. Our interest in strangeness flavor
 408 freeze-out in the early Universe [97] requires an understanding of the abundance of muons in the
 409 early Universe. The specific question needing an answer is at which temperature muons remain in
 410 abundance (chemical) equilibrium established predominantly by electromagnetic and weak interaction
 411 processes, allowing detailed-balance back-reactions to influence strangeness abundance.

In the cosmic plasma, muons can be produced by the interaction processes

$$\gamma + \gamma \longrightarrow \mu^+ + \mu^-, \quad e^+ + e^- \longrightarrow \mu^+ + \mu^-, \quad (41)$$

$$\pi^- \longrightarrow \mu^- + \bar{\nu}_\mu, \quad \pi^+ \longrightarrow \mu^+ + \nu_\mu. \quad (42)$$

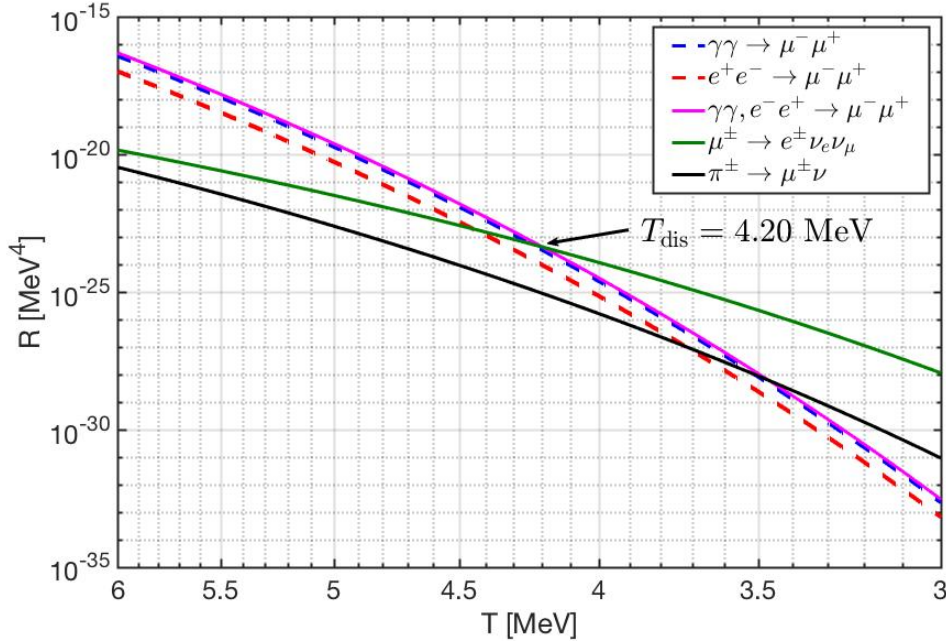


Figure 19. The thermal reaction rate per volume for different reactions as a function of temperature adapted from paper [113]. It shows that dominant reactions for μ^\pm production are $\gamma + \gamma \rightarrow \mu^+ + \mu^-$ and $e^+ + e^- \rightarrow \mu^+ + \mu^-$, and the total production rate cross the decay rate of μ^\pm at temperature $T_{\text{dis}} \approx 4.20$ MeV.

The back reaction for all the above processes is in detailed balance, provided all particles shown on the right-hand side (RHS) exist in chemical abundance equilibrium in the Universe. We recall the vacuum lifetime of pions $\tau_\pi = 2.6033 \times 10^{-8}$ sec. However, all produced muons can decay

$$\mu^- \rightarrow \nu_\mu + e^- + \bar{\nu}_e, \quad \mu^+ \rightarrow \bar{\nu}_\mu + e^+ + \nu_e \quad (43)$$

412 with the vacuum life time $\tau_\mu = 2.197 \times 10^{-6}$ sec.

The scattering angle averaged thermal reaction rate per volume for the reaction $a\bar{a} \rightarrow b\bar{b}$ in Boltzmann approximation is given by [116]

$$R_{a\bar{a} \rightarrow b\bar{b}} = \frac{g_a g_{\bar{a}}}{1 + I} \frac{T}{32\pi^4} \int_{s_{th}}^{\infty} ds \frac{s(s - 4m_a^2)}{\sqrt{s}} \sigma_{a\bar{a} \rightarrow b\bar{b}} K_1(\sqrt{s}/T), \quad (44)$$

where s_{th} is the threshold energy for the reaction, $\sigma_{a\bar{a} \rightarrow b\bar{b}}$ is the cross section for the given reaction, and we introduces the factor $1/1 + I$ to avoid the double counting of indistinguishable pairs of particles, we have $I = 1$ for an identical pair and $I = 0$ for distinguishable pair. Thermal decay rate per volume and time in the Boltzmann limit is [114]

$$R_i = \frac{g_i}{2\pi^2} \left(\frac{T^3}{\tau_i} \right) \left(\frac{m_i}{T} \right)^2 K_1(m_i/T) \quad (45)$$

413 where τ_i is the vacuum lifespan of given particle i . In the paper [113] we evaluate the production and
414 decay rates of muons in the cosmic plasma as a function of temperature. This allows for determining
415 when exactly the muon abundance disappears.

416 In Fig(19) we show the invariant thermal reaction rates per volume and time for the relevant
417 muon reactions. By comparing the production and decay rates we obtain the temperature at which
418 muons disappear from the Universe is $T_{\text{dis}} = 4.20$ MeV.

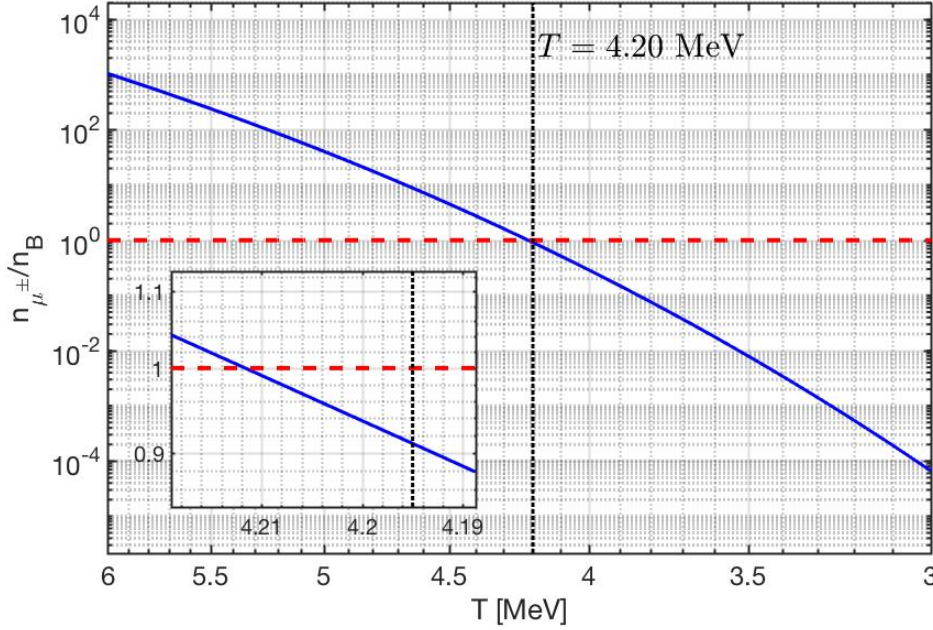


Figure 20. The density ratio between μ^\pm and baryons as a function of temperature. The density ratio at muon disappearance temperature is about $n_{\mu^\pm}/n_B(T_{\text{dis}}) \approx 0.911$.

419 As the temperature decreases in the expanding Universe, the initially dominant production rates
 420 become smaller and cross the decay rates. Muon abundance disappears as soon as any decay rate is
 421 faster than the fastest production rate. Considering the slow speed of the Universe's expansion the
 422 muon disappearance is sudden, the muon abundance thus disappears as soon as a decay rate crosses
 423 the dominant production rate. Specifically, after the Universe cools below the temperature $T_{\text{dis}} = 4.20$
 424 MeV, the dominant reaction is the muon decay.

425 In Fig(20) we show the density ratio at $T = T_{\text{dis}}$ is $n_{\mu^\pm}/n_B \approx 0.91$ [97]. This means that the
 426 muon abundance may still be able to influence baryon evolution because their number density is
 427 comparable to the baryon density. This offers a new and tantalizing model-building opportunity for
 428 baryon-antibaryon separation in the primordial Universe, strangelet formation, and perhaps other
 429 exotic primordial structure formation mechanisms.

430 4.3. Neutrino Masses and Oscillation

Neutrinos are believed to have a small, but nonzero mass due to the phenomenon of flavor oscillation. This is seen in the flux of neutrinos from the Sun, and also in terrestrial reactor experiments. In the Standard Model neutrinos are produced via weak charged current (mediated by the W boson) as flavor eigenstates. If the neutrino was truly massless, then whatever flavor was produced would be immutable as the propagating state. However, if neutrinos have mass, then they propagate through space as their mass-momentum eigenstates. A flavor eigenstate ν^α can be described as a superposition of mass eigenstates ν^k with coefficients given by the Pontecorvo–Maki–Nakagawa–Sakata (PMNS) mixing matrix which both generally complex and unitary. This is given by

$$\nu^\alpha = \sum_k^n U_{\alpha k}^* \nu^k, \quad \alpha = e, \mu, \tau, \quad k = 1, 2, 3, \dots, n \quad (46)$$

where U is the PMNS mixing matrix. The PMNS matrix is the lepton equivalent to the CKM mixing matrix which describes the misalignment between the quark flavors and their masses. The parameter δ is the CP-violating phase which is present when the number of generations is $n \geq 3$. In principle, the

number of mass eigenstates can exceed three, but is restricted to three generations in most models. By standard convention found in the literature we parameterize the rotation matrix U as

$$U = \begin{pmatrix} c_{12}c_{13} & s_{12}c_{13} & s_{13}e^{-i\delta} \\ -s_{12}c_{23} - c_{12}s_{13}s_{23}e^{i\delta} & c_{12}c_{23} - s_{12}s_{13}s_{23}e^{i\delta} & c_{13}s_{23} \\ s_{12}s_{23} - c_{12}s_{13}c_{23}e^{i\delta} & -c_{12}s_{23} - s_{12}s_{13}c_{23}e^{i\delta} & c_{13}c_{23} \end{pmatrix}, \quad (47)$$

4.31 where $c_{ij} = \cos(\theta_{ij})$ and $s_{ij} = \sin(\theta_{ij})$. In this convention, the three mixing angles $(\theta_{12}, \theta_{13}, \theta_{23})$, are
4.32 understood to be the Euler angles for generalized rotations.

Neutrino masses can be written in terms of an effective theory where the mass term contains various couplings between neutrino states determined by some BSM theory. The exact form of such a BSM theory is outside the scope of this work. In modeling the neutrino masses, we have two standard Lagrangian choices. The first is the Dirac mass given by

$$\mathcal{L}_m^{Dirac} = -\bar{\nu}_L^\alpha M_{\alpha\beta}^D \nu_R^\beta + \text{h.c.} \quad (48)$$

which requires both left L and right-handed R neutrinos. Under weak $SU(2)_L$ symmetry, such right-handed neutrinos would be sterile and otherwise not couple to the Standard Model. In general, the mass matrix M can be complex and contains off diagonal elements which arise from coupling between flavors. The PMNS mixing matrix is then responsible for diagonalizing the mass matrix and reorganizing the neutrinos into a new set of basis states. The corresponding Majorana fermion mass term in the flavor basis is then given by

$$\mathcal{L}_m^{Maj.} = -\frac{1}{2}\bar{\nu}_L^\alpha M_{\alpha\beta}^M (\nu_L^\beta)^c + \text{h.c.}, \quad (49)$$

4.33 where $\nu^c = \hat{C}(\bar{\nu})^T$ is the charge conjugate of the neutrino field. The operator $\hat{C} = i\gamma^2\gamma^0$ is the charge
4.34 conjugation operator. A third option is to consider neutrinos with both Dirac and Majorana mass
4.35 Lagrangians. If the masses are generated at some high scale, the See-Saw mechanism ensures that
4.36 the degrees of freedom separate into heavy sterile neutrinos and light nearly massless neutrinos. The
4.37 See-Saw mechanism then provides an explanation for the smallness of the neutrino masses as has been
4.38 experimentally observed. Sterile neutrinos of any mass have not yet been observed despite extensive
4.39 searching. The existence of such neutrinos, if they were ever thermally active in the early cosmos
4.40 would leave fingerprints on the Cosmic Neutrino Background (CNB) spectrum. The presence of an
4.41 abnormally large anomalous magnetic moment for the neutrino would also possibly leave traces in
4.42 the evolution of the early Universe.

The neutrino eigenmasses are generally considered to be small with values no more than 0.1 eV. Because of this, neutrinos produced during fusion within the Sun or radioactive fission in terrestrial reactors on Earth propagate relativistically. Evaluating freely propagating plane waves in the relativistic limit yields the vacuum oscillation probability between flavors ν_α and ν_β written as

$$P_{\alpha\rightarrow\beta} = \left| \sum_j U_{\alpha j}^* U_{\beta j} \exp\left(-i\frac{\Delta m_{kj}^2}{2E}L\right) \right|^2, \quad \Delta m_{kj}^2 \equiv m_k^2 - m_j^2 \quad (50)$$

4.43 where L is the distance traveled by the neutrino between production and detection. The square mass
4.44 difference Δm_{kj}^2 has been experimentally measured [104]. As oscillation only restricts the differences
4.45 in mass squares, the precise values of the masses cannot be determined from oscillation experiments
4.46 alone. It is also unknown under what hierarchical scheme the masses are organized as two of the three
4.47 neutrino eigenmasses are close together in value. If the two lightest neutrinos are close together in
4.48 mass, this is referred to as normal hierarchy, while if the two heaviest neutrinos are close together we
4.49 have an inverted hierarchy. It is important to point out that oscillation does not represent any physical

450 interaction or change in the neutrino during propagation. Rather, for a given production energy, the
 451 superposition of mass eigenstates each have unique momentum and thus unique group velocities.
 452 This mismatch in the wave propagation leads to the oscillatory probability of flavor detection as a
 453 function of distance.

454 In our work on neutrino freezeout [110], we did not consider oscillations during the freezeout
 455 period. We expect though that incorporating oscillations into the freezeout calculation would yield a
 456 smaller freezeout temperature difference between neutrino flavors as oscillation provides a mechanism
 457 in which the heavier flavors remain thermally active despite their direct production becoming
 458 shutdown. In work by Mangano et. al. [120], neutrino freezeout including flavour oscillations
 459 is shown to be a negligible effect.

460 4.4. Neutrino freezeout in early Universe

461 The relic neutrino background is believed to be a well-preserved probe of a Universe only a second old.
 462 The properties of the neutrino background are influenced by the details of the freeze-out or decoupling
 463 process at a temperature $T = \mathcal{O}(1 \text{ MeV})$. In general, The freeze-out process, whereby a particle species
 464 stops interacting and decouples from the photon background, involves several steps that lead to the
 465 final form of the free-streaming momentum distribution. We outline the freezeout properties, including
 466 what distinguishes it from the equilibrium distributions as follow[110]:

- Chemical freeze-out of a particle species occurs at the temperature, T_{ch} , when particle number changing processes slow down and the particle abundance can no longer be maintained at an equilibrium level. Prior to the chemical freeze-out temperature, number changing processes are significant and keep the particle in chemical (and thermal) equilibrium, implying that the distribution function has the Fermi-Dirac form, obtained by maximizing entropy at fixed energy

$$f_c(t, E) = \frac{1}{\exp(E/T) + 1}, \text{ for } T(t) > T_{ch}. \quad (51)$$

- Kinetic freeze-out occurs at the temperature, T_f , when momentum exchanging interactions no longer occur rapidly enough to maintain an equilibrium momentum distribution. When $T_f < T(t) < T_{ch}$, the number-changing process no longer occurs rapidly enough to keep the distribution in chemical equilibrium but there is still sufficient momentum exchange to keep the distribution in thermal equilibrium. The distribution function is therefore obtained by maximizing entropy, with fixed energy, particle number, and antiparticle number separately, implying that the distribution function has the form

$$f_k(t, E) = \frac{1}{Y^{-1} \exp(E/T) + 1}, \text{ for } T_f < T(t) < T_{ch}. \quad (52)$$

The fugacity

$$Y(t) \equiv e^{\sigma(t)} \quad (53)$$

467 controls the occupancy of phase space and is necessary once $T(t) < T_{ch}$ in order to conserve
 468 particle number. See [110] for a detailed discussion of its significance.

- For $T(t) < T_f$ there are no longer any significant interactions that couple the particle species of interest and so they begin to free-stream through the Universe, i.e. travel on geodesics without scattering. The Einstein Vlasov equation can be solved, see [112], to yield the free-streaming momentum distribution

$$f(t, E) = \frac{1}{Y^{-1} e^{\sqrt{p^2/T^2 + m^2/T_f^2}} + 1} \quad (54)$$

where the free-streaming effective temperature

$$T(t) = \frac{T_f a(t_k)}{a(t)} \quad (55)$$

is obtained by redshifting the temperature at kinetic freeze-out. The corresponding free-streaming energy density, pressure, and number densities are given by

$$\rho = \frac{d}{2\pi^2} \int_0^\infty \frac{(m^2 + p^2)^{1/2} p^2 dp}{Y^{-1} e^{\sqrt{p^2/T^2 + m^2/T_f^2} + 1}}, \quad (56)$$

$$P = \frac{d}{6\pi^2} \int_0^\infty \frac{(m^2 + p^2)^{-1/2} p^4 dp}{Y^{-1} e^{\sqrt{p^2/T^2 + m^2/T_f^2} + 1}}, \quad (57)$$

$$n = \frac{d}{2\pi^2} \int_0^\infty \frac{p^2 dp}{Y^{-1} e^{\sqrt{p^2/T^2 + m^2/T_f^2} + 1}}, \quad (58)$$

469 where d is the degeneracy of the particle species. These differ from the corresponding expressions
 470 for an equilibrium distribution in Minkowski space by the replacement $m \rightarrow mT(t)/T_f$ *only* in
 471 the exponential.

472 The separation of the freeze-out process into these three regimes is of course only an approximation.
 473 In principle, there is a smooth transition between them. However, it is a very useful approximation in
 474 cosmology. See [111,120] for methods capable of resolving these smooth transitions.

To estimate the freezeout temperature we need to solve the Boltzmann equation with different types of collision terms. In paper [103] we detail a new method for analytically simplifying the collision integrals and show that the neutrino freezeout temperature which is in turn controlled by the standard model (SM) of particle physics parameters. The freezeout temperature depends only on the magnitude of the Weinberg angle in the form $\sin^2 \theta_W$, and a dimensionless relative interaction strength parameter η ,

$$\eta \equiv M_p m_e^3 G_F^2, \quad M_p^2 \equiv \frac{1}{8\pi G_N}, \quad (59)$$

a combination of the electron mass m_e , Newton constant G_N , and the Fermi constant G_F . The dimensionless interaction strength parameter η with the vacuum present-day value is given by

$$\eta_0 \equiv M_p m_e^3 G_F^2 \Big|_0 = 0.04421. \quad (60)$$

475 The magnitude of $\sin^2 \theta_W$ is not fixed within the SM and could be subject to variation as a function
 476 of time or temperature. In Fig.(21) we show the dependence of neutrino freezeout temperatures for
 477 ν_e and $\nu_{\mu,\tau}$ on SM model parameters $\sin^2 \theta_W$ and η in detail. The impact of SM parameter values on
 478 neutrino freeze-out and the discussion of the implications and connections of this work to other areas
 479 of physics, namely Big Bang Nucleosynthesis and dark radiation can be found in detail in [103].

480 After neutrinos freezeout, the neutrino comoving entropy is independently conserved. However,
 481 the presence of electron-positron rich plasma until $T = 20$ keV provides the reaction $\gamma\gamma \rightarrow e^- e^+ \rightarrow \nu\bar{\nu}$
 482 to occur even after neutrinos decouple from the cosmic plasma. This suggests the small amount of e^\pm
 483 entropy can still transfer to neutrinos until temperature $T = 20$ keV and can modify free streaming
 484 distribution and the effective number of neutrinos.

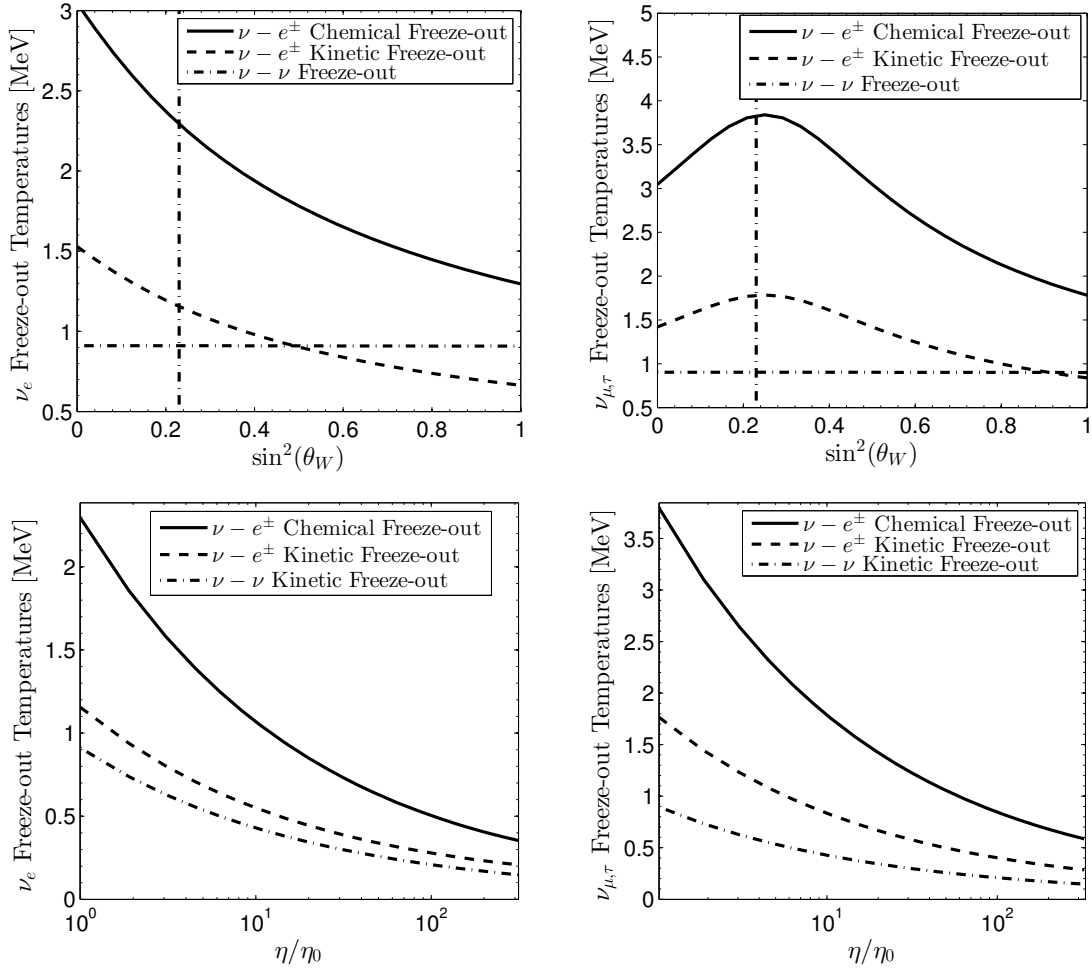


Figure 21. Freeze-out temperatures for electron neutrinos (left) and μ, τ neutrinos (right) for the three types of processes adapted from paper [103]. Top panels as functions of $\sin^2 \theta_W$ for $\eta = \eta_0$, the vertical line is $\sin^2 \theta_W = 0.23$; bottom panels as a function of relative change in interaction strength η/η_0 obtained for $\sin^2 \theta_W = 0.23$. Figure reprinted from our earlier work [103].

4.5. Effective Number of Neutrinos

The population of each flavor of neutrino is not a fixed quantity throughout the evolution of the Universe. In the earlier hot Universe, the population of neutrinos is controlled thermally and to maximize entropy, each flavor is equally filled. As the expansion factor $a(t)$ is radiation dominated for much of this period (see Fig. 3), the CMB is ultimately sensitive to the total energy density within the neutrino sector (which is sometimes referred to as the “dark radiation” contribution). This is described by the effective number of neutrinos N_ν^{eff} and captures the number of relativistic degrees of freedom.

$$N_\nu^{\text{eff}} \equiv \frac{\rho_\nu^{\text{tot}}}{\frac{7\pi^2}{120} \left(\frac{4}{11}\right)^{4/3} T_\gamma^4}, \quad (61)$$

where ρ_ν^{tot} is the total energy density in neutrinos and T_γ is the photon temperature. N_ν^{eff} is defined such that three neutrino flavors with zero participation of neutrinos in reheating during e^+e^- annihilation results in $N_\nu^{\text{eff}} = 3$. The factor of $(4/11)^{1/3}$ relates the photon temperature to the (effective) temperature of the free-streaming neutrinos after e^\pm annihilation, under the assumption of zero neutrino reheating.

Naively speaking, this number should take on the value near $N_\nu^{\text{eff}} \approx 3$, which fits within the Planck result of $N_{\nu, \text{exp}}^{\text{eff}} = 2.99 \pm 0.17$ [42]. This number in the Λ -CDM model is expected to deviate

slightly to a value of $N_{\nu, \Lambda\text{CDM}}^{\text{eff}} = 3.046$ due to an overpopulation of the ν_e electron-neutrino flavor during BBN in the production of the light elements. We also note that this number is subject to change from a more accurate assessment of lithium and tritium production, neutrino masses, as well as neutrino production from the positron disappearance event shortly after BBN. Low energy bound-state electron-positron (positronium) decay into neutrinos is suppressed as m_ν^2/m_e^2 [122,123] but may be enhanced by neutrino anomalous magnetic moment. This situation however does not describe the disappearance of the positrons which was a “hot” scattering process where the $e^+e^- \rightarrow \gamma\gamma$ amplitude outpaced the reverse $\gamma\gamma \rightarrow e^+e^-$ production process as the Universe cooled. With that in mind, the neutrino anomalous moment contribution to neutrino degrees of freedom in e^\pm epoch should be explored. The neutrino degrees of freedom are also sensitive to the presence of sterile neutrinos which is a common feature of many BSM models. We note that the Planck result is not well constrained and thus an important place to look for deviations away from standard model results.

The currently accepted theoretical value is $N_{\text{eff}} = 3.046$, after including the slight effect of neutrino reheating. The favored value of N_{eff} can be found by fitting to CMB data. In 2013 the Planck collaboration found $N_{\text{eff}} = 3.36 \pm 0.34$ (CMB only) and $N_{\text{eff}} = 3.62 \pm 0.25$ (CMB and H0). As N_{eff} is only a measure of the relativistic energy density leading up to photon decoupling, a natural alternative mechanism for obtaining $N_{\text{eff}} > 3$ is the introduction of additional, presently not discovered, weakly interacting massless particles [32,35–37] The explanations of the tension in N_{eff} has already inspired various theories, including the consideration of:

- Neutrino freezeout condition and N_ν^{eff} :
A precise study of the neutrino decoupling condition can provide precise predictions of N_ν^{eff} . A lot of studies focus on improving the calculation of decoupling, including: 1.) model in which the temperature of neutrino decoupling was a variable standard model of particle physics parameters [103], 2.) The entropy transfer from electron-positron annihilation and finite temperature correction at neutrino decoupling [29,118,119], 3.) Neutrino decoupling with flavor oscillations [120,121], provide precise predictions. 4.) Nonstandard neutrino interactions have been investigated, including neutrino electromagnetic [54–59] and nonstandard neutrino electron coupling [54]
- QGP as the possible source contribute to N_ν^{eff} :
The natural concordance of the reported CMB range of N_ν^{eff} with the range of QGP hadronization temperatures, motivates the exploration of a connection between N_ν^{eff} and the decoupling of sterile particles at and below the QGP phase transition[129]. It shows that $N_\nu^{\text{eff}} > 3.05$ can be associated with the appearance of several light particles at QGP hadronization in the early Universe that either is weakly interacting in the entire space or is allowed to interact only inside the deconfined domain, in which case their coupling would be strong. Such particles could leave a clear experimental signature in relativistic heavy ion experiments that produce the deconfined QGP phase.
- Connection between lepton asymmetry L and N_ν^{eff} :
In the current standard cosmological model, an asymmetry between leptons and anti-leptons $L \equiv [N_L - N_{\bar{L}}]/N_\gamma$ (normalized with the photon number) is in general assumed to be small (nano-scale) so that the net normalized lepton number equals the net baryon number $L = B$ where $B = [N_B - N_{\bar{B}}]/N_\gamma$. Barenboim, Kinney, and Park [126,127] note that the lepton asymmetry of the Universe is one of the most weakly constrained parameters and propose leptogenesis scenarios able to accommodate a large lepton number asymmetry surviving up to this date. The work [128] extend their qualitative discussion of these constraints by quantifying the impact of large lepton asymmetry on Universe expansion and shows that there is another ‘natural’ choice $L \simeq 1$, making the net lepton number and net photon number in the Universe similar.

In summary, the effective number of neutrinos N_ν^{eff} is a characterization of the relativistic energy content in the early Universe and independent of its source. Thus, even given a the noninteger number

541 of neutrino degrees of freedom N_V^{eff} reported experimentally, there would still remain ambiguity in
 542 regard the origin of the effect.

543 5. Electron-Positron Epoch

544 The electron-positron epoch of the early Universe was home to several significant events
 545 which have greatly shaped our contemporary Universe including neutrino decoupling, Big Bang
 546 Nucleosynthesis (BBN), the annihilation of most electrons and positrons partially re-ionizing the
 547 Universe, as well as setting the stage for the eventual recombination period which would generate
 548 the cosmic microwave background (CMB). Therefore, correctly describing the dynamics of this e^\pm
 549 plasma is of interest when considering modern cosmic mysteries such as the origin of extra-galactic
 550 magnetic fields (EGMF). While most approaches tackle magnetized plasmas from the perspective of
 551 magneto-hydrodynamics (MHD), a primarily classical or semi-classical approach, our perspective is to
 552 demonstrate that fundamental quantum statistical analysis can lead to further insights on the behavior
 553 of magnetized plasmas.

554 The properties of the electron-positron e^\pm plasma in the early Universe has not received
 555 appropriate attention in an era of precision BBN studies [100]. The presence of e^\pm pairs before
 556 and during BBN has been acknowledged by Wang, Bertulani and Balantekin [101] over a decade ago.
 557 This however was before necessary tools were developed to explore the connection between electron
 558 and neutrino plasmas [103,110,120].

559 In Fig. 5 we show that the dense e^\pm plasma in the early Universe under the hypothesis charge
 560 neutrality and entropy conservation as a function of temperature $2\text{ MeV} > T > 10\text{ keV}$ [99]. The
 561 plasma is electron-positron rich, i.e. $n_\pm \gg n_B$ in the early Universe until leptonic annihilation at $T_{\text{split}} =$
 562 20.36 keV . For $T < T_{\text{split}}$ the positron density n_{e^+} decreases dramatically because of annihilation and
 563 the residual electron density becomes equal to the proton density in accordance with charge neutrality
 564 in the Universe as a whole.

565 We can now connect back to the consideration of cosmic magnetic fields as they might have risen
 566 in the environment of early Universe plasmas noting that such primordial magnetic fields would be
 567 lensed through each of the various plasmas that existed when the Universe was far hotter and denser.
 568 As magnetic flux is conserved over co-moving surfaces, we see in Fig. 22 that the primordial relic
 569 field is expected to dilute as $B \propto 1/a(t)^2$. This means the contemporary small bounded values of
 570 $5 \times 10^{-12}\text{ T} > B_{\text{relic}} > 10^{-20}\text{ T}$ (coherent over $\mathcal{O}(1\text{ Mpc})$ distances) may have once represented large
 571 magnetic fields in the early Universe. This is relic magnetic field would then be generated by the last
 572 phase of significant magnetization in the early Universe. This figure is meant to be illustrative and
 573 it is unlikely the magnetization of the Universe would proceed unhindered and unaltered into the
 574 ultra-dense plasma phases of the early Universe. Of particular interest to us is the electron-positron
 575 plasma which existed in the early Universe especially at temperatures $T > 35\text{ keV}$ which was the
 576 last matter(antimatter) plasma in the Universe where the energy its density exceeded that of the
 577 proton/neutron baryon energy density. This dense plasma environment is where BBN occurred and
 578 where similar plasmas can still be found within exotic stars such as magnetars. The contemporary relic
 579 magnetic fields may then be an artifact of this final time of Universe-scale magnetization in a manner
 580 similar to how the CMB is a relic of the time of charge recombination.

581 The Universe is filled with magnetic fields at various scales and strengths both within galaxies
 582 and in deep extra-galactic space far and away from matter sources. Extra-galactic magnetic fields are
 583 not well constrained today, but are required by observation to be non-zero with a magnitude between
 584 $10^{-12}\text{ T} > B_{\text{EGMF}} > 10^{-20}\text{ T}$ over Mpc coherent length scales. The upper bound is constrained from the
 585 characteristics of the CMB while the lower bound is constrained by non-observation of ultra-energetic
 586 photons from blazars. There are generally considered two possible origins for extra-galactic magnetic
 587 fields: (a) matter-induced dynamo processes involving Amperian currents and (b) primordial (or relic)
 588 seed magnetic fields whose origins may go as far back as the Big Bang itself. It is currently unknown
 589 which origin accounts for extra-galactic magnetic fields today or if it some combination of the two

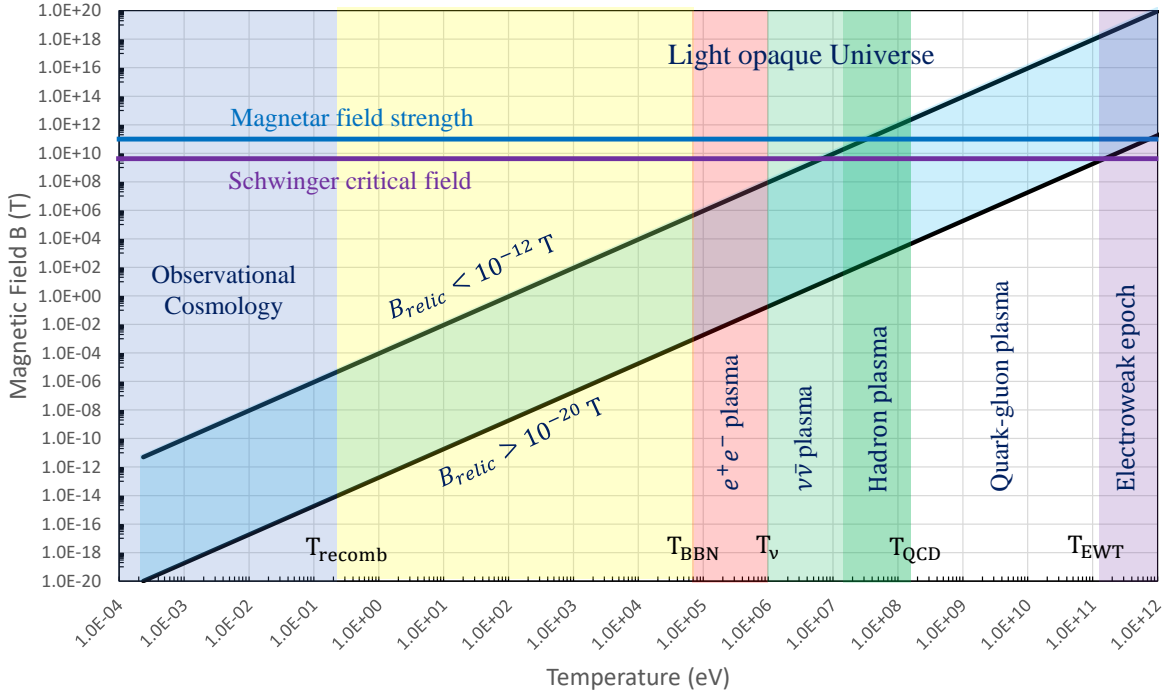


Figure 22. Qualitative value of the primordial magnetic field over the evolutionary lifespan of the Universe. The upper and lower black lines represent extrapolation of the EGMF bounds into the past. The major phases of the universe are indicated with shaded regions. The values of the Schwinger critical field (purple line) and the upper bound of surface magnetar field strength (blue line) are included for scale.

590 models. Even if magnetic fields in the Universe today are primarily driven via amplification through
 591 Amperian matter currents, such models still require primordial seed fields at some point to act as
 592 catalyst.

593 5.1. Electron-Positron Density Compared to Baryons

During the late stages of the e^\pm epoch where BBN occurred, the matter content of the Universe was still mostly dominated by the light charged leptons by many orders of magnitude even though the Hubble parameter was still mostly governed by the radiation behavior of the neutrinos and photons. The temperatures during this epoch were also cool enough that the electrons and positrons could be described non-relativistically to fairly good approximation while also still being as energy dense as the Solar core making it a relatively unique plasma environment not present elsewhere in cosmology. Considering the energy density between non-relativistic e^\pm and baryon, it can be written as

$$\chi \equiv \frac{\rho_e + \rho_{\bar{e}}}{\rho_p + \rho_n} = \frac{m_e(n_e + n_{\bar{e}})}{m_p n_p + m_n n_n} = \frac{m_e(n_e + n_{\bar{e}})}{n_B(m_p X_p + m_n X_n)} = \left(\frac{n_e + n_{\bar{e}}}{n_B}\right) \left(\frac{m_e}{m_p X_p + m_n X_n/2}\right) \quad (62)$$

where we consider all neutrons end up bound in to the ${}^4\text{He}$ after BBN and from particle data group $X_p = n_p/n_B$ and $X_n = n_n/n_B$ and are given by

$$X_p = 0.878, \quad X_n = 0.245 \quad (63)$$

and masses are given by

$$m_e = 0.511 \text{ MeV}, \quad m_p = 938.272 \text{ MeV}, \quad m_n = 939.565 \text{ MeV} \quad (64)$$

594 In Fig. 23 we plot the energy density ratio Eq. (62) as a function of temperature $10 \text{ keV} < T < 200 \text{ keV}$.
 595 It shows that the energy density of electron and positron is dominated until $T = 30.2 \text{ keV}$, i.e., we have
 596 $\rho_e \gg \rho_B$. After $T = 30.2 \text{ keV}$, we have $\rho_e \ll \rho_B$ and ratio becomes constant when is around $T = 20 \text{ keV}$
 597 because of the positron annihilation and charge neutrality.

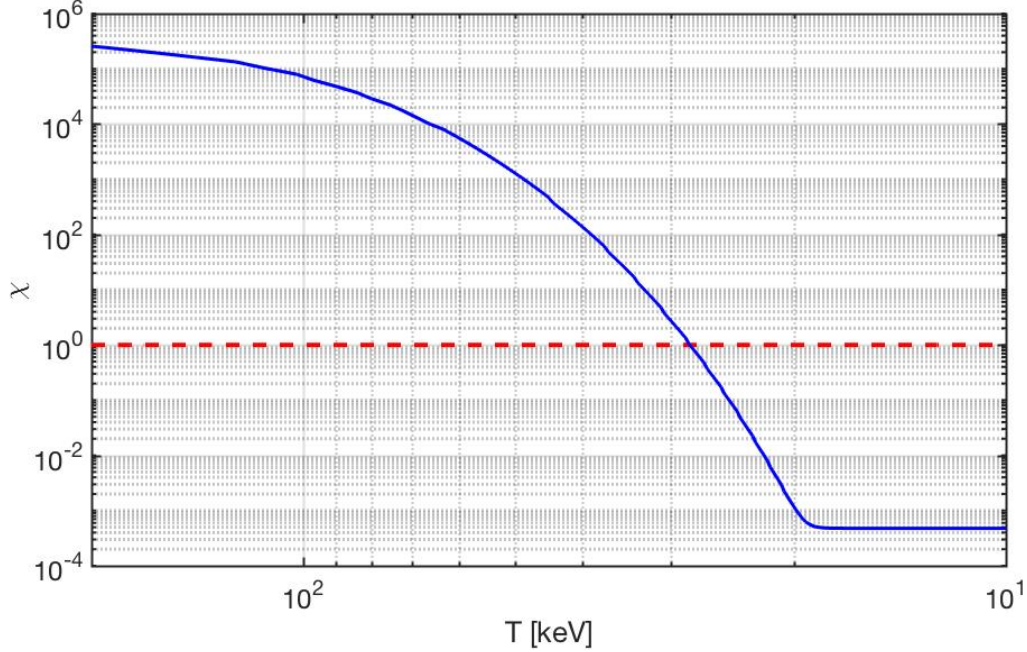


Figure 23. The energy density ratio χ (solid blue line) between e^\pm and baryons as a function of temperature from $10 \text{ keV} < T < 200 \text{ keV}$. The dashed red line represents the point where the baryon density exceeds that of the electron-positron pairs.

598 5.2. Energy Eigenvalues

As a starting point, we consider the energy eigenvalues of charged fermions within a homogeneous magnetic field. Here, we have several choices: We could assume the typical Dirac energy eigenvalues with gyro-magnetic g -factor set to $g = 2$. But as electrons, positrons and most plasma species have anomalous magnetic moments (AMM), we require a more complete model. Another option would be to modify the Dirac equation with a Pauli term, often called the Dirac-Pauli (DP) approach, via

$$\hat{H}_{\text{AMM}} = -a \frac{e}{2m_e} \frac{\sigma_{\mu\nu} F^{\mu\nu}}{2}, \quad (65)$$

where $\sigma_{\mu\nu}$ is the spin tensor proportional to the commutator of the gamma matrices and $F^{\mu\nu}$ is the EM field tensor. For the duration of this work, we will remain in natural units ($\hbar = c = k_B = 1$) unless explicitly stated otherwise. The AMM is defined via g -factor as

$$\frac{g}{2} = 1 + a. \quad (66)$$

This approach, while straightforward, would complicate the energies making analytic understanding and clarity difficult without a clear benefit. Modifying the Dirac equation with Eq. (65) yields the following eigen-energies

$$E_n^s|_{\text{DP}} = \sqrt{\left(\sqrt{m_e^2 + 2eB \left(n + \frac{1}{2} - s \right)} - \frac{eB}{2m} (g-2)s \right)^2 + p_z^2} \quad (67)$$

This model for the electron-positron plasma of the early Universe has been used in work such as Strickland et. al. [106]. Our work here is then in part a companion piece which compares and contrasts the DP model of fermions to our preferred model for the AMM via the Klein-Gordon-Pauli (KGP) equation given by

$$\left((i\partial_\mu - eA_\mu)^2 - m_e^2 - e\frac{g}{2}\frac{\sigma_{\mu\nu}F^{\mu\nu}}{2} \right) \Psi = 0. \quad (68)$$

We wish to emphasize, that each of the three above models (Dirac, DP, KGP) are distinct and have differing physical consequences and are not interchangeable which we explored in the context of hydrogen-like atoms in [107]. Recent work done in [108] discuss the benefits of KGP over other approaches for $g \neq 2$ from a quantum field theory perspective. Exploring the statistical behavior of KGP in a cosmological context can lead to new insights in magnetization which may be distinguished from pure $g = 2$ behavior of the Dirac equation or the *ad hoc* modification imposed by the Pauli term in DP. One major improvement of the KGP approach over the more standard DP approach is that the energies take eigenvalues which are mathematically similar to the Dirac energies. Considering the e^\pm plasma in a uniform magnetic field B pointing along the z -axis, the energy of e^\pm fermions can be written as

$$E_n^s = \sqrt{p_z^2 + \tilde{m}^2 + 2eBn}, \quad \tilde{m}^2 = m_e^2 + eB(1 - gs), \quad s = \pm \frac{1}{2}, \quad n = 0, 1, 2, 3, \dots \quad (69)$$

where n is the principle quantum number for the Landau levels and s is the spin quantum number. Here we introduce a notion of effective mass \tilde{m} which inherits the spin-specific part of the energy adding them to the mass. This convention is also generalizable to further non-minimal electromagnetic models with more exotic energy contributions such that we write a general replacement as

$$m_e^2 \rightarrow \tilde{m}^2(B). \quad (70)$$

This definition also pulls out the ground state Landau energy separating it from the remainder of the Landau tower of states. One restriction is that the effective mass must remain positive definite in our analysis thus we require

$$\tilde{m}^2(B) = m_e^2 + eB(1 - gs) > 0. \quad (71)$$

This condition fails under ultra-strong magnetic fields of order

$$B_{\text{crit}} = \frac{m_e^2}{ea} = \frac{\mathcal{B}_S}{a} \approx 3.8 \times 10^{12} \text{ T}, \quad (72)$$

599 where \mathcal{B}_S is the Schwinger critical field strength. For electrons, this field strength is well above the
600 window of magnetic field strengths of interest during the late e^\pm epoch.

601 5.3. Landau eigen-energies in cosmology

There is another natural scale for the magnetic field besides Eq. (72) when considering the consequences of FLRW expansion on the e^\pm fluid. As the Universe expands, different terms in the energies and thus partition function evolve as a function of the scale factor $a(t)$ which arises in the FLRW metric. We can consider the expansion to be an adiabatic process which results in a smooth shifting of the relevant dynamical quantities. From the conservation of magnetic flux through a co-moving surface, the magnetic field under expansion starting at some initial time t_0 is given by

$$B(t) = B(t_0) \frac{a(t_0)^2}{a(t)^2}. \quad (73)$$

As the Universe expands, the temperature also cools as the cosmological redshift reduces the momenta of particles in the Universe lowering their contribution to the energy content of the Universe. This cosmological redshift is written as

$$p_i(t) = p_i(t_0) \frac{a(t_0)}{a(t)}, \quad T(t) = T(t_0) \frac{a(t_0)}{a(t)}. \quad (74)$$

The momenta scale with the same factor as temperature as it is the origin of cosmological redshift. The energy of massive free particles in the Universe scales differently based on their momentum (and thus temperature). When hot and relativistic, particle energy scales with inverse scale factors like radiation. However as particles transition to non-relativistic momenta, their energies scale with the inverse square of the scale factor like magnetic flux.

$$E(t) = E(t_0) \frac{a(t_0)}{a(t)} \xrightarrow{\text{NR}} E(t_0) \frac{a(t_0)^2}{a(t)^2}. \quad (75)$$

This occurs because of the functional dependence of energy on momentum in the relativistic versus non-relativistic cases. The argument in the Boltzmann statistical factor is given by

$$X_n^s \equiv \frac{E_n^s}{T}. \quad (76)$$

We can explore this relationship for the magnetized system explicitly by writing out Eq. (76) using the KGP eigen-energies as

$$X_n^s = \sqrt{\frac{m_e^2}{T^2} + \frac{p_z^2}{T^2} + \frac{2eB}{T^2} \left(n + \frac{1}{2} - \frac{g^s}{2} \right)}, \quad (77)$$

where we now introduce the expansion scale factor via Eq. (73) - Eq. (74). The Boltzmann factor can then be written as

$$X_n^s[a(t)] = \sqrt{\frac{m_e^2}{T^2(t_0)} \frac{a(t)^2}{a(t_0)^2} + \frac{p_z^2(t_0)}{T^2(t_0)} + \frac{2eB(t_0)}{T^2(t_0)} \left(n + \frac{1}{2} - \frac{g^s}{2} \right)}. \quad (78)$$

This reveals that only the mass contribution is dynamic over cosmological time. For any given eigen-state, the mass term increases driving the state into the non-relativistic limit while the momenta and magnetic contributions are frozen by initial conditions. Following reasoning outlined in [108] and [107] we will proceed without analysis using the eigen-energies provided by the KGP equation in favor over modeling the anomalous magnetic moment as a Pauli term added to the Dirac equation (referred to at the Dirac-Pauli equation). Motivated by Eq. (78), we can introduce a dimensionless cosmic magnetic scale which is frozen in the homogeneous case as

$$b_0 \equiv \frac{eB}{T^2} = \frac{eB\hbar c^2}{(k_B T)^2} \text{ (S.I.)}, \quad (79)$$

where we've included the expression explicitly in full SI units. We can estimate the value of b_0 from the bounds of the extra-galactic magnetic field strength and the temperature of the Universe today. If the origin of deep space extra-galactic magnetic fields are relic fields from the early Universe, which today are expected to exist between $5 \times 10^{-12} \text{ T} > B_{\text{relic}} > 10^{-20} \text{ T}$, then at temperature $T = 2.7 \text{ K}$, the value of the cosmic magnetic scale is between

$$5.5 \times 10^{-5} > b_0 > 1.1 \times 10^{-11}. \quad (80)$$

602 This should remain constant in the Universe at-large up to the last epoch the Universe was sufficiently
 603 magnetized to disturb this value. As the electron-proton plasma which generated the CMB was
 604 relatively dilute over its duration, it was unlikely sufficiently magnetized to significantly alter this
 605 value over extra-galactic scales. Rather, the best candidate plasma to have been sufficiently magnetized
 606 and dense to have set the relic field magnetic scale would have been the electron-positron plasma
 607 which existed during the duration of Big Bang Nucleosynthesis (BBN) and beforehand.

Higher order non-minimal magnetic contributions which can be introduced via Eq. (70) to the eigen-energies like $\approx \mu_B^2 B^2 / T^2$ are even more suppressed over cosmological time which drives the system into minimal electromagnetic coupling with the exception of the anomalous magnetic moment in the KGP eigenenergies. It is interesting to note that cosmological expansion serves to “smooth out” the characteristics of more complex BSM electrodynamics erasing them from a statistical perspective in favor of the minimal or minimal-like dynamics. As b_0 is a constant of expansion, assuming the electron-proton plasma between the CMB and electron-positron annihilation did not greatly disturbed it, we can calculate the remnant values at the temperature $T = 50$ keV with the expression

$$B(T) = \frac{b_0}{e} T^2, \quad (81)$$

yielding a range of field strengths

$$2.3 \times 10^5 \text{ T} > B(T = 50 \text{ keV}) > 4.6 \times 10^{-4} \text{ T}, \quad (82)$$

608 during which the electron-positron plasma in the Universe had a number density comparable to that
 609 of the Solar core with $n_e = 4.49 \times 10^{24} \text{ cm}^{-3}$ at $r = 0.01 R_\odot$.

610 5.4. Electron-positron statistical physics

We now turn our attention now to the statistical behavior of the e^\pm system. We can utilize the general fermion partition function given by [67]

$$\ln \mathcal{Z} = \sum_\alpha \ln \left(1 + e^{-\beta(E-\eta)} \right), \quad (83)$$

where $\beta = 1/T$, α is the set of all quantum numbers in the system, and η is the generalized chemical potential. The magnetized e^\pm system should be considered a system of four quantum species: Particles and anti-particles, and spin aligned and anti-aligned. Taken together we consider a system where all electrons and positrons are spin aligned or anti-aligned with the magnetic field B and the partition function of the system is written as

$$\ln \mathcal{Z}_{tot} = \frac{2eBV}{(2\pi)^2} \sum_\sigma^{\pm 1} \sum_s^{\pm 1/2} \sum_{n=0}^{\infty} \int_0^{\infty} dp_z \left[\ln \left(1 + Y_\sigma^s(x) e^{-\beta E_n^s} \right) \right], \quad (84)$$

$$Y_\sigma^s(x) = \gamma(x) \lambda_\sigma^s, \quad \lambda_\sigma^s = e^{\sigma \eta_e + s \eta_s}, \quad (85)$$

where η_e is the electron chemical potential and η_s is the spin chemical potential for the generalized fugacity λ_σ^s . The parameter $\gamma(x)$ is a spatial field which controls the distribution inhomogeneity of the Fermi gas. Inhomogeneities can arise from the influence of other forces on the gas such as gravitational forces. Deviations of $\gamma \neq 1$ represent configurations of reduced entropy (maximum entropy yields the normal Fermi distribution itself with $\gamma = 1$) without pulling the system off a thermal temperature. This situation is similar to that of the quarks during QGP, but instead here the deviation is spatial rather than in time. This is precisely the kind of behavior that may arise in the e^\pm epoch as the dominant photon thermal bath keeps the Fermi gas in thermal equilibrium while spatial inequilibria could

spontaneously develop. For the remainder of this work, we will retain $\gamma(x) = 1$. The energy E_n^\pm can be written as

$$E_n^\pm = \sqrt{p_z^2 + \tilde{m}_\pm^2 + 2eBn}, \quad \tilde{m}_\pm^2 = m_e^2 + eB \left(1 \mp \frac{\delta}{2}\right), \quad (86)$$

where the \pm script refers to spin aligned and anti-aligned eigenvalues. As the temperature domain we're interested is in the $T = 50$ keV range, we can take a semi-relativistic approach of the electron-positron plasma by considering the partition function obtained in the Boltzmann approximation. In following we considering the case $\eta_s/T \ll 1$ for the first approximation and Boltzmann approximation for non-relativistic electrons and positrons. Using the Euler-Maclaurin formula to replace the sum over Landau levels with an integration yielding

$$\ln \mathcal{Z}_{tot} = \ln \mathcal{Z}_{free} + \ln \mathcal{Z}_B + \ln \mathcal{Z}_R, \quad (87)$$

where we define

$$\ln \mathcal{Z}_{free} = \frac{T^3 V}{2\pi^2} \left[2 \cosh\left(\frac{\eta_e}{T}\right) \right] \sum_{i=\pm} x_i^2 K_2(x_i), \quad (88)$$

$$\ln \mathcal{Z}_B = \frac{eBTV}{2\pi^2} \left[2 \cosh\left(\frac{\eta_e}{T}\right) \right] \sum_{i=\pm} \left[\frac{x_i}{2} K_1(x_i) + \frac{k^2 b_0}{12} K_0(x_i) \right], \quad (89)$$

$$\ln \mathcal{Z}_R = \frac{eBTV}{\pi^2} \left[2 \cosh\left(\frac{\eta_e}{T}\right) \right] R. \quad (90)$$

611 where R is the error remainder which is defined by integrals over Bernoulli polynomials. While
 612 this would require further derivation to demonstrate explicitly, the benefit of the Euler-Maclaurin
 613 approach is if the error contribution remains finite or bound for the magnetized partition function,
 614 then a correspondence between the free Fermi partition function (with noticeably modified effective
 615 mass \tilde{m}_\pm) and the magnetized Fermi partition function can be established. The mismatch between
 616 the summation and integral in the Euler-Maclaurin formula would then encapsulate the immediate
 617 magnetic response and deviation from the free particle phase space. While we label $\ln(\mathcal{Z}_{free})$ in Eq. (88)
 618 as the "free" partition function, this is not strictly true as this contribution to the overall partition
 619 function is a function of the effective mass we defined earlier in Eq. (70). When determining the
 620 magnetization of the quantum Fermi gas, derivatives of the magnetic field B will not fully vanish on
 621 this first term which will resulting in an intrinsic magnetization which is distinct from the contribution
 622 from the ground state and mismatch between the quantized Landau levels and the continuum of the
 623 free momentum. Specifically, this free Fermi contribution represents the magnetization that arises from
 624 the spin magnetic energy rather than orbital contributions.

Assuming the error remainder R is small and can be neglected, we can rewrite Eq. (88) - Eq. (89) obtaining

$$\ln \mathcal{Z}_{tot} = \frac{T^3 V}{2\pi^2} \left[2 \cosh\left(\frac{\eta_e}{T}\right) \right] \sum_{i=\pm} \left\{ x_i^2 K_2(x_i) + \frac{b_0}{2} x_i K_1(x_i) + \frac{b_0^2}{12} K_0(x_i) \right\}. \quad (91)$$

625 Eq. (91) is a surprisingly compact expression containing only tractable functions and will be our
 626 working model for the remainder of the work. Note that the above does not take into consideration
 627 density inhomogeneities and is restricted to the domain where the plasma is well described as a
 628 Maxwell-Boltzmann distribution. With that said, we have not taken the non-relativistic expansion of
 629 the eigen-energies.

630 5.5. Charge neutrality and chemical potential

In this section, we are interested in exploring the chemical potential of dense $e\bar{e}$ plasma in the early Universe under the hypothesis of charge neutrality and entropy conservation. We focus on the temperature interval at the post-BBN temperature range $20 < T < 50\text{keV}$. In this case, the charge neutrality can be written as

$$(n_e - n_{\bar{e}}) = (n_p) = \left(\frac{n_p}{n_B}\right) \left(\frac{n_B}{s_{\gamma,\nu,e}}\right) s_{\gamma,\nu,e} = X_p \left(\frac{n_B}{s_{\gamma,\nu}}\right) s_{\gamma,\nu}, \quad X_p = \frac{n_p}{n_B} \quad (92)$$

631 where n_B is the number density of baryon, and the entropy density is obtained by considering the
 632 contribution of e^\pm in entropy density is negligible compared to the photon and neutrino entropy
 633 density at post-BBN temperature $20 \text{ keV} < T < 50 \text{ keV}$ because the low density $n_e \ll n_{\gamma,\nu}$.

- Since all neutrons end up bound in to the ${}^4\text{He}$ after BBN, then the mass fraction of ${}^4\text{He}$ can be estimated as [104]

$$X_\alpha = \frac{2(n_n/n_p)}{1 + n_n/n_p} = 0.245 \pm 0.03. \quad (93)$$

Solving the ratio n_n/n_p and substituting into the X_p , we obtain

$$X_p = \frac{n_p}{n_B} = \frac{n_p}{n_p + n_n} = \frac{1}{1 + n_n/n_p} = 0.878 \pm 0.015 \quad (94)$$

- Since the comoving baryon number and entropy are conserved, hence the ratio $s_{\gamma,\nu}/n_B$ is conserved, then the entropy per baryon ratio can be written as

$$\left(\frac{s_{\gamma,\nu}}{n_B}\right) = \left(\frac{s_{\gamma,\nu}}{n_B}\right)_{t_0} = \left(\frac{n_\gamma}{n_B}\right)_{t_0} \left(\frac{s_\gamma}{n_\gamma} + \frac{n_\nu s_\nu}{n_\gamma n_\nu}\right) = \left(\frac{n_\gamma}{n_B}\right)_{t_0} \left[3.601 + \frac{9}{4} \left(\frac{T_\nu}{T_\gamma}\right)^3 4.202\right], \quad (95)$$

where the subscript t_0 denotes the present-day value and considers all neutrinos are relativistic particles today. The entropy per particle for a boson is $(s/n)_{\text{boson}} = 3.601$ and for a fermion is $(s/n)_{\text{fermion}} = 4.202$. From particle data group and standard Big Bang model [104,105], we have

$$5.8 \times 10^{-10} < \frac{n_B}{n_\gamma} < 6.5 \times 10^{-10}, \quad \frac{T_\nu}{T_\gamma} = \left(\frac{4}{11}\right)^{1/3}. \quad (96)$$

- The entropy density at temperature can be written as [105]

$$s = \frac{2\pi^2}{45} g_s T_\gamma^3, \quad g_s = \sum_{i=\text{boson}} g_i \left(\frac{T_i}{T_\gamma}\right)^3 + \frac{7}{8} \sum_{i=\text{fermion}} g_i \left(\frac{T_i}{T_\gamma}\right)^3 \quad (97)$$

634 where g_s is the effective degree of freedom that contribute to the entropy density.

On the other hand, given the partition function in Boltzmann limit Eq. (91) the net number density of electron can be written as

$$(n_e - n_{\bar{e}}) = \frac{T}{V} \frac{\partial}{\partial \eta_e} \ln \mathcal{Z}_{\text{tot}} = \frac{T^3}{2\pi^2} [2 \sinh(\eta_e/T)] \sum_{i=\pm} \left[x_i^2 K_2(x_i) + \frac{b_0}{2} x_i K_1(x_i) + \frac{b_0^2}{12} K_0(x_i) \right] \quad (98)$$

Using the charge neutrality Eq.(92) and solving the chemical potential, we obtain:

$$\sinh(\eta_e/T) = \frac{2\pi^2}{2T^3} \frac{X_p(n_B/s_{\gamma,\nu})s_{\gamma,\nu}}{\sum_{i=\pm} \left[x_i^2 K_2(x_i) + \frac{b_0}{2} x_i K_1(x_i) + \frac{b_0^2}{12} K_0(x_i) \right]} \quad (99)$$

$$\rightarrow \frac{2\pi^2 n_p}{2T^3} \frac{X_p(n_B/s_{\gamma,\nu})s_{\gamma,\nu}}{2x^2 K_2(x)}, \quad x = m_e/T, \quad \text{for } b_0 = 0 \quad (100)$$

635 It shows that for the case $b_0 = 0$ the chemical potential agrees with our earlier results [99]. In Fig. 24,
 636 we solve the Eq.(99) numerically and plot the chemical potential as a function of temperature T . It
 637 shows that the chemical potential is not sensitive to the magnetic field because the small value of
 638 $b_0 = 10^{-5} \sim 10^{-11}$ and can be neglected in Eq. (99).

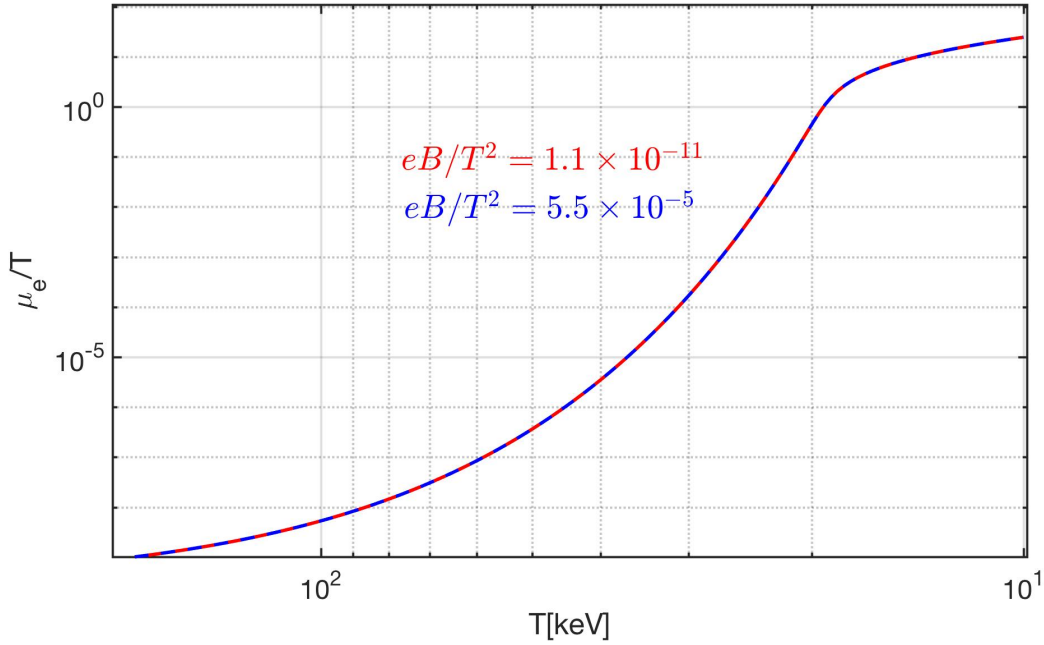


Figure 24. The chemical potential η_e/T a function of temperature $10 < T < 200$ keV. It shows that the chemical potential is not sensitive to the magnetic field b_0 .

639 In Fig. 24, we plot the chemical potential as a function of temperature T . It shows that the chemical
 640 potential is not sensitive to the magnetic field because the small value of $b_0 = 10^{-3} \sim 10^{-8}$ and can be
 641 neglected in Eq. (99).

642 5.6. Magnetization

Given the partition function Eq. (91) the magnetization can be obtained via the definition

$$M = \frac{T}{V} \frac{\partial \ln \mathcal{Z}_{tot}}{\partial B} = \frac{T}{V} \left(\frac{\partial \tilde{m}_{\pm}}{\partial B} \right) \frac{\partial \ln \mathcal{Z}_{tot}}{\partial \tilde{m}_{\pm}} \quad (101)$$

then the magnetization can be written as

$$\left(\frac{M}{B} \right) = \frac{4\pi\alpha}{2\pi^2 b_0} \left[2 \cosh \left(\frac{\eta_e}{T} \right) \right] \sum_{i=\pm} \left\{ \left[\frac{1}{2} - \frac{(1+ig/2)}{2} \left(1 + \frac{b_0^2}{12x_i^2} \right) \right] x_i K_1(x_i) + \left[\frac{1}{6} - \frac{(1+ig/2)}{4} \right] b_0 K_0(x_i) \right\}. \quad (102)$$

643 Substituting the chemical potential Eq.(99) into Eq.(102) we can solve the magnetization M/B
 644 numerically.

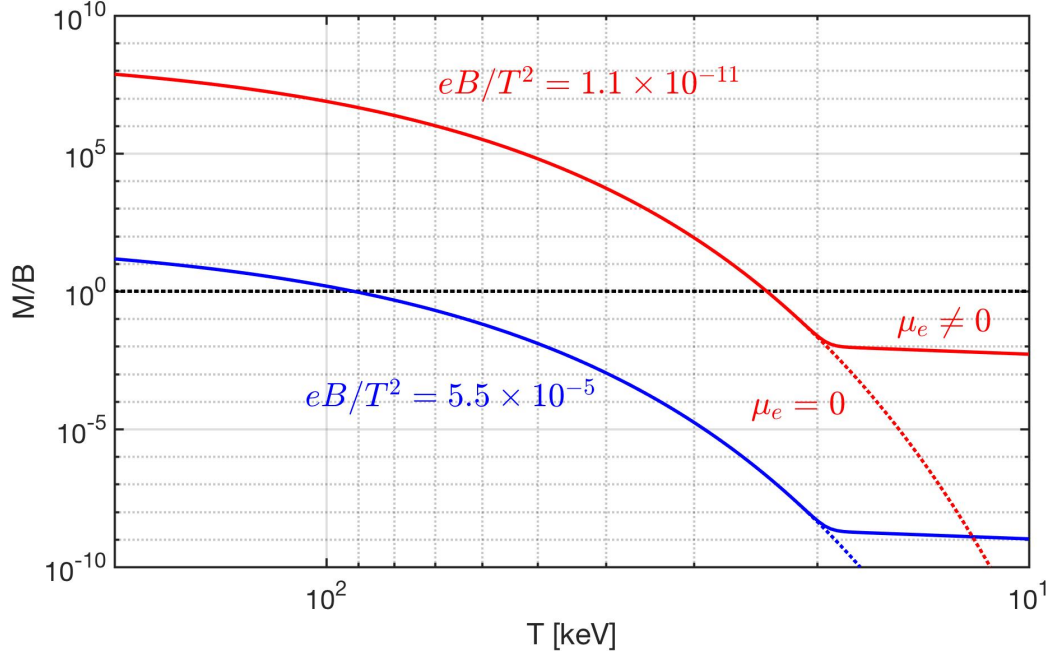


Figure 25. The magnetization M/B as a function of temperature $10 < T < 200$ keV, where the solid line represent the case $\mu_e \neq 0$ and dotted lines label the case $\mu_e = 0$. It shows that for giving b_0 we can find the temperature that $M/B > 1$ in early Universe.

Considering the case $g = 2$ the magnetization becomes

$$\left(\frac{M}{B}\right) = \left(\frac{M}{B}\right)_+ + \left(\frac{M}{B}\right)_- \quad (103)$$

645 where the functions $(M/B)_\pm$ are defined as

- Case1: $\tilde{m}_+ = \sqrt{m_e^2 + 2eB}$, and $x_+ = \tilde{m}_+/T$. The magnetization is given by

$$\left(\frac{M}{B}\right)_+ = -\frac{8\pi\alpha}{2\pi^2} \sqrt{1 + \sinh^2(\eta_e/T)} \left[\left(\frac{1}{2b_0} + \frac{b_0}{12x_+^2}\right) x_+ K_1(x_+) + \frac{1}{3} K_0(x_+) \right] \quad (104)$$

646 Substituting the magnetic field b_0 and proton density n_p/T^3 we can solve the magnetization
 647 and chemical potential numerically. In Fig. ??, we plot the magnetization M/B as a function of
 648 temperature T . It shows for the case1 the magnetization is not sensitive to the magnetic field, this
 649 is because the small value of $b_0 = 10^{-3} \sim 10^{-8}$ and can be neglected in Eq. (??) and Eq. (104).
 650

- Case 2: $\tilde{m}_- = m_e$ and $x = \tilde{m}_-/T$, then the magnetization of electron/ positron becomes

$$\left(\frac{M}{B}\right)_- = \frac{8\pi\alpha}{2\pi^2} \sqrt{1 + \sinh^2(\eta_e/T)} \left(\frac{1}{b_0} x_- K_1(x_-) + \frac{1}{6} K_0(x_-) \right) \quad (105)$$

651 Using the magnetic field b_0 and proton density n_p/T^3 we solve the magnetization numerically.
 652 In Fig. 25, we plot the magnetization M/B as a function of temperature T . It shows that the
 653 magnetization depends on the magnetic field b_0 strongly. This is because for a small magnetic
 654 field b_0 the dominant term in Eq. (105) is $xK_1(x)/b_0$. For given b_0 , the value of magnetization

655 can be larger than the magnetic field, i.e. $M/B > 1$ which shows the possibility that magnetic
 656 domains can be formed in the early Universe.

657 6. Summary

658 6.1. Primordial Plasma Outlook

659 In this survey, we looked at the major epochs in the Universe where antimatter played a large roll in
 660 expansion dynamics, and thermal and chemical equilibria within the context of the Standard Model.
 661 We emphasized that primordial QGP is an important laboratory which explores a location in the phase
 662 diagram of QCD inaccessible to relativistic colliders in both density and longevity of the plasma. After
 663 hadronization at temperature $T = 150$ MeV, the strange abundance of the Universe remains substantial
 664 until the loss of the anti-baryons at $T = 38.2$ MeV. Pions in comparison remain abundant via photon
 665 production long after the other hadrons disappear. Muons disappear at around $T = 4.2$ MeV as their
 666 decay rate outpaces their production rate.

667 For the duration of the leptonic plasma until the disappearance of the positrons, neutrinos
 668 make up the largest energy fraction in the universe driving the Universe's expansion as a radiation
 669 dominated universe. Partway through this neutrino dominated universe, at temperature $T = 1$ MeV,
 670 the neutrinos freezeout and decouple from the rest of the thermally active universe.

671 **Topics: Cover neutrinos. Freezeout. Cosmic magnetic fields. High density of e+e- above baryons**
 672 **during BBN. Protection of magnetic moment. Magnetization of e+e-. Boltzmann limit.**

673 6.2. Application to Novel Stellar Objects

674 The topics explored in this work have applications beyond early Universe cosmology. As one example,
 675 our understanding of the QGP Epoch informs the fireballs created in heavy-ion collisions performed
 676 today and vice versa [12,13,21]. The e^\pm epoch likewise because of its abundance of positrons may be
 677 useful in understanding extreme systems like those which produce gamma-ray bursts (GRB). GRBs
 678 present an interesting challenge in that a tremendous amount of matter must be converted into light
 679 in a short time-span of $t \approx 2$ seconds. Mechanisms which allow the production of large amounts of
 680 antimatter which can be subsequently annihilated offer the most direct solution. **Cite Ruffini.** We
 681 suggest that some GRB events (especially those which lack classic supernova after-signatures) **Cite**
 682 **brightest GRB ever event.** may involve novel stellar objects which naturally possess, rather than create,
 683 larger amounts of antimatter which are destroyed upon stellar collapse. Such novel stellar objects
 684 would have internal conditions not unlike the primordial plasmas of the early Universe.



Figure 26. Remo Ruffini and Johann Rafelski with a Tucson, AZ sunset on October 7th, 2012 taken at a celebratory gathering honoring the life of Fang Li-Zhi. Photo by She Sheng Xue.

685 References

- 686 1. R. Ruffini, G. Vereshchagin and S. S. Xue, "Electron-positron pairs in physics and astrophysics: from heavy
 687 nuclei to black holes," *Phys. Rept.* **487** (2010), 1-140 doi:10.1016/j.physrep.2009.10.004 [arXiv:0910.0974
 688 [astro-ph.HE]].

- 689 2. R. Ruffini and G. Vereshchagin, "Electron-positron plasma in GRBs and in cosmology," *Nuovo Cim. C* **036**
690 (2013) no.s01, 255-266 doi:10.1393/ncc/i2013-11500-0 [arXiv:1205.3512 [astro-ph.CO]].
- 691 3. W. B. Han, R. Ruffini and S. S. Xue, "Electron and positron pair production of compact stars," *Phys. Rev. D* **86**
692 (2012), 084004 doi:10.1103/PhysRevD.86.084004 [arXiv:1110.0700 [astro-ph.HE]].
- 693 4. R. Ruffini, C. L. Bianco, P. Chardonnet, F. Fraschetti and S. S. Xue, "On the interpretation of the burst structure
694 of grbs," *Astrophys. J. Lett.* **555**, L113-L116 (2001) doi:10.1086/323176 [arXiv:astro-ph/0106532 [astro-ph]].
- 695 5. A. G. Aksenov, C. L. Bianco, R. Ruffini and G. V. Vereshchagin, "GRBs and the thermalization process of
696 electron-positron plasmas," *AIP Conf. Proc.* **1000**, no.1, 309-312 (2008) doi:10.1063/1.2943471 [arXiv:0804.2807
697 [astro-ph]].
- 698 6. R. Ruffini, L. Vitagliano and S. S. Xue, "Electron-positron-photon plasma around a collapsing star,"
699 doi:10.1142/9789812702333_0030 [arXiv:astro-ph/0304306 [astro-ph]].
- 700 7. R. Belvedere, D. Pugliese, J. A. Rueda, R. Ruffini and S. S. Xue, "Neutron star equilibrium configurations
701 within a fully relativistic theory with strong, weak, electromagnetic, and gravitational interactions," *Nucl.*
702 *Phys. A* **883**, 1-24 (2012) doi:10.1016/j.nuclphysa.2012.02.018 [arXiv:1202.6500 [astro-ph.SR]].
- 703 8. R. Ruffini, J. D. Salmonson, J. R. Wilson and S. S. Xue, "On the pair-electromagnetic pulse from an
704 electromagnetic black hole surrounded by a baryonic remnant," *Astron. Astrophys.* **359** (2000), 855
705 [arXiv:astro-ph/0004257 [astro-ph]].
- 706 9. J. Rafelski, "Melting Hadrons, Boiling Quarks," *Eur. Phys. J. A* **51**, no.9, 114 (2015)
707 doi:10.1140/epja/i2015-15114-0 [arXiv:1508.03260 [nucl-th]].
- 708 10. J. Bernstein, "Kinetic theory in the expanding universe," Cambridge University Press, 1988, ISBN
709 978-0-511-56418-5 doi:10.1017/CBO9780511564185
- 710 11. G. Rodriguez [Pierre Auger], "Measurement of the ultra high energy cosmic ray energy spectrum with the
711 Pierre Auger Observatory," *Nucl. Instrum. Meth. A* **742**, 261-264 (2014) doi:10.1016/j.nima.2013.11.032
- 712 12. O. Philipsen, "The QCD equation of state from the lattice," *Prog. Part. Nucl. Phys.* **70**, 55-107 (2013)
713 doi:10.1016/j.ppnp.2012.09.003 [arXiv:1207.5999 [hep-lat]].
- 714 13. P. Braun-Munzinger and J. Wambach, "The Phase Diagram of Strongly-Interacting Matter," *Rev. Mod. Phys.*
715 **81**, 1031-1050 (2009) doi:10.1103/RevModPhys.81.1031 [arXiv:0801.4256 [hep-ph]].
- 716 14. J. Rafelski, "Formation and Observables of the Quark-Gluon Plasma," *Phys. Rept.* **88**, 331 (1982)
717 UFTP-80-1982.
- 718 15. B. V. Jacak and B. Muller, "The exploration of hot nuclear matter," *Science* **337**, 310-314 (2012)
719 doi:10.1126/science.1215901
- 720 16. A. S. Kronfeld, "Lattice Gauge Theory and the Origin of Mass," doi:10.1142/9789814425810_0018
721 [arXiv:1209.3468 [physics.hist-ph]].
- 722 17. C. D. Roberts, "Origin of the Proton Mass," *EPJ Web Conf.* **282**, 01006 (2023)
723 doi:10.1051/epiconf/202328201006 [arXiv:2211.09905 [hep-ph]].
- 724 18. C. D. Roberts, "On Mass and Matter," *AAPPS Bull.* **31**, 6 (2021) doi:10.1007/s43673-021-00005-4
725 [arXiv:2101.08340 [hep-ph]].
- 726 19. J. Rafelski and A. Schnabel, "Quark - Gluon Plasma in Nuclear Collisions at 200-GeV/A," *Phys. Lett. B* **207**,
727 6-10 (1988) doi:10.1016/0370-2693(88)90875-1
- 728 20. R. Hagedorn, "How We Got to QCD Matter from the Hadron Side: 1984," *Lect. Notes Phys.* **221**, 53-76 (1985)
729 doi:10.1007/978-3-319-17545-4_25
- 730 21. J. Rafelski, "Connecting QGP-Heavy Ion Physics to the Early Universe," *Nucl. Phys. B Proc. Suppl.* **243-244**,
731 155-162 (2013) doi:10.1016/j.nuclphysbps.2013.09.017 [arXiv:1306.2471 [astro-ph.CO]].
- 732 22. L. Lello and D. Boyanovsky, "Cosmological Implications of Light Sterile Neutrinos produced after the
733 QCD Phase Transition," *Phys. Rev. D* **91**, 063502 (2015) doi:10.1103/PhysRevD.91.063502 [arXiv:1411.2690
734 [astro-ph.CO]].
- 735 23. C. Bonati, G. Cossu, M. D'Elia, M. Mariti and F. Negro, "Effective θ term by CP-odd electromagnetic
736 background fields," *PoS LATTICE2013*, 360 (2014) doi:10.22323/1.187.0360 [arXiv:1312.2805 [hep-lat]].
- 737 24. M. D'Elia, M. Mariti and F. Negro, "Susceptibility of the QCD vacuum to CP-odd electromagnetic background
738 fields," *Phys. Rev. Lett.* **110**, no.8, 082002 (2013) doi:10.1103/PhysRevLett.110.082002 [arXiv:1209.0722
739 [hep-lat]].
- 740 25. M. J. Moravcsik, "Coulomb scattering of electrons at very small angles." *Phys. Rev.* **100.4** (1955): 1009.

- 741 26. J. R. Hoerandel, "Models of the knee in the energy spectrum of cosmic rays," *Astropart. Phys.* **21**, 241-265
742 (2004) doi:10.1016/j.astropartphys.2004.01.004 [arXiv:astro-ph/0402356 [astro-ph]].
- 743 27. A. Aab *et al.* [Pierre Auger], "Depth of maximum of air-shower profiles at the Pierre Auger Observatory.
744 II. Composition implications," *Phys. Rev. D* **90**, no.12, 122006 (2014) doi:10.1103/PhysRevD.90.122006
745 [arXiv:1409.5083 [astro-ph.HE]].
- 746 28. J. Birrell and J. Rafelski, "Proposal for Resonant Detection of Relic Massive Neutrinos," *Eur. Phys. J. C* **75**,
747 no.2, 91 (2015) doi:10.1140/epjc/s10052-015-3310-3 [arXiv:1402.3409 [hep-ph]].
- 748 29. D. A. Dicus, E. W. Kolb, A. M. Gleeson, E. C. G. Sudarshan, V. L. Teplitz and M. S. Turner, "Primordial
749 Nucleosynthesis Including Radiative, Coulomb, and Finite Temperature Corrections to Weak Rates," *Phys.*
750 *Rev. D* **26**, 2694 (1982) doi:10.1103/PhysRevD.26.2694
- 751 30. J. F. Zhang, Y. H. Li and X. Zhang, "Cosmological constraints on neutrinos after BICEP2," *Eur. Phys. J. C* **74**,
752 2954 (2014) doi:10.1140/epjc/s10052-014-2954-8 [arXiv:1404.3598 [astro-ph.CO]].
- 753 31. V. A. Kuzmin, V. A. Rubakov and M. E. Shaposhnikov, "On the Anomalous Electroweak Baryon Number
754 Nonconservation in the Early Universe," *Phys. Lett. B* **155**, 36 (1985) doi:10.1016/0370-2693(85)91028-7
- 755 32. K. N. Abazajian, M. A. Acero, S. K. Agarwalla, A. A. Aguilar-Arevalo, C. H. Albright, S. Antusch,
756 C. A. Argüelles, A. B. Balantekin, G. Barenboim and V. Barger, *et al.* "Light Sterile Neutrinos: A White
757 Paper," [arXiv:1204.5379 [hep-ph]].
- 758 33. E. Giusarma, E. Di Valentino, M. Lattanzi, A. Melchiorri and O. Mena, "Relic Neutrinos, thermal axions
759 and cosmology in early 2014," *Phys. Rev. D* **90**, no.4, 043507 (2014) doi:10.1103/PhysRevD.90.043507
760 [arXiv:1403.4852 [astro-ph.CO]].
- 761 34. A. Bazavov *et al.* [HotQCD], "Equation of state in (2+1)-flavor QCD," *Phys. Rev. D* **90**, 094503 (2014)
762 doi:10.1103/PhysRevD.90.094503 [arXiv:1407.6387 [hep-lat]].
- 763 35. G. Steigman, "Equivalent Neutrinos, Light WIMPs, and the Chimera of Dark Radiation," *Phys. Rev. D* **87**,
764 no.10, 103517 (2013) doi:10.1103/PhysRevD.87.103517 [arXiv:1303.0049 [astro-ph.CO]].
- 765 36. L. A. Anchordoqui and H. Goldberg, "Neutrino cosmology after WMAP 7-Year data and LHC first Z' bounds,"
766 *Phys. Rev. Lett.* **108**, 081805 (2012) doi:10.1103/PhysRevLett.108.081805 [arXiv:1111.7264 [hep-ph]].
- 767 37. L. A. Anchordoqui, H. Goldberg and G. Steigman, "Right-Handed Neutrinos as the Dark Radiation: Status and
768 Forecasts for the LHC," *Phys. Lett. B* **718**, 1162-1165 (2013) doi:10.1016/j.physletb.2012.12.019 [arXiv:1211.0186
769 [hep-ph]].
- 770 38. S. Borsanyi, Z. Fodor, C. Hoelbling, S. D. Katz, S. Krieg and K. K. Szabo, "Full result for the QCD equation of
771 state with 2+1 flavors," *Phys. Lett. B* **730**, 99-104 (2014) doi:10.1016/j.physletb.2014.01.007 [arXiv:1309.5258
772 [hep-lat]].
- 773 39. M. Demiański and A. G. Doroshkevich, "Beyond the standard Λ CDM cosmology: the observed structure of
774 DM halos and the shape of the power spectrum," [arXiv:1511.07989 [astro-ph.CO]].
- 775 40. P. A. R. Ade *et al.* [Planck], "Planck 2013 results. XVI. Cosmological parameters," *Astron. Astrophys.* **571**,
776 A16 (2014) doi:10.1051/0004-6361/201321591 [arXiv:1303.5076 [astro-ph.CO]].
- 777 41. P. A. R. Ade *et al.* [Planck], "Planck 2015 results. XIII. Cosmological parameters," *Astron. Astrophys.* **594**,
778 A13 (2016) doi:10.1051/0004-6361/201525830 [arXiv:1502.01589 [astro-ph.CO]].
- 779 42. N. Aghanim *et al.* [Planck], "Planck 2018 results. VI. Cosmological parameters," *Astron. Astrophys.* **641**,
780 A6 (2020) [erratum: *Astron. Astrophys.* **652**, C4 (2021)] doi:10.1051/0004-6361/201833910 [arXiv:1807.06209
781 [astro-ph.CO]].
- 782 43. T. S. Coleman and M. Roos, "Effective degrees of freedom during the radiation era," *Phys. Rev. D* **68**, 027702
783 (2003) doi:10.1103/PhysRevD.68.027702 [arXiv:astro-ph/0304281 [astro-ph]].
- 784 44. J. Hamann, S. Hannestad, G. G. Raffelt and Y. Y. Wong, "Sterile neutrinos with eV masses in cosmology:
785 How disfavoured exactly?," *JCAP* **09**, 034 (2011) doi:10.1088/1475-7516/2011/09/034 [arXiv:1108.4136
786 [astro-ph.CO]].
- 787 45. J. Kopp, M. Maltoni and T. Schwetz, "Are There Sterile Neutrinos at the eV Scale?," *Phys. Rev. Lett.* **107**,
788 091801 (2011) doi:10.1103/PhysRevLett.107.091801 [arXiv:1103.4570 [hep-ph]].
- 789 46. H. Georgi, "New Realization of Chiral Symmetry," *Phys. Rev. Lett.* **63**, 1917-1919 (1989)
790 doi:10.1103/PhysRevLett.63.1917
- 791 47. V. Castellani, S. Degl'Innocenti, G. Fiorentini, M. Lissia and B. Ricci, "Solar neutrinos: Beyond standard
792 solar models," *Phys. Rept.* **281**, 309-398 (1997) doi:10.1016/S0370-1573(96)00032-4 [arXiv:astro-ph/9606180
793 [astro-ph]].

- 794 48. O. Wantz and E. P. S. Shellard, "Axion Cosmology Revisited," *Phys. Rev. D* **82**, 123508 (2010)
795 doi:10.1103/PhysRevD.82.123508 [arXiv:0910.1066 [astro-ph.CO]].
- 796 49. J. Rafelski, J. Letessier and G. Torrieri, "Strange hadrons and their resonances: A Diagnostic tool of
797 QGP freezeout dynamics," *Phys. Rev. C* **64**, 054907 (2001) [erratum: *Phys. Rev. C* **65**, 069902 (2002)]
798 doi:10.1103/PhysRevC.64.054907 [arXiv:nucl-th/0104042 [nucl-th]].
- 799 50. J. Rafelski and J. Birrell, "Traveling Through the Universe: Back in Time to the Quark-Gluon Plasma Era," *J.*
800 *Phys. Conf. Ser.* **509**, 012014 (2014) doi:10.1088/1742-6596/509/1/012014 [arXiv:1311.0075 [nucl-th]].
- 801 51. S. Weinberg, "Gravitation and Cosmology: Principles and Applications of the General Theory of Relativity,"
802 John Wiley and Sons, 1972, ISBN 978-0-471-92567-5, 978-0-471-92567-5
- 803 52. S. Weinberg, "Goldstone Bosons as Fractional Cosmic Neutrinos," *Phys. Rev. Lett.* **110**, no.24, 241301 (2013)
804 doi:10.1103/PhysRevLett.110.241301 [arXiv:1305.1971 [astro-ph.CO]].
- 805 53. H. Yan, Z. Ma, C. Ling, C. Cheng and J. s. Huang, "First Batch of $z \approx 11$ –20 Candidate Objects Revealed by
806 the James Webb Space Telescope Early Release Observations on SMACS 0723-73," *Astrophys. J. Lett.* **942**,
807 no.1, L9 (2023) doi:10.3847/2041-8213/aca80c [arXiv:2207.11558 [astro-ph.GA]].
- 808 54. G. Mangano, G. Miele, S. Pastor, T. Pinto, O. Pisanti and P. D. Serpico, "Effects of non-standard
809 neutrino-electron interactions on relic neutrino decoupling," *Nucl. Phys. B* **756**, 100-116 (2006)
810 doi:10.1016/j.nuclphysb.2006.09.002 [arXiv:hep-ph/0607267 [hep-ph]].
- 811 55. J. A. Morgan, "Cosmological upper limit to neutrino magnetic moments," *Phys. Lett. B* **102**, 247-250 (1981)
812 doi:10.1016/0370-2693(81)90868-6
- 813 56. P. Elmfors, K. Enqvist, G. Raffelt and G. Sigl, "Neutrinos with magnetic moment: Depolarization rate in
814 plasma," *Nucl. Phys. B* **503**, 3-23 (1997) doi:10.1016/S0550-3213(97)00382-9 [arXiv:hep-ph/9703214 [hep-ph]].
- 815 57. M. Fukugita and S. Yazaki, "Reexamination of Astrophysical and Cosmological Constraints on the Magnetic
816 Moment of Neutrinos," *Phys. Rev. D* **36**, 3817 (1987) doi:10.1103/PhysRevD.36.3817
- 817 58. C. Giunti and A. Studenikin, "Neutrino electromagnetic properties," *Phys. Atom. Nucl.* **72**, 2089-2125 (2009)
818 doi:10.1134/S1063778809120126 [arXiv:0812.3646 [hep-ph]].
- 819 59. P. Vogel and J. Engel, "Neutrino Electromagnetic Form-Factors," *Phys. Rev. D* **39**, 3378 (1989)
820 doi:10.1103/PhysRevD.39.3378
- 821 60. A. Neronov and I. Vovk, "Evidence for strong extragalactic magnetic fields from Fermi observations of TeV
822 blazars," *Science* **328**, 73-75 (2010) doi:10.1126/science.1184192 [arXiv:1006.3504 [astro-ph.HE]].
- 823 61. L. A. Anchordoqui and H. Goldberg, "A Lower bound on the local extragalactic magnetic field," *Phys. Rev.*
824 *D* **65**, 021302 (2002) doi:10.1103/PhysRevD.65.021302 [arXiv:hep-ph/0106217 [hep-ph]].
- 825 62. R. Schlickeiser, U. Kolberg and P. H. Yoon, "Primordial Plasma Fluctuations. I. Magnetization of the Early
826 Universe by Dark Aperiodic Fluctuations in the Past Myon and Prior Electron-Positron Annihilation Epoch,"
827 *Astrophys. J.* **857**, no.1, 29 (2018) doi:10.3847/1538-4357/aab3dd
- 828 63. L. M. Widrow, D. Ryu, D. R. G. Schleicher, K. Subramanian, C. G. Tsagas and R. A. Treumann, "The
829 First Magnetic Fields," *Space Sci. Rev.* **166**, 37-70 (2012) doi:10.1007/s11214-011-9833-5 [arXiv:1109.4052
830 [astro-ph.CO]].
- 831 64. L. M. Widrow, "Origin of galactic and extragalactic magnetic fields," *Rev. Mod. Phys.* **74**, 775-823 (2002)
832 doi:10.1103/RevModPhys.74.775 [arXiv:astro-ph/0207240 [astro-ph]].
- 833 65. P. P. Kronberg, "Extragalactic magnetic fields," *Rept. Prog. Phys.* **57**, 325-382 (1994)
834 doi:10.1088/0034-4885/57/4/001
- 835 66. F. Vazza, N. Locatelli, K. Rajpurohit, S. Banfi, P. Domínguez-Fernández, D. Wittor, M. Angelinelli,
836 G. Inchingolo, M. Brienza and S. Hackstein, *et al.* "Magnetogenesis and the Cosmic Web: A Joint Challenge
837 for Radio Observations and Numerical Simulations," *Galaxies* **9**, no.4, 109 (2021) doi:10.3390/galaxies9040109
838 [arXiv:2111.09129 [astro-ph.CO]].
- 839 67. H. T. Elze, W. Greiner and J. Rafelski, "The relativistic ideal Fermi gas revisited," *J. Phys. G* **6**, L149-L153
840 (1980) doi:10.1088/0305-4616/6/9/003
- 841 68. A. Broderick, M. Prakash and J. M. Lattimer, "The Equation of state of neutron star matter in strong magnetic
842 fields," *Astrophys. J.* **537**, 351 (2000) doi:10.1086/309010 [arXiv:astro-ph/0001537 [astro-ph]].
- 843 69. V. Canuto and H. Y. Chiu, "Magnetic moment of a magnetized fermi gas," *Phys. Rev.* **173**, 1229-1235 (1968)
844 doi:10.1103/PhysRev.173.1229
- 845 70. V. Canuto and H. Y. Chiu, "Thermodynamic properties of a magnetized fermi gas," *Phys. Rev.* **173**, 1220-1228
846 (1968) doi:10.1103/PhysRev.173.1220

- 847 71. L. Perivolaropoulos and F. Skara, “Challenges for Λ CDM: An update,” *New Astron. Rev.* **95**, 101659 (2022)
848 doi:10.1016/j.newar.2022.101659 [arXiv:2105.05208 [astro-ph.CO]].
- 849 72. E. Di Valentino, O. Mena, S. Pan, L. Visinelli, W. Yang, A. Melchiorri, D. F. Mota, A. G. Riess and J. Silk,
850 “In the realm of the Hubble tension—a review of solutions,” *Class. Quant. Grav.* **38**, no.15, 153001 (2021)
851 doi:10.1088/1361-6382/ac086d [arXiv:2103.01183 [astro-ph.CO]].
- 852 73. P. K. Aluri, P. Cea, P. Chingangbam, M. C. Chu, R. G. Clowes, D. Hutsemékers, J. P. Kochappan, A. M. Lopez,
853 L. Liu and N. C. M. Martens, *et al.* “Is the observable Universe consistent with the cosmological principle?,”
854 *Class. Quant. Grav.* **40**, no.9, 094001 (2023) doi:10.1088/1361-6382/acbefc [arXiv:2207.05765 [astro-ph.CO]].
- 855 74. B. C. Canas, O. G. Miranda, A. Parada, M. Tortola and J. W. F. Valle, “Updating neutrino magnetic moment
856 constraints,” *Phys. Lett. B* **753**, 191-198 (2016) doi:10.1016/j.physletb.2015.12.011 [arXiv:1510.01684 [hep-ph]].
- 857 75. C. Giunti and A. Studenikin, “Neutrino electromagnetic interactions: a window to new physics,” *Rev. Mod.*
858 *Phys.* **87**, 531 (2015) doi:10.1103/RevModPhys.87.531 [arXiv:1403.6344 [hep-ph]].
- 859 76. S. Ryu, J. F. Paquet, C. Shen, G. S. Denicol, B. Schenke, S. Jeon and C. Gale, “Importance of the Bulk
860 Viscosity of QCD in Ultrarelativistic Heavy-Ion Collisions,” *Phys. Rev. Lett.* **115**, no.13, 132301 (2015)
861 doi:10.1103/PhysRevLett.115.132301 [arXiv:1502.01675 [nucl-th]].
- 862 77. H. K. Dreiner, M. Hanussek, J. S. Kim and S. Sarkar, “Gravitino cosmology with a very light neutralino,” *Phys.*
863 *Rev. D* **85**, 065027 (2012) doi:10.1103/PhysRevD.85.065027 [arXiv:1111.5715 [hep-ph]].
- 864 78. C. T. Yang and J. Rafelski, “Possibility of bottom-catalyzed matter genesis near to primordial QGP
865 hadronization,” [arXiv:2004.06771 [hep-ph]].
- 866 79. C. T. Yang and J. Rafelski, “Bottom quark chemical nonequilibrium in primordial QGP,” (to be published)
- 867 80. J. Birrell, C. T. Yang and J. Rafelski, “Relic Neutrino Freeze-out: Dependence on Natural Constants,” *Nucl.*
868 *Phys. B* **890**, 481-517 (2014) doi:10.1016/j.nuclphysb.2014.11.020 [arXiv:1406.1759 [nucl-th]].
- 869 81. J. Birrell, “Non-Equilibrium Aspects of Relic Neutrinos: From Freeze-out to the Present Day,” [arXiv:1409.4500
870 [nucl-th]].
- 871 82. J. Birrell, J. Wilkening and J. Rafelski, “Boltzmann Equation Solver Adapted to Emergent Chemical
872 Non-equilibrium,” *J. Comput. Phys.* **281**, 896-916 (2015) doi:10.1016/j.jcp.2014.10.056 [arXiv:1403.2019
873 [math.NA]].
- 874 83. J. Birrell, C. T. Yang, P. Chen and J. Rafelski, “Relic neutrinos: Physically consistent treatment of effective
875 number of neutrinos and neutrino mass,” *Phys. Rev. D* **89**, 023008 (2014) doi:10.1103/PhysRevD.89.023008
876 [arXiv:1212.6943 [astro-ph.CO]].
- 877 84. M. Blennow, E. Fernandez-Martinez, O. Mena, J. Redondo and P. Serra, “Asymmetric Dark Matter and Dark
878 Radiation,” *JCAP* **07**, 022 (2012) doi:10.1088/1475-7516/2012/07/022 [arXiv:1203.5803 [hep-ph]].
- 879 85. S. Joudaki, K. N. Abazajian and M. Kaplinghat, “Are Light Sterile Neutrinos Preferred or Disfavored by
880 Cosmology?,” *Phys. Rev. D* **87**, no.6, 065003 (2013) doi:10.1103/PhysRevD.87.065003 [arXiv:1208.4354
881 [astro-ph.CO]].
- 882 86. R. D. Peccei, “The Strong CP problem and axions,” *Lect. Notes Phys.* **741**, 3-17 (2008)
883 doi:10.1007/978-3-540-73518-2_1 [arXiv:hep-ph/0607268 [hep-ph]].
- 884 87. J. Kopp, P. A. N. Machado, M. Maltoni and T. Schwetz, “Sterile Neutrino Oscillations: The Global Picture,”
885 *JHEP* **05**, 050 (2013) doi:10.1007/JHEP05(2013)050 [arXiv:1303.3011 [hep-ph]].
- 886 88. A. Bazavov, T. Bhattacharya, M. Cheng, N. H. Christ, C. DeTar, S. Ejiri, S. Gottlieb, R. Gupta, U. M. Heller and
887 K. Huebner, *et al.* “Equation of state and QCD transition at finite temperature,” *Phys. Rev. D* **80**, 014504 (2009)
888 doi:10.1103/PhysRevD.80.014504 [arXiv:0903.4379 [hep-lat]].
- 889 89. S. Borsanyi, “Thermodynamics of the QCD transition from lattice,” *Nucl. Phys. A* **904-905**, 270c-277c (2013)
890 doi:10.1016/j.nuclphysa.2013.01.072 [arXiv:1210.6901 [hep-lat]].
- 891 90. A. Bazavov, T. Bhattacharya, M. Cheng, C. DeTar, H. T. Ding, S. Gottlieb, R. Gupta, P. Hegde, U. M. Heller
892 and F. Karsch, *et al.* “The chiral and deconfinement aspects of the QCD transition,” *Phys. Rev. D* **85**, 054503
893 (2012) doi:10.1103/PhysRevD.85.054503 [arXiv:1111.1710 [hep-lat]].
- 894 91. J. Letessier and J. Rafelski, “Hadron production and phase changes in relativistic heavy ion collisions,” *Eur.*
895 *Phys. J. A* **35**, 221-242 (2008) doi:10.1140/epja/i2007-10546-7 [arXiv:nucl-th/0504028 [nucl-th]].
- 896 92. J. Y. Ollitrault, “Anisotropy as a signature of transverse collective flow,” *Phys. Rev. D* **46**, 229-245 (1992)
897 doi:10.1103/PhysRevD.46.229

93. M. Petráň, J. Letessier, V. Petráček and J. Rafelski, "Hadron production and quark-gluon plasma hadronization in Pb-Pb collisions at $\sqrt{s_{NN}} = 2.76$ TeV," *Phys. Rev. C* **88**, no.3, 034907 (2013) doi:10.1103/PhysRevC.88.034907 [arXiv:1303.2098 [hep-ph]].
94. M. J. Fromerth and J. Rafelski, "Hadronization of the quark Universe," [arXiv:astro-ph/0211346 [astro-ph]].
95. S. Voloshin and Y. Zhang, "Flow study in relativistic nuclear collisions by Fourier expansion of Azimuthal particle distributions," *Z. Phys. C* **70**, 665-672 (1996) doi:10.1007/s002880050141 [arXiv:hep-ph/9407282 [hep-ph]].
96. M. J. Fromerth, I. Kuznetsova, L. Labun, J. Letessier and J. Rafelski, "From Quark-Gluon Universe to Neutrino Decoupling: $200 < T < 2\text{MeV}$," *Acta Phys. Polon. B* **43**, no.12, 2261-2284 (2012) doi:10.5506/APhysPolB.43.2261
97. C. T. Yang and J. Rafelski, "Cosmological strangeness abundance," *Phys. Lett. B* **827**, 136944 (2022) doi:10.1016/j.physletb.2022.136944
98. J. Birrell, Cheng Tao Yang, P. Chen and J. Rafelski, "Relic neutrinos: Physically consistent treatment of effective number of neutrinos and neutrino mass," *Phys. Rev. D* **89**, 023008 (2014) doi:10.1103/PhysRevD.89.023008 [arXiv:1212.6943 [astro-ph.CO]].
99. C. Grayson, C. T. Yang and J. Rafelski, "Electron-Positron Plasma in BBN epoch," (to be published).
100. C. Pitrou, A. Coc, J. P. Uzan and E. Vangioni, "Precision big bang nucleosynthesis with improved Helium-4 predictions," arXiv:1801.08023 [astro-ph.CO], *Phys. Rep. in press* (2018)
101. B. Wang, C. A. Bertulani and A. B. Balantekin, "Electron screening and its effects on Big-Bang nucleosynthesis," *Phys. Rev. C* **83**, 018801 (2011) doi:10.1103/PhysRevC.83.018801 [arXiv:1010.1565 [astro-ph.CO]].
102. G. Mangano, G. Miele, S. Pastor, T. Pinto, O. Pisanti and P. D. Serpico, "Relic neutrino decoupling including flavor oscillations," *Nucl. Phys. B* **729**, 221 (2005) doi:10.1016/j.nuclphysb.2005.09.041 [hep-ph/0506164].
103. J. Birrell, Cheng Tao Yang and J. Rafelski, "Relic Neutrino Freeze-out: Dependence on Natural Constants," *Nucl. Phys. B* **890**, 481 (2014) doi:10.1016/j.nuclphysb.2014.11.020 [arXiv:1406.1759 [nucl-th]].
104. R. L. Workman *et al.* [Particle Data Group], "Review of Particle Physics," *PTEP* **2022**, 083C01 (2022) doi:10.1093/ptep/ptac097
105. E. W. Kolb and M. S. Turner, *The Early Universe*, 547 pp, Front. Phys. **69**, 1 (1990), ISBN: 0201626748, 9780201626742
106. M. Strickland, V. Dexheimer and D. P. Menezes, "Bulk Properties of a Fermi Gas in a Magnetic Field," *Phys. Rev. D* **86** (2012), 125032 doi:10.1103/PhysRevD.86.125032 [arXiv:1209.3276 [nucl-th]].
107. A. Steinmetz, M. Formanek and J. Rafelski, "Magnetic Dipole Moment in Relativistic Quantum Mechanics," *Eur. Phys. J. A* **55** (2019) no.3, 40 doi:10.1140/epja/i2019-12715-5 [arXiv:1811.06233 [hep-ph]].
108. J. Rafelski, S. Evans and L. Labun, "Study of QED singular properties for variable gyromagnetic ratio $g \simeq 2$," [arXiv:2212.13165 [hep-th]].
109. M. J. Fromerth, I. Kuznetsova, L. Labun, J. Letessier and J. Rafelski, "From Quark-Gluon Universe to Neutrino Decoupling: $200 < T < 2\text{MeV}$," *Acta Phys. Polon. B* **43**, no.12, 2261-2284 (2012) doi:10.5506/APhysPolB.43.2261 [arXiv:1211.4297 [nucl-th]].
110. J. Birrell, C. T. Yang, P. Chen and J. Rafelski, "Relic neutrinos: Physically consistent treatment of effective number of neutrinos and neutrino mass," *Phys. Rev. D* **89**, 023008 (2014) doi:10.1103/PhysRevD.89.023008
111. J. Birrell, J. Wilkening and J. Rafelski, "Boltzmann Equation Solver Adapted to Emergent Chemical Non-equilibrium," *J. Comput. Phys.* **281**, 896-916 (2015) doi:10.1016/j.jcp.2014.10.056
112. Y. Choquet-Bruhat, "General Relativity and the Einstein Equations," Oxford University Press, 2009, ISBN 978-0-19-923072-3
113. J. Rafelski and C. T. Yang, "The muon abundance in the primordial Universe," *Acta Phys. Polon. B* **52**, 277 (2021) doi:10.5506/APhysPolB.52.277
114. I. Kuznetsova, D. Habs and J. Rafelski, "Pion and muon production in e^- , e^+ , gamma plasma," *Phys. Rev. D* **78**, 014027 (2008) doi:10.1103/PhysRevD.78.014027
115. I. Kuznetsova and J. Rafelski, "Unstable Hadrons in Hot Hadron Gas in Laboratory and in the Early Universe," *Phys. Rev. C* **82**, 035203 (2010) doi:10.1103/PhysRevC.82.035203 [arXiv:1002.0375 [hep-th]].
116. J. Letessier and J. Rafelski, *Hadrons and Quark-Gluon Plasma*, 397 pp, doi: 10.1017/CBO9780511534997Camb. Monogr. Part. Phys. Nucl. Phys. Cosmol. **18** (2002) ISBN: 9780521018234 (Paperback), 9780521385367 (Hardback), 9780511037276 (Online).
117. I. Kuznetsova, "Particle Production in Matter at Extreme Conditions," [arXiv:0909.0524 [hep-th]].

- 950 118. A. F. Heckler, "Astrophysical applications of quantum corrections to the equation of state of a plasma," *Phys.*
951 *Rev. D* **49**, 611-617 (1994) doi:10.1103/PhysRevD.49.611
- 952 119. N. Fornengo, C. W. Kim and J. Song, "Finite temperature effects on the neutrino decoupling in the early
953 universe," *Phys. Rev. D* **56**, 5123-5134 (1997) doi:10.1103/PhysRevD.56.5123
- 954 120. G. Mangano, G. Miele, S. Pastor, T. Pinto, O. Pisanti and P. D. Serpico, "Relic neutrino decoupling including
955 flavor oscillations," *Nucl. Phys. B* **729**, 221-234 (2005) doi:10.1016/j.nuclphysb.2005.09.041
- 956 121. G. Mangano, G. Miele, S. Pastor and M. Peloso, "A Precision calculation of the effective number of
957 cosmological neutrinos," *Phys. Lett. B* **534**, 8-16 (2002) doi:10.1016/S0370-2693(02)01622-2
- 958 122. G. S. Adkins, D. B. Cassidy and J. Pérez-Ríos, "Precision spectroscopy of positronium: Testing bound-state
959 QED theory and the search for physics beyond the Standard Model," *Phys. Rept.* **975**, 1-61 (2022)
960 doi:10.1016/j.physrep.2022.05.002
- 961 123. J. Govaerts and M. Van Caillie, "Neutrino decay of positronium in the standard model and beyond," *Phys.*
962 *Lett. B* **381**, 451-457 (1996) doi:10.1016/0370-2693(96)00623-5 [arXiv:hep-ph/9602382 [hep-ph]].
- 963 124. J. Rafelski and J. Birrell, "Traveling Through the Universe: Back in Time to the Quark-Gluon Plasma Era," *J.*
964 *Phys. Conf. Ser.* **509**, 012014 (2014) doi:10.1088/1742-6596/509/1/012014 [arXiv:1311.0075 [nucl-th]].
- 965 125. J. Rafelski, "Discovery of Quark-Gluon-Plasma: Strangeness Diaries," *Eur. Phys. J. ST* **229**, no.1, 1-140 (2020)
966 doi:10.1140/epjst/e2019-900263-x [arXiv:1911.00831 [hep-ph]].
- 967 126. G. Barenboim and W. I. Park, "A full picture of large lepton number asymmetries of the Universe," *JCAP*
968 **1704**, 048 (2017) doi:10.1088/1475-7516/2017/04/048 [arXiv:1703.08258 [hep-ph]].
- 969 127. G. Barenboim, W. H. Kinney and W. I. Park, "Resurrection of large lepton number asymmetries from
970 neutrino flavor oscillations," *Phys. Rev. D* **95**, 043506 (2017) doi:10.1103/PhysRevD.95.043506 [arXiv:1609.01584
971 [hep-ph]].
- 972 128. C. T. Yang, J. Birrell and J. Rafelski, "Lepton Number and Expansion of the Universe," [arXiv:1812.05157
973 [hep-ph]].
- 974 129. J. Birrell and J. Rafelski, "Quark-gluon plasma as the possible source of cosmological dark radiation," *Phys.*
975 *Lett. B* **741**, 77-81 (2015) doi:10.1016/j.physletb.2014.12.033
- 976 130. A. G. Aksenov, R. Ruffini, and G. V. Vereshchagin "Thermalization of Nonequilibrium
977 Electron-Positron-Photon Plasmas," *Phys. Rev. Lett.* **99**, 125003 (2007) doi: 10.1103/PhysRevLett.99.125003
- 978 131. A. G. Aksenov, R. Ruffini, and G. V. Vereshchagin "Pair plasma relaxation time scales" *Phys. Rev. E* **81**, 046401
979 (2010) doi: 10.1103/PhysRevE.81.046401